HOKKAIDO UNIVERSITY

Title	Enhanced cementation for heavy metal removal and recovery using aluminum as electron donor and electro-conductive particles as electron mediator
Author(s)	Choi, Sanghyeon
Degree Grantor	北海道大学
Degree Name	博士(工学)
Dissertation Number	甲第14684号
Issue Date	2021-09-24
DOI	https://doi.org/10.14943/doctoral.k14684
Doc URL	https://hdl.handle.net/2115/94577
Type	doctoral thesis
File Information	Choi_Sanghyeon.pdf

Hokkaido University Collection of Scholarly and Academic Papers : HUSCAP

Enhanced cementation for heavy metal removal and recovery using aluminum as electron donor and electro-conductive particles as electron mediator

A dissertation submitted in partial fulfillment of the requirements
for the degree of Doctorate in Engineering

by

SANGHYEON CHOI



Division of Sustainable Resources Engineering,
Graduate School of Engineering,
Hokkaido University, Japan
September 2021

Abstract

Cementation is a method to recover and remove metal ions from aqueous solutions by reductive deposition of the metals using another elemental metal acting as an electron donor or reducing agent. Cementation has been used in hydrometallurgical processes as well as in environmental remediation to remove toxic heavy metals from contaminated solutions. Aluminum (Al) has been considered as a promising electron donor for environmental remediation, because of its less toxicity and low standard electrode potential, allowing it to use for reducing most other metal ions without secondary contamination. Practical application of Al in cementation is, however, limited due to the presence of surface Al oxide layer(Al_2O_3), which inhibits electron transfer from Al to metal ions. Recently, a new cementation technique using the mixture of Al and activated carbon (AC) has been proposed for recovering gold ions from ammonium thiosulfate solution. In this technique, AC attached on Al surface act as an electron mediator, and electrons are transferred from Al to gold ions even without removing Al oxide layer. In this study, applicability of the cementation method using Al as an electron donor and AC as an electron mediator was investigated for removing heavy metal ions from sulfate and chloride solutions, and alternative electron mediators to AC was also studied.

Chapter 1 describes the background and objectives of this study, and a literature review on cementation using Al.

In Chapter 2, effects of AC addition on the cementation of Cd^{2+}, Co^{2+}, Ni^{2+}, and Zn^{2+} from sulfate solutions were investigated using Al powder as an electron donor. The results of solution analysis showed that at pH over 4, efficiencies of metal ion removal from solutions were higher when using both AC and Al than that with only AC or Al. The results of surface analysis for the cementation products by SEM-EDX, XPS, and AES analysis showed that the metals were deposited as an elemental form on AC attached on Al surface. The result of linear sweep voltammetry (LSV) for Al electrode in cadmium sulfate solution at pH 5, showed that current for reducing Cd ions increased by attaching AC on Al electrode surface. These results suggested that AC act as an electron mediator to enhance electron transfer from Al to heavy metal ions even in the presence of insulating surface aluminum oxide layer, and that cementation technique using AC/Al mixture can be applied to remove a wide variety of heavy metal ions from sulfate solution.

In Chapter 3, the effects of AC addition on the cementation of Pb^{2+}, Cd^{2+}, Co^{2+}, Ni^{2+}, and Zn^{2+} from chloride solutions at initial pH 4 were investigated using Al as an electron donor. In chloride solutions, insulating Al oxide layer was removed from Al surface due to formation of soluble aluminum chloride complexes, and this caused high cementation efficiency (99%) for Pb^{2+} and Cd^{2+} while the cementation efficiencies for Co^{2+}, Ni^{2+}, and Zn^{2+} were almost zero, mainly because of

competition of metal deposition and hydrogen evolution (for Co^{2+} and Ni^{2+}), and slow metal deposition rate (for Zn^{2+}). With AC/Al mixture was used, cementation of Pb^{2+} and Cd^{2+} was suppressed and cementation of Co^{2+}, Ni^{2+}, and Zn^{2+} was enhanced. Based on the results of electrochemical experiments and SEM-EDX analysis for cementation products, a possible mechanism for the suppression and enhancement of the cementation of different metal species in chloride solutions was discussed.

In Chapter 4, alternative electron mediators to AC were studied. Using fine particles of Ti oxide (TiO_2, rutile) and Si oxide (SiO_2) as an alternative to AC, cementation of Co^{2+} and Ni^{2+} from sulfate and chloride solutions were investigated with Al as an electron donor. No cementation occurred when non-conductive SiO_2 was used. When semi-conductor TiO_2 was used, enhanced cementation of Co and Ni has observed: the results showed that elemental Co and Ni were deposited on TiO_2 particles attached on Al surface, and that cementation efficiencies increased with increasing the dosage of TiO_2. These results suggest that electro-conductive particles like TiO_2 can be used as an alternative electron mediator for enhanced cementation using Al as an electron donor.

In Chapter 5, using Al particles as an electron donor and magnetite (Fe_3O_4) particles as an electron mediator, cementation of Cd^{2+} and Zn^{2+} from sulfate solutions were investigated. The results of cementation experiments showed that Cd and Zn were deposited on Fe_3O_4 particles attached on Al surface, and that the cementation efficiencies of these metals increased with increasing Fe_3O_4 dosage. The results of electrochemical impedance spectroscopy for Al electrode confirmed that charge transfer resistance was reduced when Fe_3O_4 was attached on the surface. By applying ultra-sonification and magnetic separation for cementation products, a significant portion of cemented Cd and Zn were recovered together with Fe_3O_4 in a magnetic fraction, and Al were separated to a non-magnetic fraction.

Chapter 6 summarized the important findings of this dissertation.

Table of Contents

List of Figures ..... **vi**

List of Tables ..... **x**

CHAPTER 1 – GENERAL INTRODUCTION **1**

1.1 Background and Objectives 1

1.2 Literature review on cementation using Al 2

1.2.1 Property of Al as an electron donor on cementation 2

1.2.2 Factors affecting cementation efficiencies 4

1.2.3 New cementation techniques using Al and AC 13

1.3 Outline of the dissertation 14

References 14

CHAPTER 2 – Enhanced cementation of Cd^{2+}, Co^{2+}, Ni^{2+}, and Zn^{2+} with aluminum from sulfate solutions by the addition of activated carbon as electron mediator **21**

2.1 Introduction 21

2.2 Materials and methods 22

2.2.1 Aluminum and activated carbon 22

2.2.2 Cementation methods 23

2.2.3 Surface analysis 24

2.2.4 Electrochemical measurements 24

2.3 Results and discussion 25

2.3.1 Removal of Cd^{2+} 25

2.3.2 Removal of Co^{2+} and Ni^{2+} 31

2.3.3 Removal of Zn^{2} 37

2.4 Summary 40

References 41

CHAPTER 3 – Removal of Pb^{2+}, Cd^{2+}, Co^{2+}, Ni^{2+}, and Zn^{2+} from chloride solutions by cementation using aluminum as electron donor and the effect of activated carbon addition 49

3.1 Introduction 49

3.2 Materials and methods 49

3.2.1 Cementation experiments 49

3.2.2 Cementation methods 50

3.3 Results and discussion 51

3.3.1 BET surface area of Al and AC 51

3.3.2 Removal of metal ions from chloride solutions 52

3.3.3 Surface analysis of Pb^{2+}, Cd^{2+}, Co^{2+}, Ni^{2+}, and Zn^{2+} cementation products (AC/Al-mixture) 59

3.3 Comparison of cementation of metal ions using AC/Al mixture in sulfate and chloride solutions 61

3.4 Summary 62

References 63

CHAPTER 4 – Enhanced cementation of Co^{2+} and Ni^{2+} from sulfate and chloride solutions using aluminum as electron donor and electron-conductive particles as electron mediator 68

4.1 Introduction 68

4.2 Materials and methods 69

4.2.1 Materials (Al, AC, TiO_2, and SiO_2) 69

4.2.2 Recovery of Co^{2+} and Ni^{2+} from sulfate and chloride solutions 69

4.3 Results and discussion 71

4.3.1 Recovery of Co^{2+} and Ni^{2+} 71

4.3.2 Removal of metal ions from chloride solutions 73

4.3.2 Surface analysis of deposited Co and Ni 75

4.4 Summary 77

References 78

CHAPTER 5 – Enhanced cementation of Cd^{2+} and Zn^{2+} from sulfate solutions using aluminum powder and Fe_3O_4 as an electron mediator and application of magnetic separation to concentrate cementation products **83**

5.1 Introduction 83

5.2 Materials and methods 84

5.2.1 Cementation experiments 84

5.2.2 Magnetic separation 85

5.2.3 Electrochemical measurements 86

5.3 Results and discussion 87

5.3.1 Effects of Fe_3O_4 on cementation of Cd^{2+} and Zn^{2+} with Al 87

5.3.2 Magnetic separation of cementation products 95

5.4 Summary 98

References 98

CHAPTER 6 – GENERAL CONCLUSION **101**

ACKNOLEDGEMENT **102**

List of Figures

Fig. 1-1 The schematic diagrams of cementation of metal ions involving the mechanisms (Murr and Annamalai, 1978b; Wei et al., 1994).....3

Fig. 1-2 The solubility of various metal hydroxides as a function of pH (created using the GWB ® Professional Ver. 12.0.3 software).....4

Fig. 1-3 The Eh – pH diagram of Al^{3+} – H_2O system at 25 ºC, 1.013 bar ([Al^{3+}]: 0.1 M, created using the GWB® Professional Ver. 12.0.3 software). 7

Fig. 2-1 Particle size distribution for (a) aluminum and (b) activated carbon used in this chapter.....23

Fig. 2-2 (a) The Cd^{2+} removal efficiency, (b) final pH, and (b) Al^{3+} concentration in sulfate solutions at different pH for 24 h (Al = Al^0; AC = Activated carbon).....27

Fig. 2-3 XPS spectra of the Al $2p_{3/2}$ region: (a) after the experiment using only Al at pH 5 and (b) Al before the experiment. 27

Fig. 2-4 The activity – pH diagram for (a) Al^{3+} and (b) Cd^{2+} in 0.1 M SO_4^{2-} (created using the GWB® Professional Ver. 12.0.3 software).....27

Fig. 2-5 (a) The removal efficiency of Cd^{2+} and (b) final pH in sulfate solutions at initial pH 5 for 24 h (Al = Al^0; AC = Activated carbon).....28

Fig. 2-6 SEM photomicrograph of (a) cementation products using AC/Al-mixture in 1 mM cadmium sulfate solution at pH 5.0 and EDS point analysis of each point (1 and 2).....29

Fig. 2-7 XPS spectra of cementation products using AC/Al-mixture in 1 mM cadmium sulfate solution at pH 5: spectrum of (a) Cd 3d, (b) Al $2p_{3/2}$, and (c) O 1s. 29

Fig. 2-8 Linear sweep voltammograms of without Cd^{2+} and 1 mM Cd^{2+} (scan range: OCP to –1.2 V vs. Ag/AgCl) in sulfate solutions at pH 5.0 at 25 °C using Al and AC/Al electrode (scan rate: 10 mV/s) 30

Fig. 2-9 (a) The Co^{2+} removal efficiency, (b) final pH, and (c) Al^{3+} concentration in sulfate solutions at different pH for 24 h (Al = Al^0; AC = Activated carbon).....31

Fig. 2-10 (a) The Ni^{2+} removal efficiency, (b) final pH, and (c) Al^{3+} concentration in sulfate solutions at different pH for 24 h (Al = Al^0; AC = Activated carbon).....31

Fig. 2-11 The activity – pH diagram for 1mM (a) Co^{2+} and (b) Ni^{2+} species with 0.1 M SO_4^{2-} (created using the GWB Professional Ver. 12.0.3 software).....32

Fig. 2-12 The removal efficiency and final pH of (a, b) Co and (c, d) Ni in sulfate solutions at initial pH 5 for 24 h (Al = Al^0; AC = Activated carbon). 34

Fig. 2-13 Co^{2+}, Ni^{2+} and Cd^{2+} removal efficiencies using “fresh” and “used” AC/Al-mixtures in sulfate solution at pH 5.0.....35

Fig. 2-14 SEM photomicrograph of (a) cementation products using AC/Al-mixture in 1 mM cobalt sulfate solution at pH 5.0 and EDS point analysis of each point (1 and 2).....36

Fig. 2-15 XPS spectra of cementation products using AC/Al-mixture in 1 mM cobalt sulfate solution

at pH 5: (a) spectrum of Al $2p_{3/2}$ and (b) O 1s. 36
Fig. 2-16 (a) The Zn^{2+} removal efficiency, (b) final pH, and (c) Al^{3+} concentration in sulfate solutions at different pH for 24 h (Al = Al^0; AC = Activated carbon). 38
Fig. 2-17 The removal efficiency of Zn^{2+} and final pH in sulfate solutions at initial pH 3 for 24 h (Al = Al^0, AC = Activated carbon). 38
Fig. 2-18 SEM photomicrograph of (a) Zn cementation products using AC/Al-mixture in 1 mM zinc sulfate solution at pH 3.0 and EDS point analysis of each point (1 and 2). 39
Fig. 2-19 AES results of cementation products from the Zn^{2+} removal experiments using AC/Al-mixture: (a) photomicrograph, (b) wide scan energy spectrum of the red point in (a), and (c) the narrow scan energy spectrum of the Zn peak with fitting spectra of Zn^0 and ZnO. 40
Fig. 3-1 BET nitrogen adsorption-desorption isotherm plot of (a) aluminum (Al) and (b) activated carbon (AC). 52
Fig. 3-2 (a) The removal efficiencies of Pb^{2+}, Cd^{2+}, Co^{2+}, Ni^{2+}, and Zn^{2+}, (b) the changes in pH and (c) Al concentration during the cementation using Al with time at initial pH 4.0 and 0.1 M Cl^-. 53
Fig. 3-3 The open circuit potential (OCP) of Al electrode in chloride solutions at 25 °C for 10 min (solutions: 1 mM Pb^{2+}, Cd^{2+}, Co^{2+}, Ni^{2+}, Zn^{2+} and without metal ions in 0.1 M Cl^- at initial pH 4.0). 54
Fig. 3-4 The linear sweep voltammograms of Pb, Cd, Co, Ni and Zn electrodes in chloride solutions at 25 °C (solutions: without metal ions in 0.1 M Cl^- at initial pH 4.0; sweep rate: 1.0 mV/s). 56
Fig. 3-5 The activity – pH diagram for 1 mM (a) Pb^{2+}, (b) Cd^{2+}, (c) Co^{2+}, (d) Ni^{2+} and (e) Zn^{2+} species with 0.1 M Cl^- at 25°C (created using the GWB Professional Ver. 12.0.3 software). 58
Fig. 3-6 SEM photomicrograph of cementation products using AC/Al-mixture (a) Pb, (b) Cd, (c) Co, (d) Ni and (e) Zn, and EDS point analysis of each point (1 and 2). 60
Fig. 3-7 Schematic diagram of Co^{2+} and Ni^{2+} cementation using (a) only Al and (b) AC/Al-mixture. 61
Fig. 3-8 Schematic diagram of Pb^{2+} and Cd^{2+} cementation using (a) only Al and (b) AC/Al-mixture. 62
Fig. 3-9 Schematic diagram of Zn^{2+} cementation using (a) only Al and (b) AC/Al-mixture. 62

Fig. 4-1 Particle size distribution for (a) aluminum (Al), (b) activated carbon (AC), (c) titanium dioxide (TiO_2), and (d) silicon dioxide (SiO_2) used in this chapter. 69
Fig. 4-2 The effects of (a) SiO_2, (b) AC, and (c) TiO_2 dosages on the recovery efficiency of Co^{2+} and final pH in sulfate solutions at initial pH 4.0 for 24 h. 72

Fig. 4-3 The effects of (a) SiO_2, (b) AC, and (c) TiO_2 dosages on the recovery efficiency of Ni^{2+} and final pH in sulfate solutions at initial pH 4.0 for 24 h.....72
Fig. 4-4 The activity–pH diagram for 1 mM (a) Co^{2+} and (b) Ni^{2+} species with 0.1 M SO_4^{2-} at 25 °C (created using the GWB Professional Ver. 12.0.3 software). 73
Fig. 4-5 The effects of (a) SiO_2, (b) AC, and (c) TiO_2 dosages on the recovery efficiency of Co^{2+} and final pH in chloride solutions at initial pH 4.0 for 24 h. 75
Fig. 4-6 The effects of (a) SiO_2, (b) AC, and (c) TiO_2 dosages on the recovery efficiency of Ni^{2+} and final pH in chloride solutions at initial pH 4.0 for 24 h. 75
Fig. 4-7 Auger electron spectroscopy (AES) results of the residue obtained after cementation of Co^{2+} from chloride solution using TiO_2/Al: (a) photomicrograph, (b) wide scan energy spectrum of each point, and (c) the narrow scan energy spectrum of the Co peak with fitting spectra of Co, CoO, and Co_3O_4. 76
Fig. 4-8 Auger electron spectroscopy (AES) results of the residue obtained after cementation of Ni^{2+} from chloride solution using TiO_2/Al: (a) photomicrograph, (b) wide scan energy spectrum of each points, and (c) the narrow scan energy spectrum of the Ni peak with fitting spectra of Ni and NiO.....77
Fig. 5-1 Photographs of the magnetic separation used in this study: (a) before magnetic separation, (b) during magnetic separation with stirring, and (c) after magnetic separation without stirring. 85
Fig. 5-2 The flowchart of 2-stage magnetic separation and photographs of magnetic and non-magnetic fractions obtained by magnetic separation of Cd cementation products. 86
Fig. 5-3 The schematic diagram of electrochemical experiment. 87
Fig. 5-4 The removal efficiencies of metal ions ((a) Cd^{2+} and (b) Zn^{2+}) and final pH ((c) Cd^{2+} and (d) Zn^{2+}) in sulfate solutions using Al^0 and/or Fe_3O_4 at initial pH 5.0 for 24 h and the activity – pH diagram for 1 mM (e) Cd^{2+} and (f) Zn^{2+} species with 0.1 M SO_4^{2-} at 25 °C (created using the Geochemist's Workbench® Professional Ver. 12.0.3 software with the MINTEQ database). 88
Fig. 5-5 Box plots of removal efficiencies of metal ions ((a) Cd^{2+} and (b) Zn^{2+}) in sulfate solutions using Al^0 and/or Fe_3O_4 at initial pH 5.0 for 24 h.....90
Fig. 5-6 SEM-EDS analysis of Cd- cementation product: BSE image and EDS spectra of the corresponding points. 91
Fig. 5-7 SEM-EDS analysis of Zn- cementation product: BSE image and EDS spectra of the corresponding points. 92
Fig. 5-8 Nyquist plots of (a) Al and (b) Fe_3O_4/Al electrodes (insets are equivalent circuit models for fitting EIS data), the Bode plot of (c) phase angle and (d) magnitude Z as a function of frequency for Al and Fe_3O_4/Al electrodes, and schematic diagram of Cd^{2+} and Zn^{2+}

cementation using Fe_3O_4/Al-mixture. 94
Fig. 5-9 Back-scattered electron (BSE) image of the Cd components in (a) magnetic fraction and (b) non-magnetic fraction, and EDS point analysis of each point (a-1, a-2, and b-1). 95
Fig. 5-10 Back-scattered electron (BSE) image of the Zn components in (a) magnetic fraction and (b) non-magnetic fraction, and EDS point analysis of each point (a-1, a-2, and b-1). 96
Fig. 5-11 Distribution of magnetic and non-magnetic fractions obtained by magnetic separation of (a) Cd- and (b) Zn- cementation products. 96
Fig. 5-12 The estimated flowchart for cementation using Fe_3O_4 and Al in this study. 97

List of Tables

Table 1-1 A list of studies on the cementation of metal ions using Al^0 on the effects of temperature. .6
Table 1-2 A list of studies on the cementation of metal ions using Al^0 on the effects of pH. 10
Table 1-3 A list of studies on the cementation of metal ions using Al^0 on the effects of Cl^-. 12
Table 2-1 Hydrogen overpotential values of Cd, Zn, Co, and Ni 33
Table 2-2 Initial and final pH of Co^{2+}, Ni^{2+} and Cd^{2+} removal experiments using "fresh" AC/Al-mixture and "used" AC/Al-mixture in sulfate solutions after 24 h at initial pH 5. 35
Table 3-1 Standard electrode potential of each metal and Gibbs free energy changes of cementation reaction using only aluminum at 25 °C.....53
Table 3-2 The removal efficiency of metal ions (Pb^{2+}, Cd^{2+}, Co^{2+}, Ni^{2+}, and Zn^{2+}), and the changes in pH and Al concentration during cementation using Al, AC, and Al/AC mixture in chloride solutions at initial pH 4.0 for 24 h. 57

CHAPTER 1 – GENERAL INTRODUCTION

1.1 Background and Objectives

To recover a small amount of valuable metal ions in hydrometallurgical processes and to remove toxic heavy metal ions from aqueous solutions are important issues both economically and environmentally. Among the several techniques to recover and remove metal ions, cementation, which is an electrochemical reduction reaction, is one of widely used techniques with following advantages: (1) high process efficiency, (2) low energy consumption, (3) simple operation, and (4) not require expensive and complicated facilities (Anacleto and Carvalho, 1996; Chen and Lee, 1994; Demirkran and Künkül, 2011; Farahmand et al., 2009). Cementation proceeds through two concurrent electrochemical reactions: reduction of metal ions (i.e., cathodic reaction) and oxidation of less noble metal (i.e., anodic reaction) (Brevnov et al., 2004; Wei et al., 1994). Thus, metal ions are reductively deposited on the surface of less noble metal, and its driving force is determined by the half-cell potential difference between metal ions and less noble metal in the electromotive force series (Abdel-Aziz et al., 2016; Brevnov et al., 2004; Dönmez et al., 1999).

Aluminum (Al) is a promising electron donor for environment remediation with low standard electrode potential (i.e., $E^0_{Al3+/Al} = -1.67$ V vs. SHE) and less toxicity (Hong et al., 2014; Karavasteva, 2005; Li et al., 2013), which allows reducing most other metal ions without further contamination as described by the following equation (Demirkran and Künkül, 2011):

$$2Al^0_{(s)} + 3Me^{2+}_{(aq)} = 2Al^{3+}_{(aq)} + 3Me^0_{(s)} \qquad \text{(Me: more noble metal than Al)} \qquad (1\text{-}1)$$

Although Al^0 is the most efficient electron donor, its practical application for cementation is limited due to the presence of a passive Al oxide layer (Al_2O_3) on Al^0 surface, which inhibits electron transfer from Al^0 to metal ions (Brevnov et al., 2004; Karavasteva, 2005; Malik, 1991; Reboul, et al., 1997). The surface Al_2O_3 layer is very thin but difficult to remove because it is dense and tight (1–10 nm), and even if removed, it is immediately regenerated when exposed to the water and atmosphere (Malik, 1991; McCafferty, 2003; Natishan and O'Grady, 2014; Poinern et al., 2010; Reboul, et al., 1997). Because of these reasons, numerous studies have been reported for cementation using Al^0 by removing Al_2O_3 layer: when applying high temperature, strong acidic/alkaline pH, and the addition of additives like chloride ions, the surface Al_2O_3 layer to inhibit cementation reaction can be removed. These extreme conditions are applicable for the processes using reactors, while they are very difficult to use for on-site operations of environmental remediation. Recently, a new cementation technique to recover gold ions from ammonium thiosulfate solution using a mixture of Al and activated carbon (AC) has been proposed by Jeon and coworkers (Jeon et al., 2020). The proposed mechanisms of this enhanced cementation technique (i.e., AC/Al-cementation) are as follows: attached AC on Al surface acts as an electron mediator and electron transfer could occur from Al^0 to gold ions even without the

removal of Al_2O_3 layer.

The AC/Al-cementation proposed by Jeon et al. (2020) can successfully recover gold ions from ammonium thiosulfate solutions, however, applicability of AC/Al-cementation to remove heavy metal ions from sulfate and chloride solutions has not been investigated. Moreover, applicability of alternative electron mediator to AC has also not been studied. The specific objectives of this study are as follows: (1) to investigate the applicability of AC/Al cementation to removal of heavy metal ions from sulfate and chloride solutions, (2) to develop alternative electron mediators replacing AC.

1.2 Literature review on cementation using Al

1.2.1 Property of Al as an electron donor on cementation

- Cementation process

Cementation, a spontaneous electrochemical reaction, has been widely used since the 16th century for electrochemically reducing dissolved metal ions from aqueous solutions using less noble metal (i.e., electron donor) in the hydrometallurgical industry (Djokić, 1996; Ekmekyapar et al., 2012; Karavasteva, 2009; Murr and Annamalai, 1978a). In general, cementation is concurrent reactions between anodic and cathodic reactions (Brevnov et al., 2004; Wei et al., 1994), and the overall reaction is represented by the following equation:

$$n\,A^0{}_{(s)} + m\,B^{b+}{}_{(aq)} = n\,A^{a+}{}_{(aq)} + m\,B^0{}_{(s)} \qquad (na = mb) \qquad (1\text{-}2)$$

Where, A is a less noble metal (electron donor) and B, a metal that is removed from an aqueous solution. This reaction occurs spontaneously when the Gibbs free energy change of the reaction (ΔG^0) is negative. The relation between the Gibbs free energy change and standard electrode potential of anodic and cathodic reactions can be expressed by the following equation (Uhlig and Revie, 1985):

$$\Delta G^0{}_{cell} = -n\,F\Delta E^0{}_{cell} \qquad (\Delta E^0{}_{cell} = E^0{}_{Cathodic} - E^0{}_{Anodic}) \qquad (1\text{-}3)$$

where n and F represent the number of electrons transferred and Faraday's constant, respectively.

As shown in Fig. 1-1, cementation process is composed of five steps (Murr and Annamalai, 1978b; Wei et al., 1994): (1) metal ions (B^{b+}) diffusion to surface of electron donor (metal A^0) from bulk solution, (2) adsorption of B^{b+} onto the A^0 surface, (3) electron exchange between B^{b+} and A^0, (4) release of A^{a+} from the anodic site, and (5) diffusion of A^{a+} into the bulk solution. In general, steps (1) and (5) are mass transfer processes, and (2) – (4) are electrochemical reactions. Factors like pH, temperature, hydrogen evolution, and additives affect the rates of steps (1) – (5) and overall reaction (Eq. 1-2).

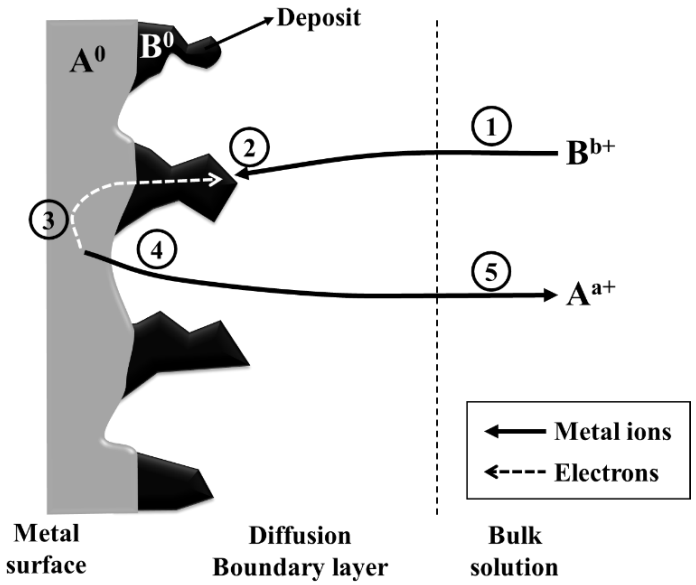


Fig. 1-1 The schematic diagrams of cementation of metal ions involving the mechanisms (Murr and Annamalai, 1978b; Wei et al., 1994).

- Property of Al

Because the standard electrode potential of aluminum (Al) is very low (i.e., $E^0_{Al3+/Al0}$ = –1.66 V vs. SHE), Al can be used as electron donor for cementation to remove most of other metal ions. Although cementation using Al^0 can achieve high efficiency for removal of most metal ions, its practical application is limited because it is covered with an insulating passive Al oxide layer (Al_2O_3), inhibiting electron transfer from Al^0 to metal ions (Anacleto and Carvalho, 1996; Brevnov et al., 2004; Karavasteva, 2005).

When Al^0 is exposed to oxygen in the atmosphere, stable Al_2O_3 layer forms immediately on its surface (Li et al., 2013; McCafferty, 2003; Poinern et al., 2010; Reboul, et al., 1997). The thickness of Al_2O_3 layer depends on the production conditions and it has been reported to be 4.8 nm (Strohmeier, 1990), 4.0 nm (Yu et al., 2000), and 4.0 nm (Zähr et al., 2012) for air-exposed aluminum, with an average of 1–10 nm (Poinern et al., 2010; Uhlig and Revie, 1985). This Al_2O_3 layer is thin but hard and stable in a neutral medium, so it can prevent corrosion of Al^0 (Park et al., 2020; Poinern et al., 2010; Xhanari and Finšgar, 2019). Moreover, even if corrosion occurs, it can be considered that continuous oxidation of Al^0 is difficult due to regeneration of Al_2O_3 layer (Malik, 1991; McCafferty, 2003; Reboul, et al., 1997; Takahashi et al., 2009). When Al^0 is oxidized in aqueous solutions during cementation, aluminum ions (Al^{3+}) are released, and they are precipitated as hydroxide (Fig. 1-2). When this aluminum hydroxide covers on Al^0 surface, they act as an insulation layer and suppresses further reactions for cementation (Abdollahi et al., 2015; Hong et al., 2014; Karavasteva, 2005; Li et al., 2013; Park et al., 2018; Reboul, et al., 1997; Seng et al., 2019).

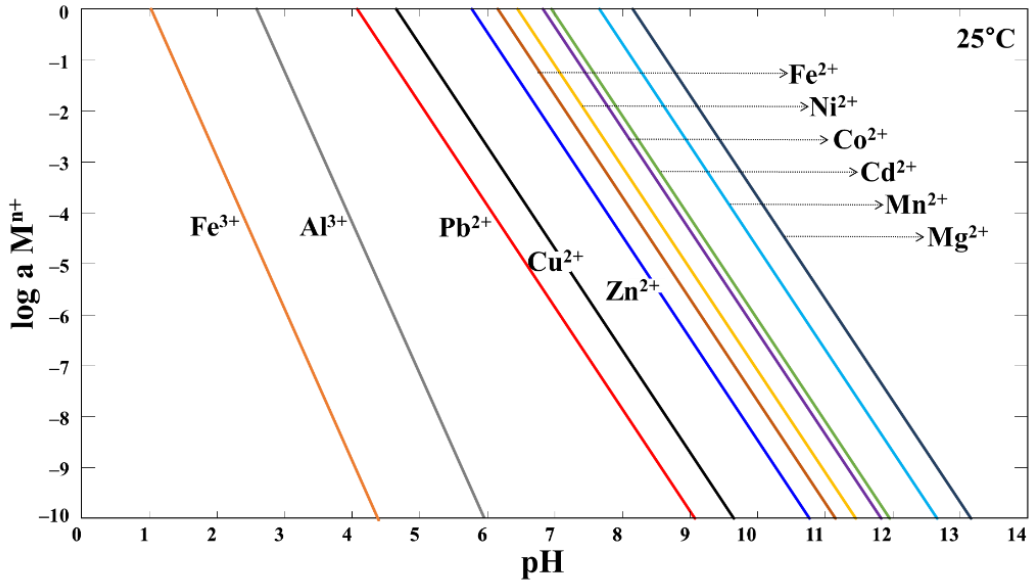


Fig. 1-2 The solubility of various metal hydroxides as a function of pH (created using the GWB ® Professional Ver. 12.0.3 software).

1.2.2 Factors affecting cementation efficiencies

Several techniques have been reported to enhance the efficiency of cementation using Al^0 by removing Al_2O_3 layer at high temperature, strongly acidic/alkaline pH, and in the presence of additives such as chloride ions. This section summarizes the factors to enhance cementation efficiency by the removal of Al_2O_3 layer.

- Effects of temperature

Many studies have confirmed that cementation efficiency increases with increasing temperature as shown in Table 1-1. Annamalai et al. (1978) investigated the kinetic studies on the cementation of Cu ions in chloride solution using Al^0 disc and the effects of temperature. At 15 °C, the specific rate constant (k) was very low while it increased rapidly as the temperature increased to 33 °C. Ekmekyapar et al. (2012) examined the effects of temperature on the study of kinetics on the cementation of Cu ions in acetic leachate using Al^0 disc, and they observed that the rate constant increase rapidly as the temperature increased from 20 °C to 60 °C. Based on these results, they suggested that the increase of rate constant was caused by the break down (i.e., removal) of the Al_2O_3 layer via high temperature. This is supported by the leaching experiment of alumina (Al_2O_3). Sarker et al. (2015) demonstrated that the leaching efficiency of alumina (Al_2O_3) increased with increasing temperature from 25 °C to 100 °C using 4 M HCl solution.

Lee et al. (1997) investigated the recovery of Au and Ag ions from thiourea solution using Al^0 powder. The recovery efficiencies of Au and Ag ions at 15 °C were 60% and 20%, respectively, and increased to around 99% as the temperature increased to 25–35 °C. They suggested that high temperature caused removal of Al_2O_3 layer and causes higher cementation efficiency for gold and silver recovery.

As summarized in Table 1-1, the effects of temperature are more clear in the following studies: (1) Cu ions recovery in sulfate solutions (Demirkran and Künkül, 2011; Dönmez et al., 1999), (2) Au ions recovery in thiocyanate solution (Wang et al., 2007), (3) Pb ions recovery in chloride solution (Abdollahi et al., 2015; Farahmand et al., 2009), and In ions recovery in chloride solution (Hong et al., 2014; Lee et al., 2014). These results showed that the importance of high temperature for cementation process using Al^0.

Table 1-1 A list of studies on the cementation of metal ions using Al^0 on the effects of temperature.

Year	Aluminum type	Target metal ions	Solutions	pH	Speed (min^{-1})	Time (min)	Cl^- (mg/L)	Temp. (°C)	Comment	Ref.
1978	Al disc (ø 2.22 cm, 99.99%)	Cu ions (100 mg/L)	in chloride solution	2.5	1250	-	75	15–70	Rate constant increased with increasing temperature	(Annamalai et al., 1978)
1997	Al power (–200 mesh, > 99%)	Au ions (96 mg/L) Ag ions (534 mg/L)	in thiourea solution	< 1.5	300	60	x	15–35	Au ≒ 60%, Ag ≒ 20% (15 °C) Au 99%, Ag 99% (> 25 °C)	(Lee et al., 1997)
1999	Al disc (ø 2.2 cm, –)	Cu ions (635.46 mg/L)	in sulfate solution	2.5	5027	45	x	20–50	≒ 53% (20 °C, 15 min) ≒ 80% (50 °C, 15 min)	(Dönmez et al., 1999)
2007	Al power (D_{50}: 168.9 µm, 99.0%)	Au ions (10 mg/L)	in thiocyanate solution	2	500	60	x	6–50	≒ 70% (6 °C, 60 min) 99% (25 °C, 60 min) 99% (50 °C, 15 min)	(Wang et al., 2007)
2009	Al powder (–125 +88 µm, 99.5%)	Pb ions (3000 mg/L)	in chloride solution	–	110	90	–	40–70	≒ 50% (40 °C) 94% (70 °C)	(Farahmand et al., 2009)
2011	Al powder (–2.0 +1.5 mm)	Cu ions (1589 mg/L)	in sulfate solution	1	71	90	x	40–80	≒ 60% (40 °C) ≒ 99% (80 °C)	(Demirkran and Künkül, 2011)
2012	Al disc (ø 50 mm, –)	Cu ions (159–1271 mg/L)	in acetic acid solution	1–3.26	200–500	90	x	20–60	Cemented Cu fraction increased with increasing temperature	(Ekmekyapar et al., 2012)
2014	Al plate (-)	In ions (266 mg/L)	in chloride solution	0.4	–	120	–	0–60	18% (40 °C) 89% (60 °C)	(Hong et al., 2014)
2014	Al plate (15 x 3 mm, 99.9%)	In ions (400 mg/L)	in chloride solution	0.15	–	180	–	40–80	40% (40 °C, 10 min) 70% (60 °C, 10 min)	(Lee et al., 2014)
2015	Al powder (-)	Pb ions (5630–16360 mg/L)	in chloride solution	4	100	90	300 x10^3	40–70	87% (40 °C, 40 min) 93% (70 °C, 40 min)	(Abdollahi et al., 2015)

Note: “x” means not present and “–” means not reported.

➢ Effects of acidic and alkaline pH

Maintaining the appropriate pH of an aqueous solution is an important technique to enhance cementation efficiency using Al^0 (Abdollahi et al., 2015; Karavasteva, 2005). As shown in Fig. 1-3, Al_2O_3 layer is stable in neutral pH ranges, but it is dissolved in acidic and alkaline conditions to be stable species as Al^{3+} and $Al(OH)_4^-$ or AlO_2^- respectively (Reboul, et al., 1997; Stubblebine et al., 2016; Tak et al., 2006; Uhlig and Revie, 1985; Xhanari and Finšgar, 2019).

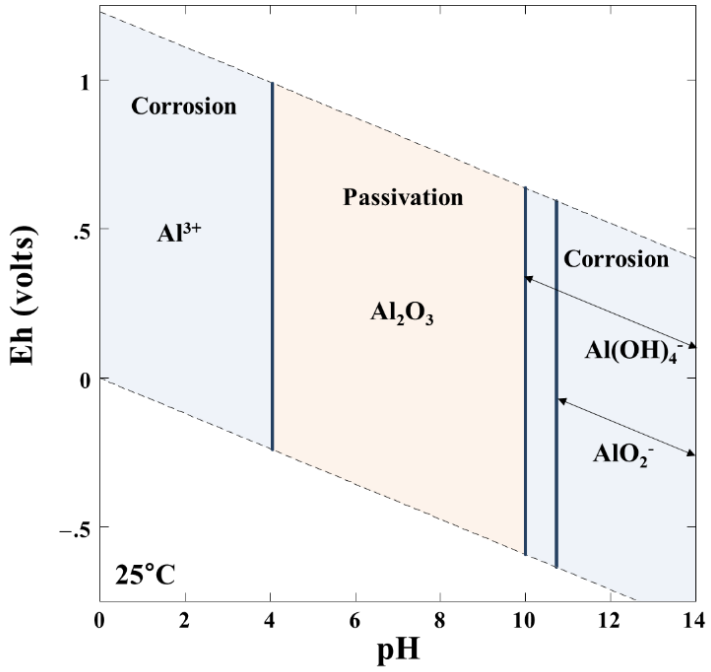


Fig. 1-3 The Eh – pH diagram of Al^{3+} – H_2O system at 25 ºC, 1.013 bar ([Al^{3+}]: 0.1 M, created using the GWB® Professional Ver. 12.0.3 software).

Stubblebine et al. (2016) studied the corrosion behavior of Al_2O_3 and Al^0 in acidic media using a thermodynamic Eh – pH diagram. At low pH, dissolution of Al_2O_3 layer on Al^0 surface is as expressed in Eq. 1-4.

$$Al_2O_{3(s)} + 6H^+_{(aq)} = 2Al^{3+}_{(aq)} + 3H_2O_{(aq)} \quad (1\text{-}4)$$

After removing Al_2O_3 layer on Al^0 surface at low pH, an oxidation-reduction reaction takes place on the exposed Al^0 surface as explained in Fig. 1-2. Two reactions can occur on the Al^0 surface: (1) cementation of metal ions (Eq. 1-1) and (2) hydrogen evolution reaction (HER) (Eq. 1-5; MacKinnon and Ingraham, 1971; Reboul, et al., 1997; Stubblebine et al., 2016).

$$2Al^0_{(s)} + 6H^+_{(aq)} = 2Al^{3+}_{(aq)} + 3H_{2(g)} \quad (1\text{-}5)$$

In cementation process, HER is an unwanted side reaction, causing the decreases in cementation efficiency by competition with metal ions reduction and the excessive consumption of Al^0 (Anacleto and Carvalho, 1996; Nelson et al., 2000). The rate of HER depends on the hydrogen overpotential of cemented metal; hydrogen evolution became faster when hydrogen overpotential is low (Beyene et al., 2018; Ezaki et al., 1993; Ku and Chen, 1992; Uhlig and Revie, 1985).

Because Al_2O_3 is an amphoteric substance that can react with alkaline media as well as acidic media, so cementation using Al^0 in an alkaline solution can also be an alternative technique (Bi et al., 2021). The dissolution of Al_2O_3 layer in alkaline solution is mainly caused by the reactions with OH^- as shown by Eqs. 1-6 to 1-9, and products of Al_2O_3 dissolution are AlO_2^- and $Al(OH)_4^-$ (Brouwers and Eijk, 2003; Mendibide et al., 2021; Stubblebine et al., 2016; Tossell, 1999; Xhanari and Finšgar, 2019).

$$Al_2O_{3(s)} + 2OH^-_{(aq)} = 2AlO_2^-{}_{(aq)} + H_2O_{(l)} \quad (1\text{-}6)$$

$$AlO_2^-{}_{(aq)} + 2H_2O_{(l)} = Al(OH)_4^-{}_{(aq)} \quad (1\text{-}7)$$

$$Al_2O_{3(s)} + 3H_2O_{(l)} = 2Al(OH)_{3(s)} \quad (1\text{-}8)$$

$$Al(OH)_{3(s)} + OH^-_{(aq)} = Al(OH)_4^-{}_{(aq)} \quad (1\text{-}9)$$

As shown in Eqs. 1-10 to 1-11, under strongly alkaline conditions, the following hydrogen evolution occurs and these reactions consumed Al^0 (Djokić, 1996; Mendibide et al., 2021; Stubblebine et al., 2016; Xhanari and Finšgar, 2019).

$$2Al_{(s)} + 2H_2O_{(l)} + 2OH^-_{(aq)} = 2AlO_2^-{}_{(aq)} + 3H_{2(g)} \quad (1\text{-}10)$$

$$2Al_{(s)} + 2OH^-_{(aq)} + 6H_2O_{(l)} = 2Al(OH)_4^-{}_{(aq)} + 3H_{2(g)} \quad (1\text{-}11)$$

When the pH value moves to the neutral condition, dissolved Al^{3+} and $Al(OH)_4^-$ precipitates as Al hydroxide on the Al^0 surface due to their low stability (Eqs. 1-12 to 1-14), suppressing the further cementation process (Arima et al., 2002; Demirkran and Künkül, 2011; Lee et al., 2019; May et al., 1979).

$$Al^{3+}_{(aq)} + 3OH^-_{(aq)} = Al(OH)_{3(s)} \quad (1\text{-}12)$$

$$Al^{3+}_{(aq)} + 3H_2O_{(l)} = Al(OH)_{3(s)} + 3H^+ \quad (1\text{-}13)$$

$$Al(OH)_4^-{}_{(aq)} + H^+_{(aq)} = Al(OH)_{3(s)} + H_2O_{(l)} \quad (1\text{-}14)$$

As discussed above, removal of Al_2O_3 layer, hydrogen evolution, consumption of Al^0 and Al hydroxide precipitation depends on pH, and maintaining appropriate pH is important on cementation using Al^0 (Demirkran and Künkül, 2011; Karavasteva, 2005; Kim et al., 2011; Ku and Chen, 1992).

Wang et al. (2007), Demirkran and Künkül (2011), and Ekmekyapar et al. (2012) demonstrated that at pH 1 to 3, cementation efficiency was high because of the removal of Al_2O_3 layer. MacKinnon

and Ingraham (1970), Chen and Lee (1994), studied the kinetic rate constant of cementation of Cu ions from sulfate and chloride solutions at acidic to neutral pH. They observed that the specific rate constant became smallest at a neutral pH because of the presence of Al_2O_3 layer. Anacleto and Carvalho (1996) investigated cementation of Hg ions from chloride solutions using Al^0 powder, and they demonstrated that recovery efficiency was over 80% at pH from 1–7, suggesting that cementation using Al^0 as electron donor was possible at acidic to neutral pH in chloride solutions. On the other hand, in sulfate solutions efficiency of cementation using Al^0 at acidic to neutral pH is limited: Dönmez et al. (1999) reported that recovery of Cu was less than 10% in sulfate solution at pH 5.2. This may be due to the Al_2O_3 layer is not removed in sulfate solution at neutral pH.

Arima et al. (2002) demonstrated that the cementation efficiency of Au ions in ammonium thiosulfate solution was 80% at pH 10 while it was 0% at pH 9.5. At pH 10, $Al(OH)_4^-$ was stable and this caused the removal of insulating Al_2O_3 layer, while at pH 9.5, $Al(OH)_4^-$ was not stable and Al_2O_3 layer was not removed, causing a lower efficiency of cementation. The experimental conditions and results of the effect of pH on cementation using Al^0 are summarized in Table 1-2.

Table 1-2 A list of studies on the cementation of metal ions using Al^0 on the effects of pH.

Year	Aluminum type	Target metal ions	Solutions	pH	Speed (min^{-1})	Time (min)	Cl^- (mg/L)	Temp. (°C)	Comment	Ref.
1970	Al disc (ø 2.22 cm, 99.99%)	Cu ions (100 mg/L)	in sulfate solution	0–1	1250	-	x	50	Cementation efficiency increased with increasing $[H^+]$	(MacKinnon and Ingraham, 1970)
1994	Al disc (ø 46.8 mm, –)	Cu ions (200 mg/L)	in chloride solution	1–4	800	–	220	30	Rate constant value is slow when pH over 4	(Chen and Lee, 1994)
1996	Al powder (D_{50}: 70µm, >90.5%)	Hg ions (500 mg/L)	in chloride solution	1–7	–	30	$100x10^3$	18	≒ 80% (pH 1) ≒ 99% (pH 3) ≒ 80% (pH 7)	(Anacleto and Carvalho, 1996)
1999	Al disc (ø 2.2 cm, –)	Cu ions (635.46 mg/L)	in sulfate solution	1–5.2	5027	45	x	30	99% (pH 1) ≒ 10% (pH 5.2)	(Dönmez et al., 1999)
2002	Al powder (45µm, –)	Au ions (8 mg/L)	in ammonium thiosulfate solution	9.5–10.5	–	60	x	Room temp.	≒ 0% (pH 9.5) > 80% (pH > 10)	(Arima et al., 2002)
2007	Al power (D_{50}: 168.9 µm, 99.0%)	Au ions (10 mg/L)	in thiocyanate solution	1–3	500	60	x	25	99% (pH 1, 50 min) ≒ 80% (pH 3, 60 min)	(Wang et al., 2007)z
2011	Al powder (–2.0 +1.5 mm)	Cu ions (1589 mg/L)	in sulfate solution	1–2	71	60	x	70	≒ 90% (pH 1) ≒ 80% (pH 2)	(Demirkran and Künkül, 2011)
2012	Al disc (ø 50 mm, –)	Cu ions (159–1271 mg/L)	in acetic acid solution	1–3.26	200–500	90	x	20–60	Cemented Cu fraction increased with decreasing pH	(Ekmekyapar et al., 2012)

Note: “x” means not present and “–” means not reported.

➢ Effects of chloride ions

Pitting corrosion, a typical reaction destroying Al^0 caused by anions such as Cl^- in aqueous solutions, is used as a technique for the enhancement of cementation via removal of Al_2O_3 layer. (McCafferty, 2003; Natishan and O'Grady, 2014; Reboul, et al., 1997; Sarker et al., 2015; Tak et al., 2006). The removal of Al_2O_3 layer via Cl^- involves as follows (McCafferty, 2003; Natishan and O'Grady, 2014; Reboul, et al., 1997): (1) Cl^- adsorption on Al_2O_3 layer's micro-flaws, (2) hydrogen evolution occurred at Al_2O_3/Al^0 interface, (3) formation and growth of blister due to the gas pressure increase, and (4) removal of Al_2O_3 layer by a larger scale blister breaks and localized corrosion.

Adsorption of Cl^- is enhanced at pH lower than 9, because the point of zero charge (PZC) of Al is around 9 and negatively charged Cl^- is attracted to the positively charged surface of Al at pH lower than 9 (McCafferty, 2003; Natishan and O'Grady, 2014; Reboul, et al., 1997).

In the presence of Cl^-, Al_2O_3 layer is dissolved according to Eq. 1-15 (Reboul, et al., 1997; Sarker et al., 2015).

$$Al_2O_{3(s)} + 6HCl_{(aq)} = 2AlCl_{3(aq)} + 3H_2O_{(l)} \quad (1\text{-}15)$$

When Al^0 surface is exposed to the solution, hydrogen evolution (Eq. 1-16) occurs (Reboul, et al., 1997; Tak et al., 2006).

$$Al_{(s)} + HCl_{(aq)} = AlCl_{3(aq)} + H_{2(g)} \quad (1\text{-}16)$$

In addition to Al_2O_3 removal, Cl^- enhances cementation reaction by increasing the exchange current density and preventing passivation of Al surface (Hong et al., 2014; Vasil'ev et al., 2010).

Effects of Cl^- concentration on the cementation using Al^0 has been investigated in many studies. Annamalai et al. (1978) investigated the effect of Cl^- concentration on Cu ion cementation using Al^0. They showed that the specific rate constant of cementation increased as the concentration of Cl^- increased up to 25 mg/L and then maintained a constant value above 25 mg/L, suggesting that a small amount of Cl^- is enough to remove Al_2O_3 layer. The different sources of Cl^- (e.g., KCl, NaCl, $AlCl_3 \cdot 6H_2O$, $CuCl_2 \cdot 2H_2O$, and HCl) have not significantly affected the Cu ion cementation using Al^0 (Annamalai and Murr, 1978; Wei et al., 1994).

Cementation of valuable metal ions from hydrochloric leaching solutions using Al^0 has been investigated by many researchers (e.g., Ag and Pb recovery from zinc leaching residue; In and Sn recovery from indium tin oxide) (Farahmand et al., 2009; Hong et al., 2014; Lee et al., 2014; Raghavan et al., 1998). In this case, further addition of Cl^- is not required, so there is an advantage that cementation using Al^0 can be used immediately as a follow-up process after leaching. Table 1-3 is the list of cementation research using Al^0 on the effects of Cl^-.

Table 1-3 A list of studies on the cementation of metal ions using Al^0 on the effects of Cl^-.

Year	Aluminum type	Target metal ions	pH	Speed (min^{-1})	Time (min)	Cl^-	Temp. (°C)	Comment	Ref.
1978	Al disc (ø 2.22 cm, 99.99%)	Cu (100 mg/L)	2.5	1250	–	75 mg/L	50	Specific rate constant increased with increasing [Cl^-]	(Annamalai et al., 1978)
1978	Al disc (ø 2.22 cm, 99.99%)	Cu (100 mg/L)	2.5	1250	–	75 mg/L	40	Using different sources of Cl^-	(Annamalai and Murr, 1978)
1994	Al disc (ø 46.8 mm, –)	Cu (50–300 mg/L)	3	800	100	–	30	$AlCl_3 \cdot 6H_2O$ added to remove Al_2O_3	(Wei et al., 1994)
1996	Al powder (D_{50}: 70μm, >90.5%)	Hg (500 mg/L)	7	–	30	100 g/L	18	≒ 80%	(Anacleto and Carvalho, 1996)
2020	Al powder (0.4–0.45 μm, 99.8%)	In (6.83 g/L)	0.4	200	20	0.75 M	25	91.69% (in HCl) < 1% (in H_2SO_4 and HNO_3)	(Rahmawati and Liu, 2020)

Note: "–" means not reported.

Effects of other anions were also reported. Halogens like F^- and Br^- are also effective to enhance cementation using Al_0 as electron donor, while SO_4^{2-} did not enhance the cementation(Li et al., 2013). This is because that SO_4^{2-} inhibits the pitting corrosion by inducing rapid regeneration of the passive oxide layer on Al^0 surface (Li et al., 2013; Reboul, et al., 1997; Rudd and Scully, 1980; Tak et al., 2006).

- Effects of morphology of cemented metal

There is a strong relationship between the morphology of cemented metal when using Al^0 as electron donor and cementation rate. A featherlike dendrite-type precipitate was observed when cementation rate was high, while a bulbous-type precipitate was observed when the rate was low (Annamalai et al., 1978; Chen and Lee, 1994; Li et al., 2013; Wei et al., 1994). Specific surface area is larger with a featherlike dendrite-type precipitate than with a bulbous-type precipitate (Chen and Lee, 1994; Hong et al., 2014). This surface area difference may cause mass transfer rate, which is an important factor to determine cementation rate.

- Effects of chelating agent

Chelating agents for heavy metal ions (Fu and Wang, 2011; O'Connell et al., 2008) affect the efficiency of cementation using Al^0 in aqueous solutions. Chen and Lee (1994) investigated the effects of chelating agents such as EDTA, NTA, and citrate on Cu ions cementation using Al disc. The specific rate constant depended on the type of chelating agent: the rate increased with citrate, while decreased with EDTA and NTA. When Al_2O_3 layer is removed at low pH, citrate can enhance the cementation efficiency by precipitating a fine dendrite-type precipitate, but it acts as an inhibitor of Al_2O_3 layer removal from chloride solution due to competitive adsorption with Cl^- (Rudd and Scully, 1980; Toujas et al., 2017). Wei et al. (1994) studied the effects of EDTA concentration on Cu ions cementation using Al disc, and they demonstrated that the specific rate constant decreased with increasing EDTA concentration based on the calculation of kinetic model and surface analysis results. In the presence of NTA or EDTA, the cementation rate decreased because diffusion and reduction of metal ions were inhibited by stable chelated species (Chen and Lee, 1994).

1.2.3 New cementation techniques using Al and AC

As mentioned earlier, the presence of Al_2O_3 layer on Al^0 surface suppresses cementation reaction by inhibiting electron transfer from Al^0 to metal ions. Many researchers have been studied removal of Al_2O_3 layer to enhance cementation. Recently, Jeon et al. (2020) reported a new cementation technique using Al and AC for the recovery of Au-thiosulfate complex from the ammonium thiosulfate solution. They conducted cementation experiments under the following conditions: 0.15 g of Al and/or 0.15 g of AC in the 10 ml of ammonium thiosulfate solutions (i.e., pH: 9–10, 100 mg/L Au ions, 1 M $Na_2S_2O_3$, 0.5 M NH_3, 0.25 M $(NH_4)_2SO_4$, and 10 mM $CuSO_4$) at 25 °C for 24 h. Without AC the recovery of Au from the solution was negligible. With AC, the cementation efficiency of Au was significantly enhanced. Based on the surface analysis results, they suggested a possible mechanism as follow: Al acts as an electron donor (i.e., anode) and AC attached to Al surface served as an electron mediator (i.e., cathode) from Al to Au-thiosulfate complex despite the presence of Al_2O_3 layer, thereby promoting Au recovery.

1.3 Outline of the dissertation

The dissertation consists of six chapters. The key contents of each chapter are as follows:

Chapter 1 gives the general background, objectives of this study, and literature reviews on cementation using Al.

Chapter 2 investigates the effects of AC addition on the cementation of Cd^{2+}, Co^{2+}, Ni^{2+}, and Zn^{2+} from sulfate solutions using Al powder as an electron donor, and mechanisms are detailed based on surface analysis and electrochemical experiments.

Chapter 3 investigates the effects of AC addition in the absence of Al_2O_3 layer on the cementation of Pb^{2+}, Cd^{2+}, Co^{2+}, Ni^{2+}, and Zn^{2+} from chloride solutions using Al powder as an electron donor. Suppression and enhancement cementation of different metal species are discussed based on surface analysis and electrochemical experiments.

Chapter 4 examines TiO_2 and SiO_2 as alternative electron mediators to AC for Co^{2+} and Ni^{2+} cementation using Al powder.

Chapter 5 investigates Cd^{2+} and Zn^{2+} cementation from sulfate solution using Al powder as an electron donor and Fe_3O_4 as electron mediator and proposes detailed mechanisms by electrochemical experiments and surface analysis. The effect of magnetic separation for cementation products is studied to separate cemented Cd and Zn in magnetic fractions.

Chapter 6 gives the summary and general conclusion of this dissertation.

References

Abdel-Aziz, M.H., El-Ashtoukhy, E.S.Z., Bassyouni, M., 2016. Recovery of Copper from Effluents by Cementation on Aluminum in a Multirotating Cylinder-Agitated Vessel. Metall. Mater. Trans. B Process Metall. Mater. Process. Sci. 47, 657–665. https://doi.org/10.1007/s11663-015-0467-y

Abdollahi, P., Yoozbashizadeh, H., Moradkhani, D., Behnian, D., 2015. A Study on Cementation Process of Lead from Brine Leaching Solution by Aluminum Powder. OALib 02, 1–6. https://doi.org/10.4236/oalib.1100990

Anacleto, A.L., Carvalho, J.R., 1996. Mercury cementation from chloride solutions using iron, zinc and aluminium. Miner. Eng. 9, 385–397. https://doi.org/10.1016/0892-6875(96)00025-8

Annamalai, V., Hiskey, J.B., Murr, L.E., 1978. The effects of kinetic variables on the structure of copper

deposits cemented on pure aluminum discs: A scanning electron microscopic study. Hydrometallurgy 3, 163–180. https://doi.org/10.1016/0304-386X(78)90018-X

Annamalai, V., Murr, L.E., 1978. Effects of the source of chloride ion and surface corrosion patterns on the kinetics of the copper-aluminum cementation system. Hydrometallurgy 3, 249–263. https://doi.org/10.1016/0304-386X(78)90026-9

Arima, H., Fujita, T., Yen, W.T., 2002. Gold cementation from ammonium thiosulfate solution by zinc, copper and aluminium powders. Mater. Trans. 43, 485–493. https://doi.org/10.2320/matertrans.43.485

Beyene, B.B., Mane, S.B., Hung, C.H., 2018. Electrochemical Hydrogen Evolution by Cobalt (II) Porphyrins: Effects of Ligand Modification on Catalytica Activity, Efficiency and Overpotential. J. Electrochem. Soc. 165, H481–H487. https://doi.org/10.1149/2.0481809jes

Bi, Z., Li, K., Jiang, C., Zhang, J., Ma, S., Sun, M., Wang, Z., Li, H., 2021. Performance and transition mechanism from acidity to basicity of amphoteric oxides (Al2O3 and B2O3) in SiO2–CaO–Al2O3–B2O3 system: A molecular dynamics study. Ceram. Int. 47, 12252–12260. https://doi.org/10.1016/j.ceramint.2021.01.074

Brevnov, D.A., Olson, T.S., López, G.P., Atanassov, P., 2004. Electroless deposition of silver by galvanic displacement on aluminum alloyed with copper. J. Phys. Chem. B 108, 17531–17536. https://doi.org/10.1021/jp047096u

Brouwers, H.J.H., Eijk, R.J. Van, 2003. Chemical Reaction of Fly Ash. 11th Int. Congr. Chem. Cem. 791–800.

Chen, H.J., Lee, C., 1994. Effects of the Type of Chelating Agent and Deposit Morphology on the Kinetics of the Copper-Aluminum Cementation System. Langmuir 10, 3880–3886. https://doi.org/10.1021/la00022a079

Demirkran, N., Künkül, A., 2011. Recovering of copper with metallic aluminum. Trans. Nonferrous Met. Soc. China (English Ed. 21, 2778–2782. https://doi.org/10.1016/S1003-6326(11)61123-0

Djokić, S.S., 1996. Cementation of Copper on Aluminum in Alkaline Solutions. J. Electrochem. Soc. 143, 1300–1305. https://doi.org/10.1149/1.1836634

Dönmez, B., Sevim, F., Saraç, H., 1999. Kinetic study of the cementation of copper from sulphate solutions onto a rotating aluminum disc. Hydrometallurgy 53, 145–154. https://doi.org/10.1016/S0304-386X(99)00042-0

Ekmekyapar, A., Tanaydin, M., Demirkiran, N., 2012. Investigation of copper cementation kinetics by

rotating aluminum disc from the leach solutions containing copperions. Physicochem. Probl. Miner. Process. 48, 355–367. https://doi.org/10.5277/ppmp120203

Ezaki, H., Morinaga, M., Watanabe, S., 1993. Hydrogen overpotential for transition metals and alloys, and its interpretation using an electronic model. Electrochim. Acta 38, 557–564. https://doi.org/10.1016/0013-4686(93)85012-N

Farahmand, F., Moradkhani, D., Sadegh Safarzadeh, M., Rashchi, F., 2009. Optimization and kinetics of the cementation of lead with aluminum powder. Hydrometallurgy 98, 81–85. https://doi.org/10.1016/j.hydromet.2009.04.001

Fu, F., Wang, Q., 2011. Removal of heavy metal ions from wastewaters: A review. J. Environ. Manage. 92, 407–418. https://doi.org/10.1016/j.jenvman.2010.11.011

Hong, H.S., Kim, G.H., Hong, M.H., Lee, S., Lee, J.C., 2014. Indium ion cementation onto aluminum plates in hydrochloric acid solutions: A kinetic perspective. Int. J. Mater. Res. 105, 177–182. https://doi.org/10.3139/146.111004

Jeon, S., Tabelin, C.B., Takahashi, H., Park, I., Ito, M., Hiroyoshi, N., 2020. Enhanced cementation of gold via galvanic interactions using activated carbon and zero-valent aluminum: A novel approach to recover gold ions from ammonium thiosulfate medium. Hydrometallurgy 191, 105165. https://doi.org/10.1016/j.hydromet.2019.105165

Karavasteva, M., 2009. The effect of nonylphenylpolyethylene glycol on the kinetics and morphology of silver cemented using zinc, iron, copper and aluminum. Hydrometallurgy 95, 337–340. https://doi.org/10.1016/j.hydromet.2008.07.005

Karavasteva, M., 2005. Kinetics and deposit morphology of copper cementation onto zinc, iron and aluminium. Hydrometallurgy 76, 149–152. https://doi.org/10.1016/j.hydromet.2004.10.003

Kim, M.-S., Kim, B.-S., Kim, E.-Y., Kim, S.-K., Ryu, J.-W., Lee, J.-C., 2011. Recovery of Platinum Group Metals from the Leach Solution of Spent Automotive Catalysts by Cementation. J. Korean Inst. Resour. Recycl. https://doi.org/10.7844/kirr.2011.20.4.036

Ku, Y., Chen, C.H., 1992. Kinetic Study of Copper Deposition on Iron by Cementation Reaction. Sep. Sci. Technol. 27, 1259–1275. https://doi.org/10.1080/01496399208019424

Lee, H.Y., Kim, S.G., Oh, J.K., 1997. Cementation behavior of gold and silver onto Zn, Al, and Fe powders from acid thiourea solutions. Can. Metall. Q. 36, 149–155. https://doi.org/10.1179/cmq.1997.36.3.149

Lee, S., Kim, G.H., Ryu, S.S., Hong, H.S., 2014. Recovery of indium powders from indium chloride

solutions by cementation. Can. Metall. Q. 53, 232–239. https://doi.org/10.1179/1879139513Y.0000000122

Lee, S.S., Schmidt, M., Sturchio, N.C., Nagy, K.L., Fenter, P., 2019. Effect of pH on the Formation of Gibbsite-Layer Films at the Muscovite (001)-Water Interface. J. Phys. Chem. C 123, 6560–6571. https://doi.org/10.1021/acs.jpcc.8b12122

Li, W., Cochell, T., Manthiram, A., 2013. Activation of aluminum as an effective reducing agent by pitting corrosion for wet-chemical synthesis. Sci. Rep. 3, 1–7. https://doi.org/10.1038/srep01229

MacKinnon, D.J., Ingraham, T.R., 1971. Copper cementation on aluminum canning sheet. Can. Metall. Q. 10, 197–201. https://doi.org/10.1179/cmq.1971.10.3.197

MacKinnon, D.J., Ingraham, T.R., 1970. Kinetics of Cu(ll) cementation on a pure aluminum disc in acidic sulphate solutions. Can. Metall. Q. 9, 443–448. https://doi.org/10.1179/cmq.1970.9.3.443

Malik, F., 1991. A study of passive films on valve metals. Thin Solid Films 206, 345–348. https://doi.org/10.1016/0040-6090(91)90448-7

May, H.M., Helmke, P.A., Jackson, M.L., 1979. Gibbsite solubility and thermodynamic properties of hydroxy-aluminum ions in aqueous solution at 25°C. Geochim. Cosmochim. Acta 43, 861–868. https://doi.org/10.1016/0016-7037(79)90224-2

McCafferty, E., 2003. Sequence of steps in the pitting of aluminum by chloride ions. Corros. Sci. 45, 1421–1438. https://doi.org/10.1016/S0010-938X(02)00231-7

Mendibide, C., Dusquesnes, V., Deydier, V., Bourbon, X., Crusset, D., 2021. Corrosion behavior of aluminum alloy 5754 in cement-based matrix-simulating nuclear waste disposal conditions. Mater. Corros. 72, 383–395. https://doi.org/10.1002/maco.202011687

Murr, L.E., Annamalai, V., 1978a. Characterization of copper nucleation and growth from aqueous solution on aluminum: A transmission electron microscopy study of copper cementation. Thin Solid Films 54, 189–195. https://doi.org/10.1016/0040-6090(78)90198-0

Murr, L.E., Annamalai, V., 1978b. An Electron Microscopic Study of Nucleation and Growth in Electrochemical Displacement Reactions: A Comparison of the Cu/Fe and Cu/AI Cementation Systems. Metall. Trans. B 9, 515–525. https://doi.org/10.1007/BF03257198

Natishan, P.M., O'Grady, W.E., 2014. Chloride Ion Interactions with Oxide-Covered Aluminum Leading to Pitting Corrosion: A Review. J. Electrochem. Soc. 161, C421–C432. https://doi.org/10.1149/2.1011409jes

Nelson, A., Wang, W., Demopoulos, G.P., Houlachi, G., 2000. Removal of cobalt from zinc electrolyte by cementation: A critical review. Miner. Process. Extr. Metall. Rev. 20, 325–356. https://doi.org/10.1080/08827500008547436

O'Connell, D.W., Birkinshaw, C., O'Dwyer, T.F., 2008. Heavy metal adsorbents prepared from the modification of cellulose: A review. Bioresour. Technol. 99, 6709–6724. https://doi.org/10.1016/j.biortech.2008.01.036

Park, I., Tabelin, C.B., Seno, K., Jeon, S., Inano, H., Ito, M., Hiroyoshi, N., 2020. Carrier-microencapsulation of arsenopyrite using Al-catecholate complex: nature of oxidation products, effects on anodic and cathodic reactions, and coating stability under simulated weathering conditions. Heliyon 6, e03189. https://doi.org/10.1016/j.heliyon.2020.e03189

Park, I., Tabelin, C.B., Seno, K., Jeon, S., Ito, M., Hiroyoshi, N., 2018. Simultaneous suppression of acid mine drainage formation and arsenic release by Carrier-microencapsulation using aluminum-catecholate complexes. Chemosphere 205, 414–425. https://doi.org/10.1016/j.chemosphere.2018.04.088

Poinern, G.E.J., Ali, N., Fawcett, D., 2010. Progress in nano-engineered anodic aluminum oxide membrane development, Materials. https://doi.org/10.3390/ma4030487

Raghavan, R., Mohanan, P.K., Patnaik, S.C., 1998. Innovative processing technique to produce zinc concentrate from zinc leach residue with simultaneous recovery of lead and silver. Hydrometallurgy 48, 225–237. https://doi.org/10.1016/S0304-386X(97)00082-0

Rahmawati, A., Liu, J.C., 2020. Recovery of indium from extractants of waste indium tin oxide (ITO) by aluminum cementation. J. Mater. Cycles Waste Manag. 22, 326–332. https://doi.org/10.1007/s10163-019-00916-3

Reboul, M.C., Warner, T.J., Mayer, H., Barouk, B., 1997. A Ten Step Mechanism for the Pitting Corrosion of Aluminium Alloys. Corros. Rev. 15, 471–496. https://doi.org/10.1515/CORRREV.1997.15.3-4.471

Rudd, W.J., Scully, J.C., 1980. The function of the repassivation process in the inhibition of pitting corrosion on aluminium. Corros. Sci. 20, 611–631. https://doi.org/10.1016/0010-938X(80)90098-0

Sarker, M.S.R., Alam, M.Z., Qadir, M.R., Gafur, M.A., Moniruzzaman, M., 2015. Extraction and characterization of alumina nanopowders from aluminum dross by acid dissolution process. Int. J. Miner. Metall. Mater. 22, 429–436. https://doi.org/10.1007/s12613-015-1090-2

Seng, S., Tabelin, C.B., Kojima, M., Hiroyoshi, N., Ito, M., 2019. Galvanic microencapsulation (GME)

using zero-valent aluminum and zero-valent iron to suppress pyrite oxidation. Mater. Trans. 60, 277–286. https://doi.org/10.2320/matertrans.M-M2018851

Strohmeier, B.R., 1990. An ESCA method for determining the oxide thickness on aluminum alloys. Surf. Interface Anal. 15, 51–56. https://doi.org/10.1002/sia.740150109

Stubblebine, M.J., Yao, Q., Supowit, J., Catton, I., 2016. A new method for evaluating heat pipe fluid compatibility. Appl. Therm. Eng. 101, 796–803. https://doi.org/10.1016/j.applthermaleng.2016.04.020

Tak, Y., Kang, J., Choi, J., 2006. Electrochemical Properties of Metal Aluminum and Its Application. J. Korean Ind. Eng. Chem. 17, 335–342.

Takahashi, H., Sakairi, M., Kikuchi, T., 2009. Anodic Oxide Films on Aluminum: Their Significance for Corrosion Protection and Micro- and Nano-Technologies. https://doi.org/10.1007/978-0-387-92263-8_2

Tossell, J.A., 1999. Theoretical studies on aluminate and sodium aluminate species in models for aqueous solution: A1(OH)3, Al(OH)4-, and NaAl(OH)4. Am. Mineral. 84, 1641–1649. https://doi.org/10.2138/am-1999-1019

Toujas, S., Vázquez, M., Valcarce, M.B., 2017. Unexpected effect of citrate ions on the corrosion process of carbon steel in alkaline solutions. Corros. Sci. 128, 94–99. https://doi.org/10.1016/j.corsci.2017.08.018

Uhlig, H.H., Revie, R.W., 1985. Corrosion and corrosion control: and introduction of corrosion science and engineering, 4th ed. A john wiley & sons, New York.

Vasil'ev, E.A., Darintseva, A.B., Naboichenko, S.S., 2010. Experimental investigations of cementation of indium. Russ. J. Non-Ferrous Met. 51, 268–272. https://doi.org/10.3103/S1067821210040024

Wang, Z., Chen, D., Chen, L., 2007. Application of fluoride to enhance aluminum cementation of gold from acidic thiocyanate solution. Hydrometallurgy 89, 196–206. https://doi.org/10.1016/j.hydromet.2007.07.005

Wei, W.Y., Lee, C., Chen, H.J., 1994. Modeling and Analysis of the Cementation Process on a Rotating Disk. Langmuir 10, 1980–1986. https://doi.org/10.1021/la00018a058

Xhanari, K., Finšgar, M., 2019. Organic corrosion inhibitors for aluminum and its alloys in chloride and alkaline solutions: A review. Arab. J. Chem. 12, 4646–4663. https://doi.org/10.1016/j.arabjc.2016.08.009

Yu, S.Y., O'Grady, W.E., Ramaker, D.E., Natishan, P.M., 2000. Chloride Ingress into Aluminum Prior to Pitting Corrosion An Investigation by XANES and XPS. J. Electrochem. Soc. 147, 2952. https://doi.org/10.1149/1.1393630

Zähr, J., Oswald, S., Türpe, M., Ullrich, H.J., Füssel, U., 2012. Characterisation of oxide and hydroxide layers on technical aluminum materials using XPS. Vacuum 86, 1216–1219. https://doi.org/10.1016/j.vacuum.2011.04.004

CHAPTER 2 – Enhanced cementation of Cd^{2+}, Co^{2+}, Ni^{2+}, and Zn^{2+} with aluminum from sulfate solutions by the addition of activated carbon as electron mediator

2.1 Introduction

Cementation is an electrochemical reduction process usually used in the hydrometallurgical industry to recover or remove dissolved metal ions (Nelson et al., 2000). This reaction spontaneously proceeds via the difference in the standard reduction potentials, and more noble metal ions are reductively cemented on the surface of reductant metal (i.e., electron donors) in the same aqueous system. The overall cementation reaction is described by the following equation (Abdel-Aziz et al., 2016; Dönmez et al., 1999; Gouvea and Morais, 2007; Hsu and Tran, 1996; Navarro et al., 2004):

$$n\,A^{0}{}_{(s)} + m\,B^{b+}{}_{(aq)} = n\,A^{a+}{}_{(aq)} + m\,B^{0}{}_{(s)} \qquad (na = mb) \qquad (2\text{-}1)$$

where A and B represent the reductant and target metals, respectively.

Equation 2-1 can be divided further into two half-cell reactions as follows:

$$\text{anodic reaction: } n\,A^{0} \rightarrow n\,A^{a+} + na\,e^{-} \qquad (2\text{-}2)$$

$$\text{cathodic reaction: } m\,B^{b+} + mb\,e^{-} \rightarrow m\,B^{0} \qquad (2\text{-}3)$$

The anodic reaction (Eq. 2-2) represents the oxidative dissolution of reductant (A^0) while the cathodic reaction (Eq. 2-3) refers to the cementation of target metal ion B^{b+} on the reductant.

Various cementation systems using low electrode potential reductants such as iron ($E^0_{Fe2+/Fe}$ = –0.45 V vs. SHE), zinc ($E^0_{Zn2+/Zn}$ = –0.76 V vs. SHE), and aluminum ($E^0_{Al3+/Al}$= –1.67 V vs. SHE) have been studied (Boyanov et al., 2004; Choi et al., 2020; Jeon et al., 2020b; Ku and Chen, 1992; Makhloufi et al., 2000; Silwamba et al., 2020b, 2020a; Tables et al., 2018). Among them, Al^0 is theoretically considered as a promising electron donor because of its low standard electrode potential, which makes it possible to recover almost all metal ions; however, its application is limited due to the presence of dense insulating aluminum oxide (Al_2O_3) layer inhibiting electron transfer from Al^0 to metal ions (Anacleto and Carvalho, 1996; Annamalai and Murr, 1978; Choi et al., 2021; Li et al., 2013a; Murr and Annamalai, 1978a, 1978b). When the Al oxide layer is removed from the surface, Al can be used as an electron donor for cementation. To remove the Al oxide layer, however, high temperatures, acid/alkaline solutions, or high concentration of chloride ions are needed (Demirkran and Künkül, 2011; Djokić, 1996; Ekmekyapar et al., 2012; Farahmand et al., 2009; Li et al., 2013a), and these extreme conditions make it difficult to use Al as an electron donor in the practical cementation processes.

Recently, Jeon et al. (2020b) investigated the effects of activated carbon (AC) addition on the

efficiency of cementation using Al as an electron donor for recovering gold ions from ammonium thiosulfate solution (Jeon et al., 2020a, 2020b). The results showed that cementation efficiencies of the metal ions were significantly enhanced by the addition of activated carbon (AC) even when an insulating Al oxide layer covered on the Al surface (Jeon et al., 2020a, 2020b). This "enhanced cementation using AC/Al-mixture" can be operated under mild conditions; i.e., it does not require extreme operating conditions such as high temperatures, and high concentrations of chemical reagents such as acid, base, and chloride ions. This new method may, therefore, provide a practical way to use Al, one of the strongest reductants (electron donor) for cementation to recover metal ions from dilute solutions.

In this chapter, enhanced cementation using AC/Al-mixture was investigated to recover/remove heavy metal ions other than gold ions under mild conditions. Batch-type experiments were conducted to investigate the applicability of "AC/Al-cementation" for the recovery/removal of cadmium (Cd), cobalt (Co), nickel (Ni), and zinc (Zn) from sulfate solutions. These heavy metals were selected not only because they are challenging to remove by conventional neutralization-precipitation strategies but also due to their emerging importance in batteries and renewable energy technologies (Bernhoft, 2013; Choi et al., 2020; Douglas. S. Flett, 2004; Gupta et al., 1997; Lupi and Pasquali, 2003; Peeters et al., 2020; Silwamba et al., 2020b; Tabelin et al., 2021; Zhang et al., 1998). In addition, these heavy metals have different hydrogen overpotentials (higher overpotentials with Cd^{2+} and Zn^{2+}, and lower overpotentials with Co^{2+} and Ni^{2+}) (Beyene et al., 2018; Ezaki et al., 1993; Hickling and Salt, 1940; Uhlig and Revie, 1985), which can advance our understanding of how hydrogen overpotential affects cementation.

2.2 Materials and methods

2.2.1 Aluminum and activated carbon

As an electron donor, Al powder (99.99%, Wako Pure Chemical Industries, Ltd., Osaka, Japan) was used, and AC powder (99.99%, Wako Pure Chemical Industries, Ltd., Osaka, Japan) was used as an electron mediator. Particle size distribution of these materials, measured by laser diffraction (Microtrac® MT3300SX, Nikkiso Co. Ltd., Osaka, Japan), is shown in Fig. 2-1. The median diameters (D_{50}) of Al and AC were 21.3 and 38.1 μm, respectively.

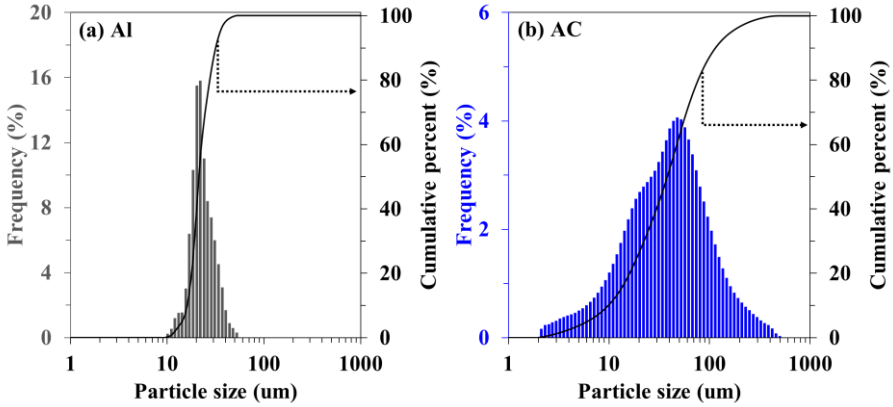


Fig. 2-1 Particle size distribution for (a) aluminum and (b) activated carbon used in this chapter.

2.2.2 Cementation methods

When Sulfate solutions containing 1 mM Cd^{2+}, Co^{2+}, Ni^{2+}, or Zn^{2+} were prepared by dissolving $CdSO_4 \cdot nH_2O$ (99.5%, Wako Pure Chemical Industries, Ltd., Japan), $CoSO_4 \cdot 7H_2O$ (99.0%, Wako Pure Chemical Industries, Ltd., Japan), $NiSO_4 \cdot 6H_2O$ (99.0%, Wako Pure Chemical Industries, Ltd., Japan), or $ZnSO_4 \cdot 7H_2O$ (99.5%, Wako Pure Chemical Industries, Ltd., Japan) in deionized (DI) water (18 MΩ·cm, Mill-Q® Integral Water Purification System, Merck Millipore, USA). The initial pH was adjusted using 1 M H_2SO_4 (Wako Pure Chemical Industries, Ltd., Japan). Total SO_4^{2-} concentration was fixed to 0.1 M using Na_2SO_4 (99.0%, Wako Pure Chemical Industries, Ltd., Japan) to normalize the effects of this anion on cementation.

To investigate the removal/recovery efficiency of heavy metal ions from sulfate solutions, 10 mL of prepared solution (initial pH of 1, 2, 3, 4, and 5) was poured into a 50-mL Erlenmeyer flask and then purged with ultrapure N_2 (99.9%) for 15 min to remove dissolved oxygen. Afterward, 0.1 g of Al and/or 0.1 g of AC was introduced into the flask and then re-purged with ultrapure N_2 for 5 min. After this, the flask was tightly capped with a rubber stopper and parafilm, and shaken at 25 °C for 24 h in a thermostat water bath shaker (Cool bath shaker, ML-10F, Taitec Corporation, Japan) with 40 mm of shaking amplitude and 120 min^{-1} of shaking frequency (Note that these parameters were selected based on our preliminary experiments). At pre-determined time intervals, flasks were collected from the shaker and the final pH of suspensions was measured. The suspensions were then filtered through syringe-driven membrane filters (pore size: 0.2 μm, LMS Co., Ltd., Japan), and the filtrates were immediately diluted with 0.1 M HNO_3. The concentrations of metal ions in the filtrates were analyzed using inductively coupled plasma atomic emission spectroscopy (ICP-AES, ICPE-9820, Shimadzu Corporation, Japan) (margin of error = ±2%) and removal/recovery efficiency (R) was calculated according to the following equation:

$$R = \frac{C_i - C_f}{C_i} \, x \, 100 \quad (2\text{-}4)$$

where C_i and C_f are the initial and final concentrations of metal ions, respectively. The amount of metal ion removed per unit mass from solution (q) was also calculated as follows:

$$q = \frac{(C_i - C_f)V}{m} \quad (2\text{-}5)$$

where q is the amount of metal ion removed per unit mass (mg/g), V is a volume of solution (L), and m is the mass of Al (g) and/or AC (g) used. When an AC/Al-mixture was used, m is the combined masses of AC (0.1 g) and Al (0.1 g).

2.2.3 Surface analysis

The cementation products were collected by vacuum filtration (pore size: 0.2 μm, Merck Millipore, USA), washed thoroughly with DI water, dried in a vacuum oven at 40 °C for 24 h, and then analyzed by scanning electron microscopy with energy-dispersive X-ray spectroscopy (SEM-EDS, JSM-IT200^{TM}, JEOL Co., Ltd., Japan), X-ray photoelectron spectroscopy (XPS, JPS-9200, JEOL Co., Ltd., Japan) and auger electron spectroscopy (AES, JAMP-9500F, JEOL Co., Ltd., Japan). The XPS analysis was conducted using a monochromatized Al Kα X-ray source (hv = 1486.6 eV) operated at 100 W (voltage: 10 kV; current: 10 mA) under ultra-high vacuum (~10^{-7} Pa). All spectra were calibrated and corrected using the C1s binding energy of adventitious carbon (284.0 eV). Background subtraction and curve fitting were done using the SPECSURF analysis software by applying a true Shirley background and 80%–20% Gaussian–Lorentzian curve fitting model (Park et al., 2021; Shirley, 1972). Auger electron spectroscopy (AES) analysis was conducted under a pressure of less than 10^{-7} Pa, probe energy of 10 kV, and probe current of 19.7 nA. The spectra were then analyzed using Spectra Investigator AES software.

2.2.4 Electrochemical measurements

2.2.4.1 Linear sweep voltammetry (LSV)

To understand reduction reactions of Cd^{2+} on the surfaces of Al and AC/Al, linear sweep voltammetry was carried out using a potentiostat (SP-300, Biologic, France) with a conventional three-electrode system. For this, Al rod (99.999 %, 10 mm φ; AL-012651, Nilaco Corp.), Ag/AgCl electrode filled with saturated KCl, and platinum (Pt) electrode were used as working, reference, and counter electrodes, respectively. The Al working electrode was polished using wet 1200-grit silicon carbide papers using a polishing machine (Saphir 250 M1, ATM, Germany). After this, the electrode was

further ground using 1 μm diamond paste on a polishing cloth plate using the polishing machine, ultrasonically cleaned for 3 min in DI water to remove impurities on Al surface, and re-washed with DI water. After this, the Al working electrode was exposed to air to make Al_2O_3 layer on Al^0 surface for 7 days. The Al electrode with AC was prepared as follows: (1) AC was mixed with acetone and suspended by ultra-sonification, and (2) the acetone suspension was put on the whole surface of the polished Al electrode. The Al and AC/Al electrodes were used as a working electrode after the evaporation of acetone. Three electrodes were immersed into the prepared solution (e.g., pH 5 1 mM Cd^{2+} with 0.1 M SO_4^{2-} as a supporting electrolyte), deoxygenated by N_2 purging, and equilibrated at 25 °C for 30 min. After equilibration at the open circuit potential (OCP), LSV was measured starting from OCP to –1.2 V vs. Ag/AgCl at the scan rate of 10 mV/s.

2.3 Results and discussion

2.3.1 Removal of Cd^{2+}

2.3.1.1 Effects of pH

Figures 2-2(a), (b), and (c) show the Cd^{2+} removal efficiency, final pH, and Al concentration, respectively in sulfate solution using AC, Al, and AC/Al-mixtures at different initial pH for 24 h. When only AC was added, the removal efficiency was less than 4% at pH 1–3 and around 25% at pH 4–5. The Cd^{2+} removal by AC could be attributed to adsorption onto negatively charged surface functional groups like *n*(–COOH) as described in Eq. 2-6 (Ali et al., 2012; Dil et al., 2016; Gao et al., 2018; Gupta and Saleh, 2013; Iida et al., 2013; Kadirvelu et al., 2001; Karnib et al., 2014; Mar et al., 2013; Sulyman et al., 2017).

$$M^{n+} + n(\text{–COOH}) \leftrightarrow (\text{–COO})_n M + nH^+ \quad (2\text{-}6)$$

At low pH, surface functional groups on AC remains protonated (i.e., uncharged) because of the high H^+ concentration that limited Cd^{2+} removal by adsorption (Burakov et al., 2018; Gao et al., 2018; Iida et al., 2013; Kadirvelu et al., 2001; Karnib et al., 2014; Saleh and Gupta, 2014; Sulyman et al., 2017). As the pH is increased, these surface functional groups are deprotonated, become more negatively charged, and promote Cd^{2+} adsorption via electrostatic interactions (Eq. 2-6) (Burakov et al., 2018; Dil et al., 2016; Gupta et al., 2014, 2013, 2002; Nekouei et al., 2015).

The removal efficiency using only Al was even lower than AC at ~2% (pH 4–5), suggesting that cementation of Cd^{2+} on Al was negligible. Figures 2-3(a) and (b) illustrate the XPS spectra of Al before and after the Cd^{2+} removal experiments at pH 5, respectively. The Al $2p_{3/2}$ peaks were unchanged before and after the experiment with a binding energy of 72.6 eV from Al metal and of 75.6 eV from

Al oxide layer; that is, both Al and Al_2O_3 were present in the samples (Kaplowitz et al., 2014; Naumkin et al., 2012; Zähr et al., 2012). Before and after experiments, the Al metal and Al_2O_3 peaks have similar FWHM of around 1.2±0.1 and 0.7±0.1, respectively. The curve fitting results also showed that Al_2O_3 before the experiment was 84.5% and only slightly decreased to 83.5% after the experiments, which means that the insulating Al_2O_3 layer on Al was stable at pH 5. This deduction is supported by the activity-pH diagram for Al^{3+} in 0.1 M SO_4^{2-} predicting Al_2O_3 stability at pH 5 (Fig. 2-4(a)), the very low Al^{3+} concentrations (< 0.1 mg/L) measured at pH 5, and previous reports on Al_2O_3 solubility (Park et al., 2020; Tabelin et al., 2017a). At pH below 3, Al^{3+} concentration increased with decreasing initial pH (Figs. 2-2(c) and 2-4(a)), indicating that Al_2O_3 dissolved under strongly acidic conditions, then electron transfer from Al to Cd^{2+} could occur spontaneously due to standard redox potential differences between Cd^{2+}/Cd redox pair (–0.40 V vs. SHE) and Al^{3+}/Al redox pair (–1.67 V vs. SHE). This promoted Cd^{2+} reduction to elemental Cd (Cd^0) on Al as described in Eq. 2-7.

$$3\ Cd^{2+} + 2\ Al^0 \rightarrow 3\ Cd^0 + 2\ Al^{3+} \quad (2\text{-}7)$$

The final pH was also markedly higher at initial pH 2–3, which could be attributed to two phenomena: (1) buffering effects of Al_2O_3 (Tabelin et al., 2017b), and (2) H^+ consumption due to H_2 formation on Al (Eq. 2-8), which will be discussed in detail later.

$$2\ H^+ + 2\ e^- \rightarrow H_2 \quad (2\text{-}8)$$

When only AC was used, the increase in pH was smaller than the AC/Al-mixture, confirming that the pH increase was mainly due to the reaction of proton with Al or Al_2O_3. Slight increase of final pH was observed in the experiments with only AC, which could be attributed to protonation (i.e., H^+ adsorption) of AC surface functional groups as explained previously (Dil et al., 2016; Suhas et al., 2016).

In the case of AC/Al-mixture, Cd^{2+} removal efficiency increased to ~50% at pH 4–5, which were higher than either AC only or Al only. As noted earlier, Al was covered with Al_2O_3 at pH 4–5, so the enhanced removal of Cd^{2+} was likely because of electrochemical interactions between Al and AC, a phenomenon that will be discussed in more detail in the surface analysis section. Although Cd^{2+} removal via precipitation as Cd-hydroxide and/or carbonate is another possible mechanism, this can be neglected because the maximum final pH in the experiments was 5.1 where Cd^{2+} solubility remains high (Figs. 2-2(b) and 2-4(b); Tabelin et al., 2020b).

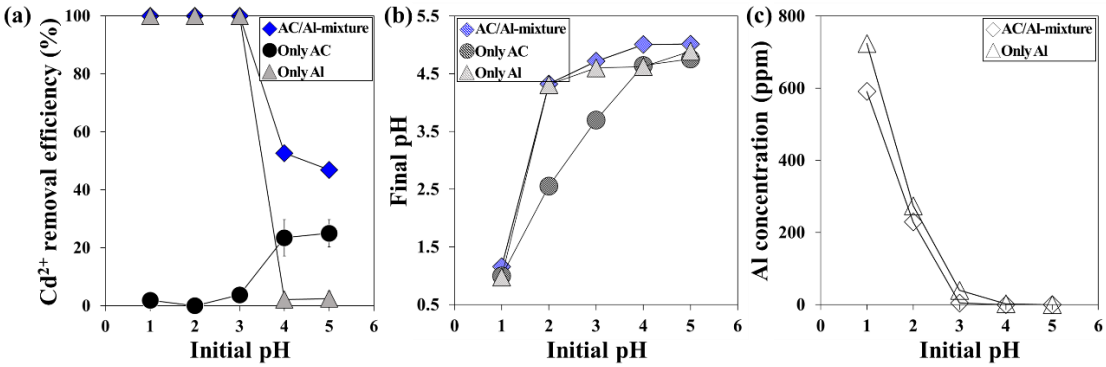


Fig. 2-2 (a) The Cd^{2+} removal efficiency, (b) final pH, and (b) Al^{3+} concentration in sulfate solutions at different pH for 24 h (Al = Al^0; AC = Activated carbon).

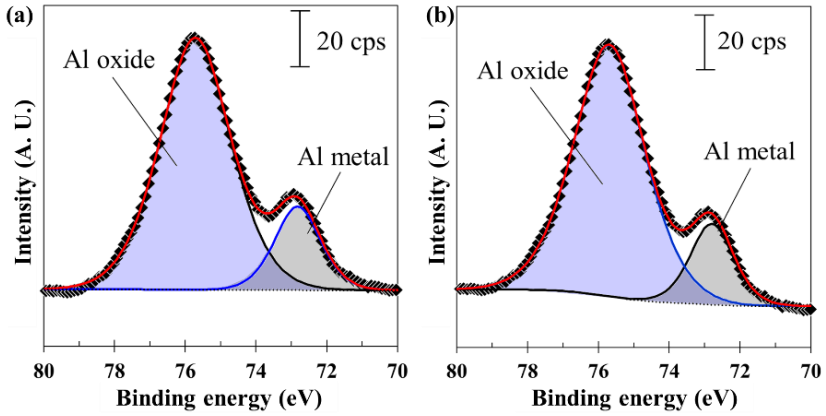


Fig. 2-3 XPS spectra of the Al $2p_{3/2}$ region: (a) after the experiment using only Al at pH 5 and (b) Al before the experiment.

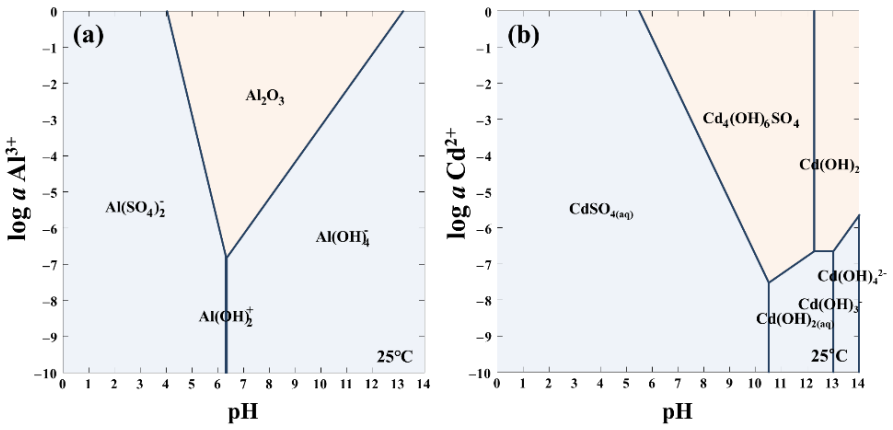


Fig. 2-4 The activity – pH diagram for (a) Al^{3+} and (b) Cd^{2+} in 0.1 M SO_4^{2-} (created using the GWB® Professional Ver. 12.0.3 software).

2.3.1.2 Effects of time

Figures 2-5(a) and (b) show the removal efficiency of Cd^{2+} and final pH in sulfate solution using AC, Al, and AC/Al-mixture as a function of time (initial pH: 5.0). When only Al was used, removal efficiencies were almost 0% regardless of the experiment duration. When only AC was added, Cd^{2+} removal efficiency reached 21% within 1 h, which remained unchanged until 24 h. The pH also decreased to 4.7 but stabilized quickly after just 1 h.

When both Al and AC were added, the removal efficiency increased to 21% after 1 h and increased continuously with time to reach 45% after 6 h. After 24 h, the amount of Cd^{2+} removed per unit mass of AC/Al-mixture was 2.1 mg/g (Eq. 2-5). Given that Cd^{2+} removal by Al was negligible, the increase in Cd^{2+} removal after 1 h cannot be explained by adsorption to AC only. These results suggest a synergistic interaction between AC and Al that enhanced Cd^{2+} removal in sulfate solution. During the experiments, the pH remained in the range of 4.8–5.1 regardless of Al and AC.

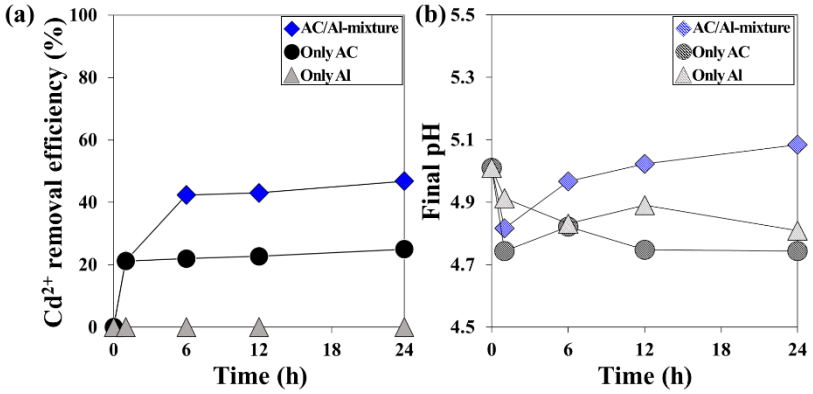


Fig. 2-5 (a) The removal efficiency of Cd^{2+} and (b) final pH in sulfate solutions at initial pH 5 for 24 h (Al = Al^0; AC = Activated carbon).

2.3.1.3 Surface analysis of Cd-bearing products

Figure 2-6 shows the SEM photomicrograph and EDS point analysis of cementation products obtained after Cd^{2+} removal experiments using AC/Al-mixture at pH 5 for 24 h. The SEM photomicrograph (BSE) has bright regions (e.g., Point 1) attached to a dark particle (Point 2). Based on the EDS spectra, Al was the major component detected in Point 2 while in Point 1, Al and O peaks were detected together with Cd and C peaks. These results suggest that Cd was likely deposited on AC rather than on Al.

Figure 2-7 shows the XPS spectra of Cd 3d, Al $2p_{3/2}$, and O 1s of cementation products obtained after Cd^{2+} removal experiments using AC/Al-mixture at pH 5 after 24 h. The XPS spectrum of Cd 3d with fitted Gaussian-Lorentzian models is shown in Fig. 2-7(a). The spin-orbit splitting components—

main Cd $3d_{5/2}$ and spin-orbit Cd $3d_{3/2}$—in Cd 3d peak appeared at 405.0 eV and 411.8 eV (Fig. 2-7(a)). The measured difference between the Cd $3d_{5/2}$ and Cd $3d_{3/2}$ was 6.8 eV, which is consistent with reported values for Cd binding energy separation (Li et al., 2013b; Marychurch and Morris, 1985). The peak detected at 405.1 eV (Cd $3d_{5/2}$) corresponded to Cd^0, which means that Cd^{2+} was removed via cementation. CdO formation was also implied by the binding energy (B.E.) at 404.2 eV, and the formation of CdO was also corroborated by O 1s spectrum (Fig. 2-7(c)) (Naumkin et al., 2012). Direct CdO precipitation around pH 5 is thermodynamically unfavorable (Tabelin et al., 2020b), so its formation was likely the consequence of Cd^0 oxidation during drying of products before the XPS analysis. The spectrum of Al 2p3/2 (Fig. 2-7(b)) and O 1s (Fig. 2-7(c)) identified peaks of Al_2O_3 at binding energies of 74.1 eV and 531.2 eV, and $Al(OH)_3$ peaks at binding energies of 74.9 eV and 532.3 eV (Figs. 2-7(b) and (c)) (Fang et al., 2013; He et al., 1993; Kloprogge et al., 2006; Maslakov et al., 2012; Park et al., 2020; Shi et al., 2013). This means that the enhanced cementation of Cd^{2+} using AC/Al-mixture occurred via Al_2O_3 layer on Al surface. Dissolved Al^{3+} were not observed after cementation experiments (Fig. 2-2(c)), which indicates that dissolved Al^{3+} (Eq. 2-7) precipitated on the Al surface as hydroxide form due to the high pH (Fig. 2-2(b)).

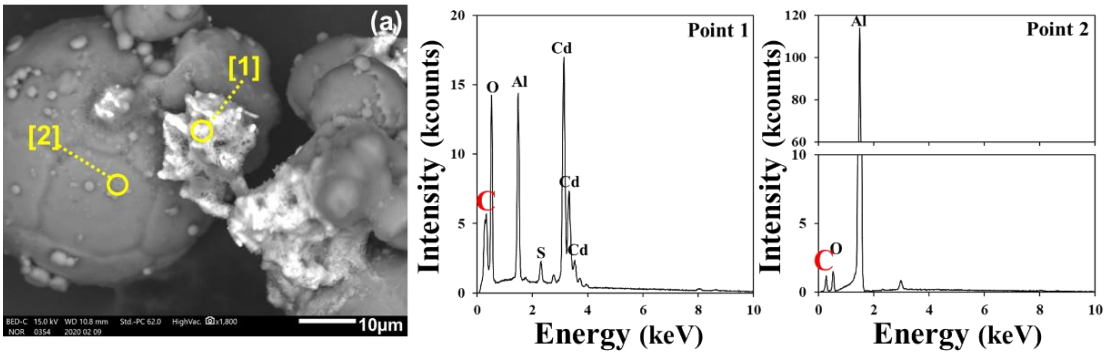


Fig. 2-6 SEM photomicrograph of (a) cementation products using AC/Al-mixture in 1 mM cadmium sulfate solution at pH 5.0 and EDS point analysis of each point (1 and 2).

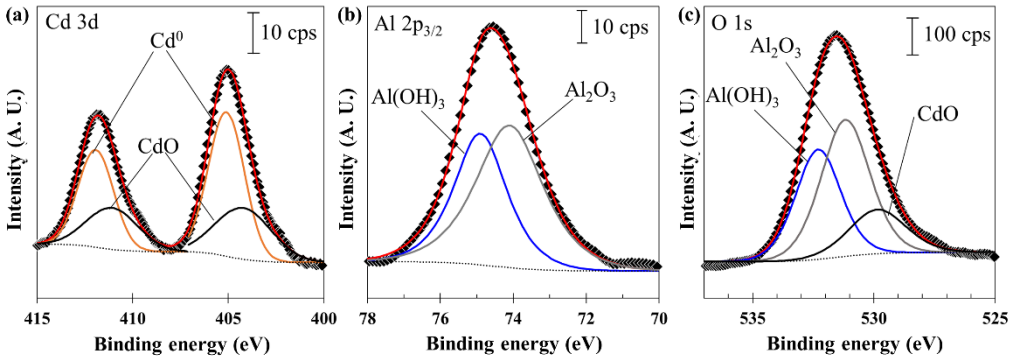


Fig. 2-7 XPS spectra of cementation products using AC/Al-mixture in 1 mM cadmium sulfate solution at pH 5: spectrum of (a) Cd 3d, (b) Al $2p_{3/2}$, and (c) O 1s.

2.3.1.4 Linear sweep voltammetry (LSV)

Figure 2-8 shows the cathodic linear sweep voltammograms for Al and AC/Al electrodes in sulfate solutions with and without 1 mM Cd^{2+} at pH 5. Linear sweep voltammograms for Al electrode showed that there was no current peak without Cd^{2+} while a cathodic current peak was observed at –0.97 V with Cd^{2+}, suggesting that Cd^{2+} reduction (Eq. 2-9) occurred on Al electrode even though the electrode surface was covered with insulating Al oxide layer at pH 5.

$$Cd^{2+} + 2\ e^{-} \rightarrow Cd^{0} \qquad (2\text{-}9)$$

This may be due to the presence of cracks in the Al oxide layer.

When AC was attached on Al electrode (i.e., AC/Al electrode was used), a larger cathodic current peak was observed. This result suggests that Cd^{2+} reduction became more active with attached AC and that AC act as electron mediator from Al to metal ions.

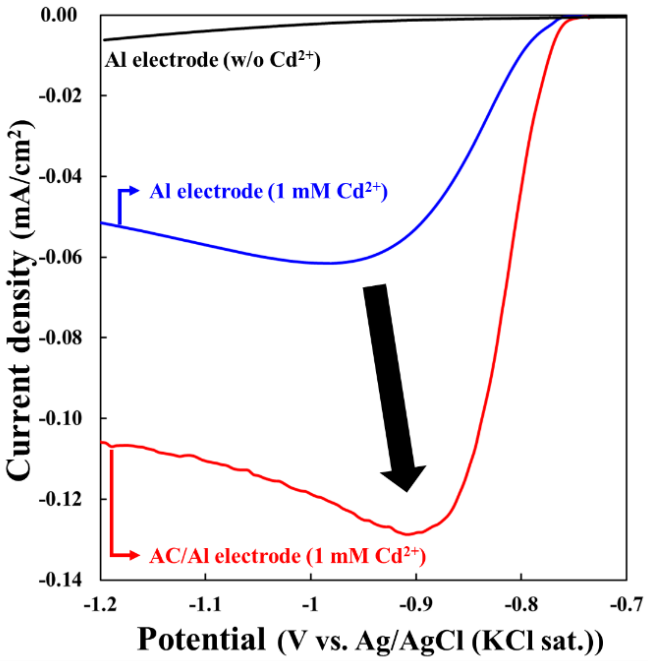


Fig. 2-8 Linear sweep voltammograms of without Cd^{2+} and 1 mM Cd^{2+} (scan range: OCP to –1.2 V vs. Ag/AgCl) in sulfate solutions at pH 5.0 at 25 °C using Al and AC/Al electrode (scan rate: 10 mV/s)

Based on the results in Sections 2.3.1.1 – 2.3.1.4, better removal of Cd^{2+} by cementation in AC/Al-mixture can be interpreted by assuming that AC provided an electron mediator from Al to Cd^{2+} and this mechanism occurred even in the presence of Al_2O_3 on Al.

2.3.2 Removal of Co^{2+} and Ni^{2+}

2.3.2.1 Effects of pH

Figures 2-9 and 2-10 show the removal efficiency, final pH, and Al^{3+} concentrations after 24 h at initial pH of 1–5 for Co^{2+} and Ni^{2+}, respectively. The Al^{3+} concentration was almost zero at pH over 4 but increased with decreasing pH below 3. With Al, the removal efficiencies were almost 0% in the entire pH range considered in the experiments even if Al^{3+} concentration increased at pH below 2. When only AC was used, Co^{2+} and Ni^{2+} were adsorbed on AC and the removal efficiency increased with increasing pH with maximum removal reaching ~32% for Co^{2+} and ~45% for Ni^{2+}. When AC/Al-mixture was used, higher removal efficiencies were observed and the maximum removal efficiencies at pH 5 were 57% for Co^{2+} and 61% for Ni^{2+}. The maximum final pH was 5.0 and 5.1 for the Co^{2+} and Ni^{2+} removal experiments, respectively (Figs. 2-9(b) and 2-10(b)), and precipitations of Co^{2+} and Ni^{2+} as hydroxides under these conditions were thermodynamically unfavorable (Fig. 2-11).

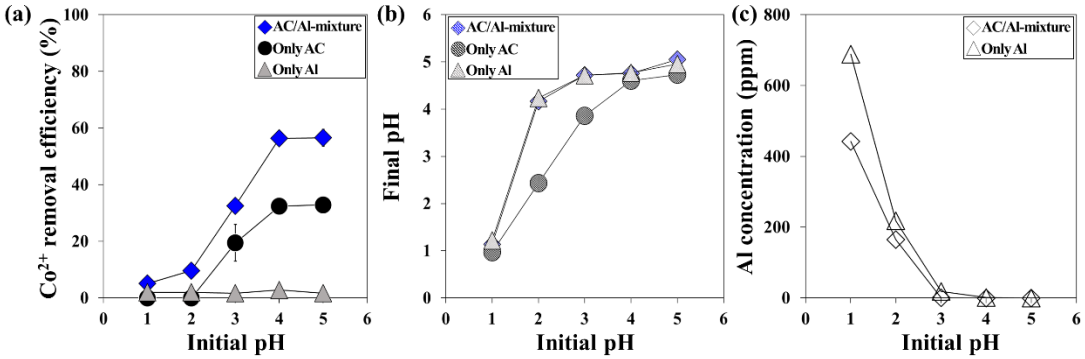


Fig. 2-9 (a) The Co^{2+} removal efficiency, (b) final pH, and (c) Al^{3+} concentration in sulfate solutions at different pH for 24 h (Al = Al^0; AC = Activated carbon).

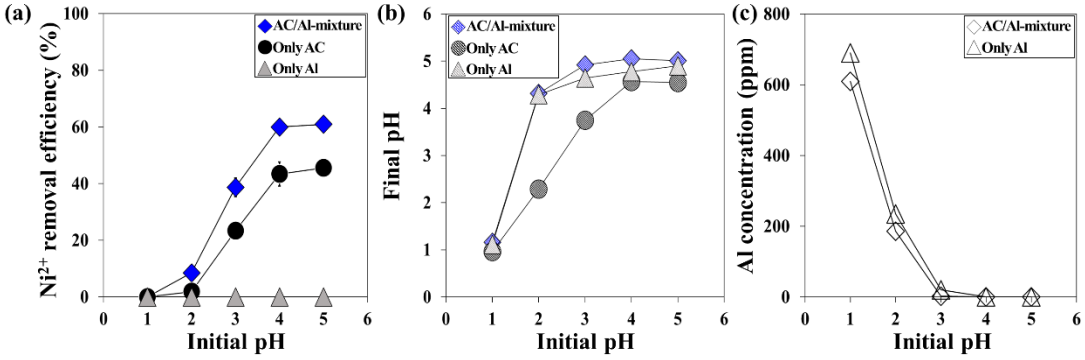


Fig. 2-10 (a) The Ni^{2+} removal efficiency, (b) final pH, and (c) Al^{3+} concentration in sulfate solutions at different pH for 24 h (Al = Al^0; AC = Activated carbon).

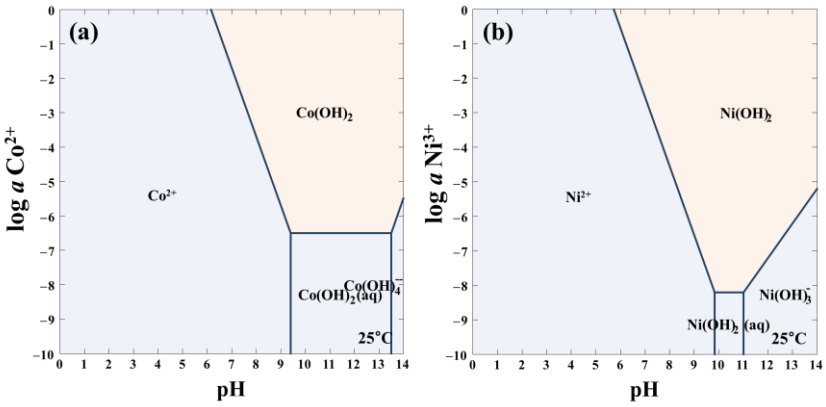


Fig. 2-11 The activity – pH diagram for 1mM (a) Co^{2+} and (b) Ni^{2+} species with 0.1 M SO_4^{2-} (created using the GWB Professional Ver. 12.0.3 software).

Generally, proton (H^+) concentration or pH is an important factor in the cementation of metal ions with Al as a reductant. On the one hand, the high concentrations of H^+ could dissolve the insulating Al_2O_3 layer on Al and enhance cementation (Dönmez et al., 1999). On the other hand, high concentrations of protons may inhibit cementation when H^+ are reduced to form hydrogen gas (H_2) as described in Eq. 2-8 (Bøckman and Østvold, 2000). Because this half-cell cathodic reaction (Eq. 2-8) consumes electrons, it competes with metal ion reduction (Eq. 2-3) and suppresses the extent of cementation on Al.

Previous electrochemical studies on the reaction rates of hydrogen evolution using different metal electrodes reported that the rate is mainly dependent on hydrogen overpotential, a parameter defined as the voltage required for hydrogen evolution on a given metal surface (Beyene et al., 2018; Ezaki et al., 1993; Hickling and Salt, 1940). Hydrogen evolution is sluggish when hydrogen overpotential is high but fast when the overpotential is low.

As shown in Table 2-1, the hydrogen overpotential of Co is around 0.3–0.4 V while that of Ni is around 0.3 V (Ezaki et al., 1993; Hickling and Salt, 1940). These values are lower than that of Cd (0.99 V) and thus, the reduction of H^+ to H_2 occurs more readily on Co and Ni than Cd (Hickling and Salt, 1940). Because of this, it is postulated that small amounts of Co and Ni deposited on Al could promote hydrogen reduction and hydrogen gas evolution that competes with the continued cementation of Co^{2+} and Ni^{2+} on Al.

Table 2-1 Hydrogen overpotential values of Cd, Zn, Co, and Ni

Metal	Temperature (°C)	Solution	ŋ at 1 mA/cm^2 (V)	Reference
Cd	-	-	0.99	(Hickling and Salt, 1940)
Zn	20	0.5 M H_2SO_4	0.94	(Uhlig and Revie, 1985)
Co	30	0.5 M H_2SO_4	0.3 – 0.4	(Ezaki et al., 1993)
Ni	30	0.5 M H_2SO_4	0.3	(Ezaki et al., 1993; Hickling and Salt, 1940)

Note: "–" means not reported.

2.3.2.2 Effects of time

Figures 2-12(a) – (d) show the removal efficiency and pH of Co^{2+} and Ni^{2+} from sulfate solution using AC, Al, and AC/Al-mixture as a function of time (initial pH: 5.0). When only Al was used, the removal efficiencies of Co^{2+} and Ni^{2+} were almost 0% regardless of time. When only AC was used, Co^{2+} and Ni^{2+} adsorption occurred and the removal efficiencies increased to 31% for Co^{2+} and 41% for Ni^{2+} within 1 h, and remained virtually constant until 24 h. When AC/Al-mixture was used, higher removal efficiencies for Co^{2+} and Ni^{2+} were observed, and the removal efficiencies were 31% for Co^{2+} and 41% for Ni^{2+} at 1 h. These values increased to 57% for Co^{2+} and 61% for Ni^{2+} after 24 h, which were equivalent to removal amounts per unit mass of AC/Al-mixture of 1.4 mg/g and 1.5 mg/g for Co^{2+} and Ni^{2+}, respectively. The pH slightly decreased to 4.70 for Co^{2+} and Ni^{2+} within 1 h, then increased to 5.0 for Co^{2+} and 5.1 for Ni^{2+} after 24 h. As discussed in Sections 2.3.1.1 and 2.3.1.2, adsorption of metal ions on AC was rapid that saturated adsorption sites quickly. The succeeding increase in metal removal efficiencies in Al/AC-mixtures after 1 h is difficult to interpret by adsorption alone because this process usually reaches steady-state condition in a short time (Sulyman et al., 2017). The succeeding increase in the metal removal efficiencies suggests that a slow chemical process like cementation at low temperature is related to metal removal (Lee et al., 1997).

The experimental results in Figs. 2-12(a) and (c) suggest that when AC/Al-mixture was used, Ni^{2+} and Co^{2+} cementation was enhanced because AC acted as an electron mediator from Al to Co^{2+} and Ni^{2+}. The extent of cementation was, however, limited because of the high hydrogen overpotential of AC, which consumed electrons by hydrogen formation and competed for metal ion reduction. This suggests that continuous metal deposition until the surface of AC is covered could be possible provided that competition from hydrogen formation is suppressed. The details of the mechanism proposed here are not fully understood and further study is needed.

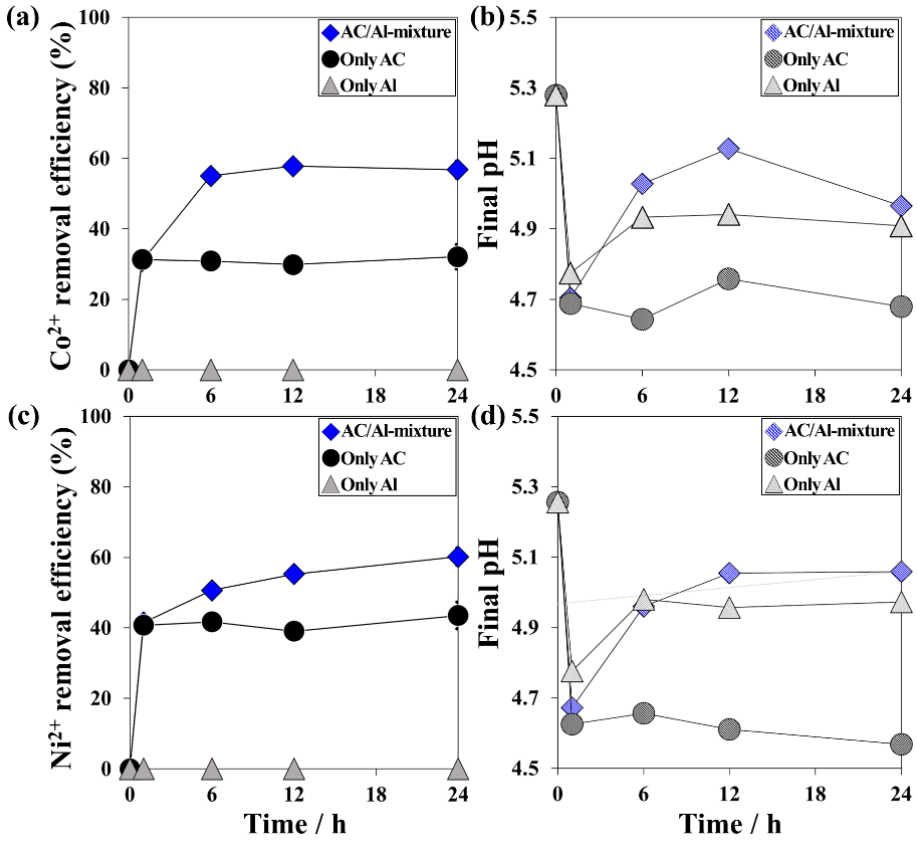


Fig. 2-12 The removal efficiency and final pH of (a, b) Co and (c, d) Ni in sulfate solutions at initial pH 5 for 24 h (Al = Al^0; AC = Activated carbon).

2.3.2.3 Limitation of cementation using AC/Al-mixture

As shown in Figs. 2-5(a), 2-12(a) and (c), the removal at pH 5 of Cd^{2+}, Co^{2+}, and Ni^{2+} almost stopped after 6 h. To identify the reason for this limited cementation, cementation experiments using cementation products (AC/Al-mixture) were conducted. In this series of experiments, used AC/Al-mixtures were prepared and resuspended in a fresh sulfate solution containing 1 mM metal ions to investigate metal ion removal by the used mixture. The detail of experimental procedure is described follows: used AC/Al-mixture was prepared by mixing 0.3 g of Al, 0.3 g of AC and 30 mL sulfate solution containing 1 mM metal ions (pH 5) in a 100-mL centrifuge tube using a roller mixer (Mix Rotor Variable 5 rollers, VMR-5R, AS ONE Corporation, Japan) (Rotation speed, 110 rpm; temperature, room temperature; gas condition, N_2). After 24 h, the solution was removed from the tube by a centrifugation-decantation technique using Table Centrifuge 5220, KUBOTA, Japan (at 2500 rpm for 3 minutes) and 30 mL of fresh sulfate solution containing 1 mM metal ions (pH 5) was added to the tube containing the cementation products (used-AC/Al mixture). The mixture was then mixed in the same manner described above and metal removal from fresh solution was determined after 24 h.

Figure. 2-13 compares the removal efficiencies of metal ions using fresh AC/Al-mixtures and used AC/Al-mixtures. The removal efficiencies were lower with used AC/Al-mixture than with fresh AC/Al-mixture, suggesting that AC/Al-mixture lost a majority of its ability to remove metal ions when re-used in the metal ion removal experiments. Table 2-2 shows the initial and final pH of the metal ion removal experiments. It was observed that there was an insignificant difference between using fresh and used AC/Al-mixtures.

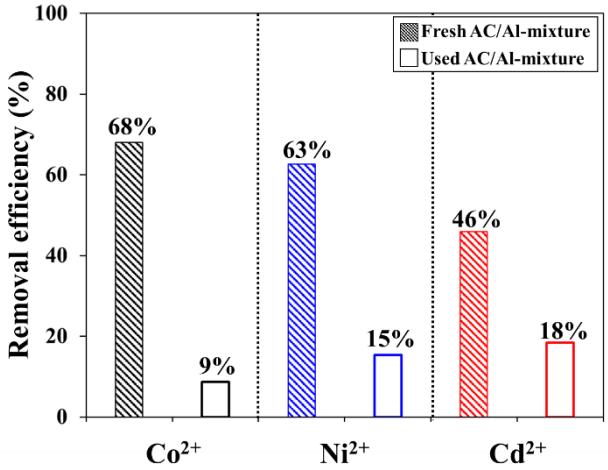


Fig. 2-13 Co^{2+}, Ni^{2+} and Cd^{2+} removal efficiencies using "fresh" and "used" AC/Al-mixtures in sulfate solution at pH 5.0.

Table 2-2 Initial and final pH of Co^{2+}, Ni^{2+} and Cd^{2+} removal experiments using "fresh" AC/Al-mixture and "used" AC/Al-mixture in sulfate solutions after 24 h at initial pH 5.

Solutions	Initial pH	Final pH	
		"Fresh" AC/Al-mixture	"Used" AC/Al-mixture
1 mM $CoSO_4$	5.2	5.1	5.3
1 mM $NiSO_4$	5.1	5.0	5.1
1 mM $CdSO_4$	5.0	5.1	5.3

Figure 2-14(a) shows the SEM photomicrograph (BSE) of the cementation products of Co^{2+} removal experiment using fresh AC/Al-mixture. There is a dark Al particle and a small bright particle attached on the Al particle. The small bright particle is cemented Co because a strong Co signal was detected in the EDS spectrum at Point 1 in this area. This cemented Co was covered with a gray-colored layer, which is most probably an aluminum precipitate because in the EDS spectrum at Point 2, a stronger Al signal was detected together with a weaker Co signal. This suggests that Al^{3+} released from Al was likely re-precipitated and covered the surface of cemented Co.

To identify Al compounds precipitated on deposited Co, XPS observation for the cementation product was conducted. Figure 2-15 shows XPS spectra of Al $2p_{3/2}$ and O 1s. In both Al $2p_{3/2}$ and O 1s

spectra, strong peaks were observed, and each peak can be deconvoluted with two peaks. The deconvoluted peaks at 74.1 eV and 74.9 eV in Al $2p_{3/2}$ spectrum and at 531.2 and 532.3 eV in O 1s spectrum matched with Al_2O_3 and $Al(OH)_3$ signals, respectively (Fang et al., 2013; He et al., 1993; Maslakov et al., 2012; Park et al., 2020; Shi et al., 2013). In XPS spectrum for Al powder before cementation experiments (Fig. 2-3) showed that there were only Al_2O_3 peaks. From these results, it can be concluded that Al precipitate covered on deposited Cd in the cementation product was $Al(OH)_3$.

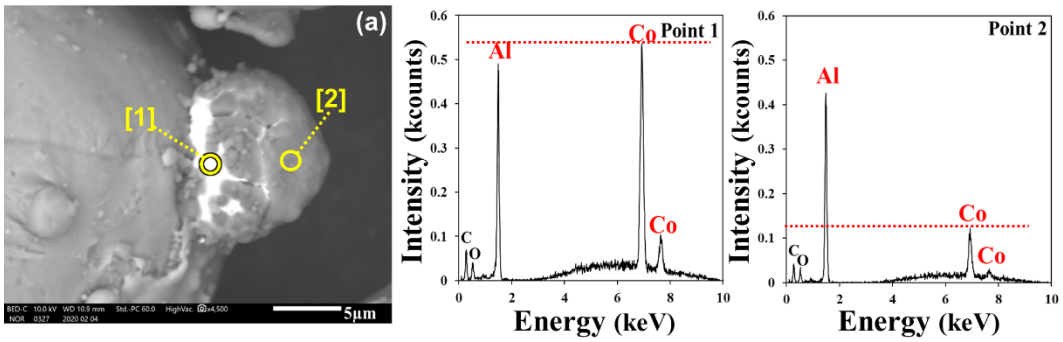


Fig. 2-14 SEM photomicrograph of (a) cementation products using AC/Al-mixture in 1 mM cobalt sulfate solution at pH 5.0 and EDS point analysis of each point (1 and 2).

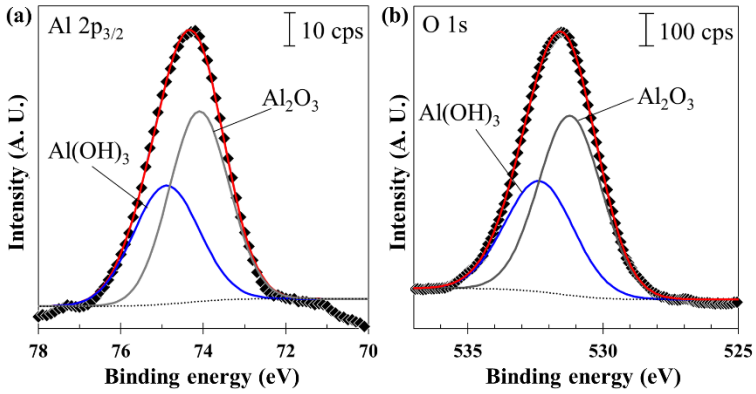


Fig. 2-15 XPS spectra of cementation products using AC/Al-mixture in 1 mM cobalt sulfate solution at pH 5: (a) spectrum of Al $2p_{3/2}$ and (b) O 1s.

At the surface of the cemented Co, H^+ is preferentially consumed by hydrogen evolution (Eq. 2-8), causing a higher "interfacial" pH than in the bulk solution phase. This deduction is supported by negligible Al^{3+} concentration using AC/Al-mixture at initial pH 5 (Fig. 2-9(c)). Considering this, the layer on cemented Co is likely $Al(OH)_3$ formed as described in Eq. 2-10 (Ali et al., 2012).

$$Al^{3+}_{(aq)} + 3\ H_2O_{(l)} \rightarrow Al(OH)_{3(s)} + 3\ H^+_{(aq)} \qquad (2\text{-}10)$$

This aluminum hydroxide layer covering cemented Co may suppress cementation of Co^{2+} and limit the overall removal of this metal ion.

2.3.3 Removal of Zn^2

2.3.3.1 Effects of pH

Figures 2-16(a) – (c) show the Zn^{2+} removal efficiency and final pH, and Al concentration, respectively in sulfate solution at different initial pH for 24 h. When only AC was used, Zn^{2+} adsorbed on AC and the maximum removal efficiency was around 30% at pH 5. When only Al was used, the removal efficiency was negligible from pH 1 to 5, although the standard redox potential of Zn^{2+}/Zn (–0.76 V vs. SHE) is higher than Al^{3+}/Al (–1.67 V vs. SHE). At higher pH (4–5), Al_2O_3 likely inhibited Zn^{2+} cementation on Al. Even at lower pH (1–3), where Al_2O_3 was removed and Al concentration increased (Fig. 2-16(c)), Zn^{2+} cementation efficiency remained almost 0% (Eq. 2-11).

$$2\ Al^0_{(s)} + 3\ Zn^{2+}_{(aq)} \rightarrow 2\ Al^{3+}_{(s)} + 3\ Zn^0_{(aq)} \quad (2\text{-}11)$$

One of the possible reasons for the suppression of Zn^{2+}cementation on Al at lower pH is the competition between cementation reaction (Eq. 2-11) and hydrogen evolution (Eq. 2-8). Hydrogen overpotential of Zn (i.e., 0.94 V) is higher than that of Co (i.e., 0.3 V) and Ni (i.e., 0.3–0.4 V) and very close to that of Cd (i.e., 0.99 V) (Ezaki et al., 1993; Hickling and Salt, 1940; Uhlig and Revie, 1985), suggesting that hydrogen evolution on Zn was not significant. Considering this, there would be another reason for the suppression of Zn cementation on Al.

The relative rates of diffusion of hydrogen on Zn and Cd are quite different; that is, it is high in Zn and low in Cd (Gabe, 1997), which indicates that hydrogen evolution reaction occurs more easily on Zn than on Cd. Because of this, the low current efficiencies of Zn reduction and high current efficiencies of Cd reduction were reported in several literatures and investigations (Gabe, 1997; Ivanov, 2004; Recéndiz et al., 2007; Wernick, 1932). In addition, the standard Gibbs free energy change, ΔG^0, for Zn cementation (Eq. 2-11) is –519.282 kJ/mol, which is less negative than that of Cd cementation (Eq. 2-7; –729.427 kJ/mol). Therefore, the thermodynamic driving force for Zn cementation is weaker than for Cd cementation. Furthermore, Cd^{2+} and Zn^{2+} cementation kinetic is essential which needs further study.

As shown in Fig. 2-16(a), when using AC/Al-mixture, the removal efficiencies were over 80% at pH 2–3, and this value was much higher than that observed with only Al or with only AC, suggesting that the addition of AC enhanced Zn cementation using Al. At pH 4–5, the removal efficiencies were less than 60%, indicating that Zn removal using AC/Al-mixture is dependent on pH. The maximum final pH was 5.1 (Fig. 2-16(b)) and under this condition.

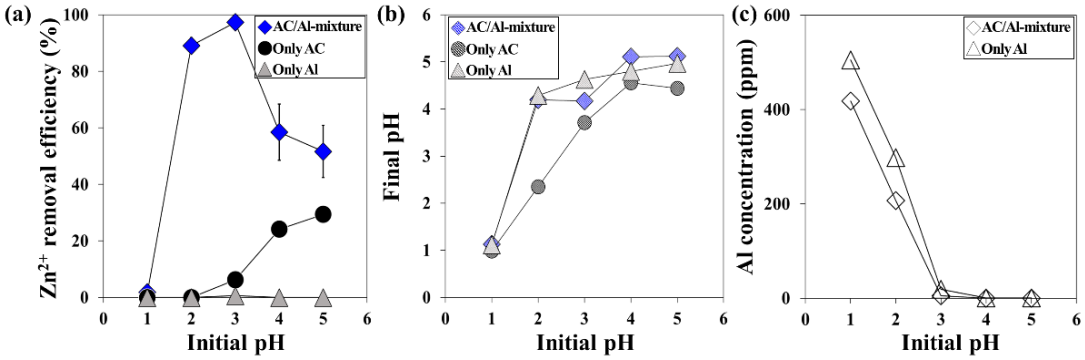


Fig. 2-16 (a) The Zn^{2+} removal efficiency, (b) final pH, and (c) Al^{3+} concentration in sulfate solutions at different pH for 24 h (Al = Al^0; AC = Activated carbon).

2.3.3.2 Effects of time

Figures 2-17(a) and (b) show the removal efficiency of Zn^{2+} and pH as a function of time (initial pH: 3.0). The removal efficiencies were almost 0% with Al only and less than 10% with AC only. With AC/Al-mixture, the removal efficiency increased continuously with time and reached over 96% (2.8 mg/g AC/Al-mixture) after 24 h. The pH increased from 3.0 to 4.8 after 12 h, then it remained almost constant until 24 h. This result suggests that Zn removal with Al was enhanced by the addition of AC.

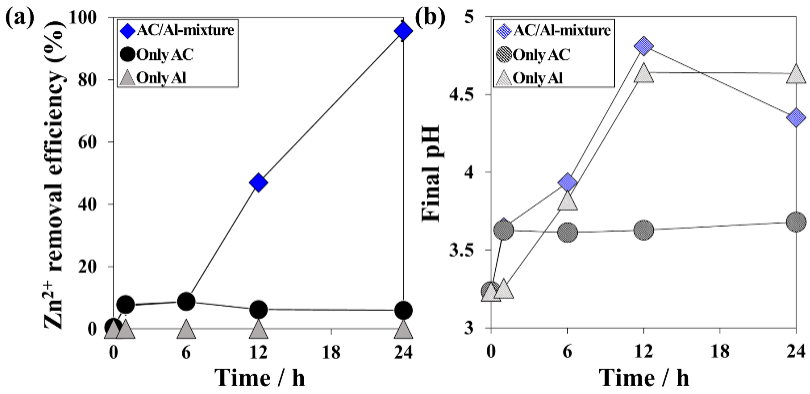


Fig. 2-17 The removal efficiency of Zn^{2+} and final pH in sulfate solutions at initial pH 3 for 24 h (Al = Al^0, AC = Activated carbon).

2.3.3.3 Surface analysis of Zn-bearing products

Figure 2-18 shows the SEM photomicrographs (Fig. 2-18(a)) and EDS point analysis (1 and 2) of cementation products obtained after Zn^{2+} removal experiments using AC/Al-mixture at pH 3. As shown in the SEM photomicrograph (Fig. 2-18(a)), a bright region (point 1) is sandwiched between two dark "particles" (point 2). In the EDS spectra, Al and O peaks were detected in Point 2 on the surface of a dark particle while Zn, Al, O, and C peaks were detected in Point 1 on the bright region, suggesting that C was present with Zn.

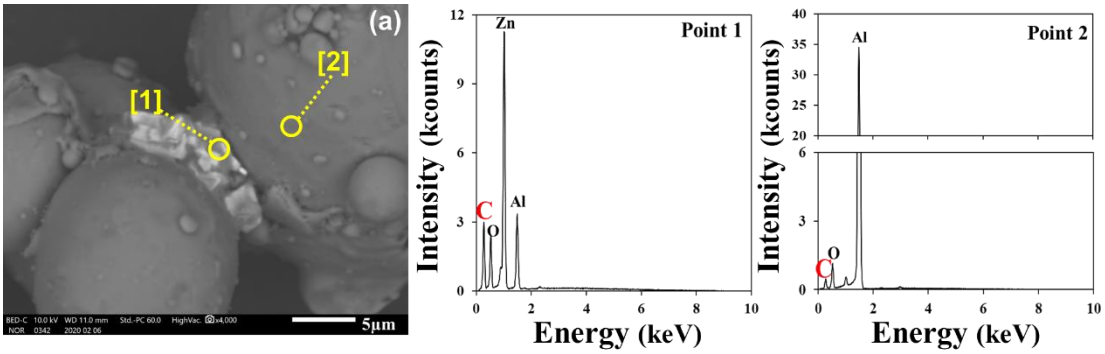


Fig. 2-18 SEM photomicrograph of (a) Zn cementation products using AC/Al-mixture in 1 mM zinc sulfate solution at pH 3.0 and EDS point analysis of each point (1 and 2).

To identify the elemental composition of deposited Zn, cementation products of Zn^{2+} removal experiment using AC/Al-mixture were analyzed by AES. Figure 2-19 shows the AES photomicrographs (Fig. 2-19(a)) and scan results of cementation products from the Zn^{2+} removal experiments. In the wide AES spectrum, the peaks corresponding to C, O, Zn, and Al were detected (Fig. 2-19(b)). The narrow AES spectrum in the range of 960–1030 eV was fitted with reference spectra of Zn^0 and ZnO (Fig. 2-19(c)). From the fitting result, it was confirmed that Zn in the products was composed of Zn^0 (17.6%) and ZnO (82.4%). Because AES analysis is a surface sensitive (Kohli, 2012), the detected ZnO signal could be from the oxidized surface layer on Zn, which was formed during drying and sample preparation before AES analysis.

The results of the surface analysis of cementation products can be summarized as follows: (1) Zn was cemented together with carbon AC on Al based on the SEM-EDS analysis, and (2) Zn^0 was present with its oxidized form (i.e., ZnO) based on the XPS and AES analyses. Overall, the above results showed that Al is the primary electron donor (i.e., anode) while AC attached on Al acted as an electron mediator (i.e., cathode) from Al to Zn^{2+}, which was then cemented on AC. This mechanism is similar to the enhanced cementation of gold-thiosulfate complex using AC/Al-mixture proposed by Jeon et al. (2020b).

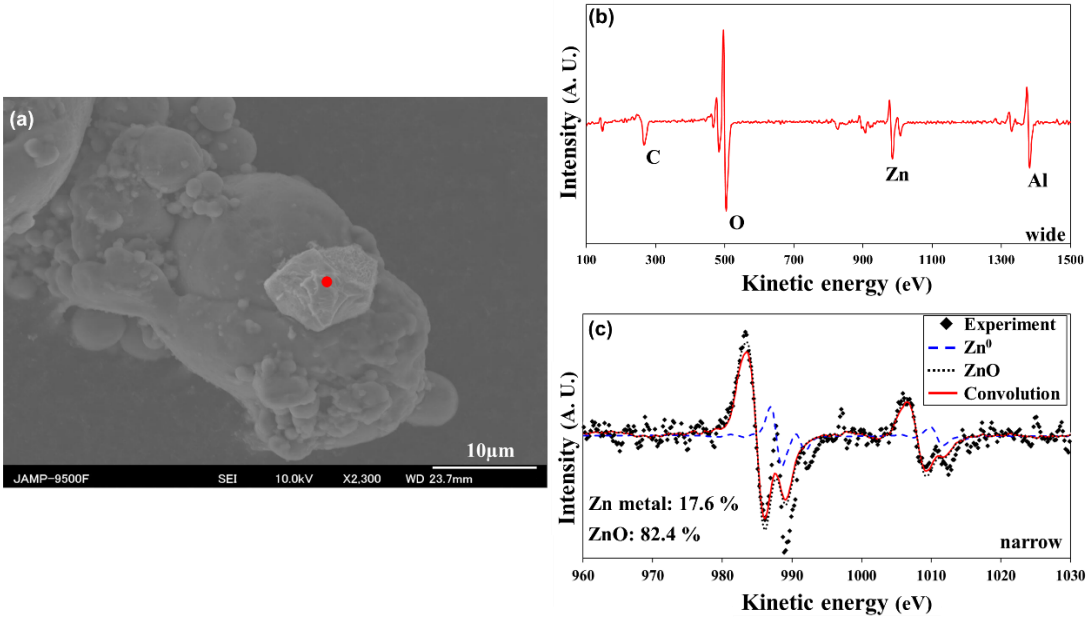


Fig. 2-19 AES results of cementation products from the Zn^{2+} removal experiments using AC/Al-mixture: (a) photomicrograph, (b) wide scan energy spectrum of the red point in (a), and (c) the narrow scan energy spectrum of the Zn peak with fitting spectra of Zn^0 and ZnO.

2.4 Summary

This chapter investigated the removal/recovery of Cd^{2+}, Co^{2+}, Ni^{2+}, and Zn^{2+} in sulfate solutions via enhanced cementation using Al and AC. The results showed that removal/recovery efficiencies of Cd^{2+}, Co^{2+}, Ni^{2+}, and Zn^{2+} were higher in the AC/Al-mixture than those in AC or Al only experiments. The results of surface analyses of cementation products showed that these heavy metals were deposited on AC attached on Al in elemental (zero-valent) forms. The removal efficiencies varied depending on the target heavy metal ion, which is mainly due to the differences in Gibbs free energy change for cementation and hydrogen overpotential of different metals. Precipitation of $Al(OH)_3$ induced by H^+ consumption on the cemented metal further suppressed metal ion removal from sulfate solutions. Overall, the role of AC during the "AC/Al-cementation" technique is as an electron "bridge" between Al (electron donor) and metal ions (electron acceptor) in solution warranting further electrochemical studies.

References

Abdel-Aziz, M.H., El-Ashtoukhy, E.S.Z., Bassyouni, M., 2016. Recovery of Copper from Effluents by Cementation on Aluminum in a Multirotating Cylinder-Agitated Vessel. Metall. Mater. Trans. B Process Metall. Mater. Process. Sci. 47, 657–665. https://doi.org/10.1007/s11663-015-0467-y

Ali, I., Gupta, V.K., Khan, T.A., Asim, M., 2012. Removal of arsenate from aqueous solution by electro-coagulation method using Al-Fe electrodes. Int. J. Electrochem. Sci. 7, 1898–1907.

Anacleto, A.L., Carvalho, J.R., 1996. Mercury cementation from chloride solutions using iron, zinc and aluminium. Miner. Eng. 9, 385–397. https://doi.org/10.1016/0892-6875(96)00025-8

Annamalai, V., Murr, L.E., 1978. Effects of the source of chloride ion and surface corrosion patterns on the kinetics of the copper-aluminum cementation system. Hydrometallurgy 3, 249–263. https://doi.org/10.1016/0304-386X(78)90026-9

Bernhoft, R.A., 2013. Cadmium toxicity and treatment. Sci. World J. 2013. https://doi.org/10.1155/2013/394652

Beyene, B.B., Mane, S.B., Hung, C.H., 2018. Electrochemical Hydrogen Evolution by Cobalt (II) Porphyrins: Effects of Ligand Modification on Catalytica Activity, Efficiency and Overpotential. J. Electrochem. Soc. 165, H481–H487. https://doi.org/10.1149/2.0481809jes

Bøckman, O., Østvold, T., 2000. Products formed during cobalt cementation on zinc in zinc sulfate electrolytes. Hydrometallurgy 54, 65–78. https://doi.org/10.1016/S0304-386X(99)00059-6

Boyanov, B.S., Konareva, V. V., Kolev, N.K., 2004. Purification of zinc sulfate solutions from cobalt and nickel through activated cementation. Hydrometallurgy 73, 163–168. https://doi.org/10.1016/j.hydromet.2003.09.002

Burakov, A.E., Galunin, E. V., Burakova, I. V., Kucherova, A.E., Agarwal, S., Tkachev, A.G., Gupta, V.K., 2018. Adsorption of heavy metals on conventional and nanostructured materials for wastewater treatment purposes: A review. Ecotoxicol. Environ. Saf. 148, 702–712. https://doi.org/10.1016/j.ecoenv.2017.11.034

Choi, S., Jeon, S., Park, I., Ito, M., Hiroyoshi, N., 2021. Enhanced cementation of Co2+ and Ni2+ from sulfate and chloride solutions using aluminum as electron donor and conductive particles as an electron pathway. Metals (Basel). 11, 1–12. https://doi.org/10.3390/met11020248

Choi, S., Yoo, K., Alorro, R.D., Tabelin, C.B., 2020. Cementation of Co ion in leach solution using Zn powder followed by magnetic separation of cementation-precipitate for recovery of unreacted Zn powder. Miner. Eng. 145. https://doi.org/10.1016/j.mineng.2019.106061

Demirkran, N., Künkül, A., 2011. Recovering of copper with metallic aluminum. Trans. Nonferrous Met. Soc. China (English Ed. 21, 2778–2782. https://doi.org/10.1016/S1003-6326(11)61123-0

Dil, E.A., Ghaedi, M., Ghaedi, A.M., Asfaram, A., Goudarzi, A., Hajati, S., Soylak, M., Agarwal, S., Gupta, V.K., 2016. Modeling of quaternary dyes adsorption onto ZnO-NR-AC artificial neural network: Analysis by derivative spectrophotometry. J. Ind. Eng. Chem. 34, 186–197. https://doi.org/10.1016/j.jiec.2015.11.010

Djokić, S.S., 1996. Cementation of Copper on Aluminum in Alkaline Solutions. J. Electrochem. Soc. 143, 1300–1305. https://doi.org/10.1149/1.1836634

Dönmez, B., Sevim, F., Saraç, H., 1999. Kinetic study of the cementation of copper from sulphate solutions onto a rotating aluminum disc. Hydrometallurgy 53, 145–154. https://doi.org/10.1016/S0304-386X(99)00042-0

Douglas. S. Flett, 2004. Cobalt-Nickel Separation in Hydrometallurgy: a Review. Chem. Sustain. Dev. 12, 81–91.

Ekmekyapar, A., Tanaydin, M., Demirkiran, N., 2012. Investigation of copper cementation kinetics by rotating aluminum disc from the leach solutions containing copperions. Physicochem. Probl. Miner. Process. 48, 355–367. https://doi.org/10.5277/ppmp120203

Ezaki, H., Morinaga, M., Watanabe, S., 1993. Hydrogen overpotential for transition metals and alloys, and its interpretation using an electronic model. Electrochim. Acta 38, 557–564. https://doi.org/10.1016/0013-4686(93)85012-N

Fang, R.-C., Sun, Q.-Q., Zhou, P., Yang, W., Wang, P.-F., Zhang, D.W., 2013. High-performance bilayer flexible resistive random access memory based on low-temperature thermal atomic layer deposition. Nanoscale Res. Lett. 8, 92. https://doi.org/10.1186/1556-276x-8-92

Farahmand, F., Moradkhani, D., Sadegh Safarzadeh, M., Rashchi, F., 2009. Optimization and kinetics of the cementation of lead with aluminum powder. Hydrometallurgy 98, 81–85. https://doi.org/10.1016/j.hydromet.2009.04.001

Gabe, D.R., 1997. The role of hydrogen in metal electrodeposition processes. J. Appl. Electrochem. 27, 908–915. https://doi.org/10.1023/A:1018497401365

Gao, X., Wu, L., Xu, Q., Tian, W., Li, Z., Kobayashi, N., 2018. Adsorption kinetics and mechanisms of copper ions on activated carbons derived from pinewood sawdust by fast H3PO4 activation. Environ. Sci. Pollut. Res. 25, 7907–7915. https://doi.org/10.1007/s11356-017-1079-7

Gouvea, L.R., Morais, C.A., 2007. Recovery of zinc and cadmium from industrial waste by

leaching/cementation. Miner. Eng. 20, 956–958. https://doi.org/10.1016/j.mineng.2007.04.016

Gupta, V.K., Ali, I., Saleh, T.A., Siddiqui, M.N., Agarwal, S., 2013. Chromium removal from water by activated carbon developed from waste rubber tires. Environ. Sci. Pollut. Res. 20, 1261–1268. https://doi.org/10.1007/s11356-012-0950-9

Gupta, V.K., Jain, C.K., Ali, I., Chandra, S., Agarwal, S., 2002. Removal of lindane and malathion from wastewater using bagasse fly ash - A sugar industry waste. Water Res. 36, 2483–2490. https://doi.org/10.1016/S0043-1354(01)00474-2

Gupta, V.K., Nayak, A., Agarwal, S., Tyagi, I., 2014. Potential of activated carbon from waste rubber tire for the adsorption of phenolics: Effect of pre-treatment conditions. J. Colloid Interface Sci. 417, 420–430. https://doi.org/10.1016/j.jcis.2013.11.067

Gupta, V.K., Rastogi, A., Dwivedi, M.K., Mohan, D., 1997. Process development for the removal of zinc and cadmium from wastewater using slag - A blast furnace waste material, Separation Science and Technology. https://doi.org/10.1080/01496399708002227

Gupta, V.K., Saleh, T.A., 2013. Sorption of pollutants by porous carbon, carbon nanotubes and fullerene- An overview. Environ. Sci. Pollut. Res. 20, 2828–2843. https://doi.org/10.1007/s11356-013-1524-1

He, H., Alberti, K., Barr, T.L., Klinowski, J., 1993. ESCA studies of aluminophosphate molecular sieves. J. Phys. Chem. 97, 13703–13707. https://doi.org/10.1021/j100153a045

Hickling, A., Salt, F.W., 1940. Studies in hydrogen overvoltage at high current densities: Part 1 - The influence of electrode material, current density, and time, in aqueous solution. Trans. Faraday Soc. 36, 1226–1235. https://doi.org/10.1039/TF9403601226

Hsu, Y.J., Tran, T., 1996. Selective removal of gold from copper-gold cyanide liquors by cementation using zinc. Miner. Eng. 9, 1–13. https://doi.org/10.1016/0892-6875(95)00127-1

Iida, T., Amano, Y., Machida, M., Imazeki, F., 2013. Effect of surface property of activated carbon on adsorption of nitrate ion. Chem. Pharm. Bull. 61, 1173–1177. https://doi.org/10.1248/cpb.c13-00422

Ivanov, I., 2004. Increased current efficiency of zinc electrowinning in the presence of metal impurities by addition of organic inhibitors. Hydrometallurgy 72, 73–78. https://doi.org/10.1016/S0304-386X(03)00129-4

Jeon, S., Tabelin, C.B., Park, I., Nagata, Y., Ito, M., Hiroyoshi, N., 2020a. Ammonium thiosulfate extraction of gold from printed circuit boards (PCBs) of end-of-life mobile phones and its recovery from pregnant leach solution by cementation. Hydrometallurgy 191, 105214.

https://doi.org/10.1016/j.hydromet.2019.105214

Jeon, S., Tabelin, C.B., Takahashi, H., Park, I., Ito, M., Hiroyoshi, N., 2020b. Enhanced cementation of gold via galvanic interactions using activated carbon and zero-valent aluminum: A novel approach to recover gold ions from ammonium thiosulfate medium. Hydrometallurgy 191, 105165. https://doi.org/10.1016/j.hydromet.2019.105165

Kadirvelu, K., Thamaraiselvi, K., Namasivayam, C., 2001. Removal of heavy metals from industrial wastewaters by adsorption onto activated carbon prepared from an agricultural solid waste. Bioresour. Technol. 76, 63–65. https://doi.org/10.1016/S0960-8524(00)00072-9

Kaplowitz, D.A., Jian, G., Gaskell, K., Jacob, R., Zachariah, M.R., 2014. Synthesis and Reactive Properties of Iron Oxide-Coated Nanoaluminum. J. Energ. Mater. 32, 95–105. https://doi.org/10.1080/07370652.2013.767288

Karnib, M., Kabbani, A., Holail, H., Olama, Z., 2014. Heavy metals removal using activated carbon, silica and silica activated carbon composite. Energy Procedia 50, 113–120. https://doi.org/10.1016/j.egypro.2014.06.014

Kloprogge, J.T., Duong, L. V., Wood, B.J., Frost, R.L., 2006. XPS study of the major minerals in bauxite: Gibbsite, bayerite and (pseudo-)boehmite. J. Colloid Interface Sci. 296, 572–576. https://doi.org/10.1016/j.jcis.2005.09.054

Kohli, R., 2012. Methods for Monitoring and Measuring Cleanliness of Surfaces, Developments in Surface Contamination and Cleaning: Detection, Characterization, and Analysis of Contaminants. Elsevier. https://doi.org/10.1016/B978-1-4377-7883-0.00003-1

Ku, Y., Chen, C.H., 1992. Kinetic Study of Copper Deposition on Iron by Cementation Reaction. Sep. Sci. Technol. 27, 1259–1275. https://doi.org/10.1080/01496399208019424

Lee, H.Y., Kim, S.G., Oh, J.K., 1997. Cementation behavior of gold and silver onto Zn, Al, and Fe powders from acid thiourea solutions. Can. Metall. Q. 36, 149–155. https://doi.org/10.1179/cmq.1997.36.3.149

Li, W., Cochell, T., Manthiram, A., 2013a. Activation of aluminum as an effective reducing agent by pitting corrosion for wet-chemical synthesis. Sci. Rep. 3, 1–7. https://doi.org/10.1038/srep01229

Li, W., Li, M., Xie, S., Zhai, T., Yu, M., Liang, C., Ouyang, X., Lu, X., Li, H., Tong, Y., 2013b. Improving the photoelectrochemical and photocatalytic performance of CdO nanorods with CdS decoration. CrystEngComm 15, 4212–4216. https://doi.org/10.1039/c3ce40092a

Lupi, C., Pasquali, M., 2003. Electrolytic nickel recovery from lithium-ion batteries. Miner. Eng. 16,

537–542. https://doi.org/10.1016/S0892-6875(03)00080-3

Makhloufi, L., Saidani, B., Hammache, H., 2000. Removal of lead ions from acidic aqueous solutions by cementation on iron. Water Res. 34, 2517–2524. https://doi.org/10.1016/S0043-1354(99)00405-4

Mar, K.K., Karnawati, D., Sarto, Putra, D.P.E., Igarashi, T., Tabelin, C.B., 2013. Comparison of Arsenic Adsorption on Lignite, Bentonite, Shale, and Iron Sand from Indonesia. Procedia Earth Planet. Sci. 6, 242–250. https://doi.org/10.1016/j.proeps.2013.01.033

Marychurch, M., Morris, G.C., 1985. X-ray photoelectron spectra of crystal and thin film cadmium sulphide. Surf. Sci. 154, 251–254. https://doi.org/10.1016/0039-6028(85)90035-4

Maslakov, K.I., Teterin, A.Y., Teterin, Y.A., Ivanov, K.E., Yudintsev, S. V., Stefanovskii, S. V., 2012. X-ray photoelectron study of murataite ceramics containing Th, U, Np, and Pu. Radiochemistry 54, 115–121. https://doi.org/10.1134/S1066362212020026

Murr, L.E., Annamalai, V., 1978a. Characterization of copper nucleation and growth from aqueous solution on aluminum: A transmission electron microscopy study of copper cementation. Thin Solid Films 54, 189–195. https://doi.org/10.1016/0040-6090(78)90198-0

Murr, L.E., Annamalai, V., 1978b. An Electron Microscopic Study of Nucleation and Growth in Electrochemical Displacement Reactions: A Comparison of the Cu/Fe and Cu/AI Cementation Systems. Metall. Trans. B 9, 515–525. https://doi.org/10.1007/BF03257198

Naumkin, A. V., Kraut-Vass, A., Gaarenstroom, S.W., Powell, C.J., 2012. NIST X-ray Photoelectron Spectroscopy Database [WWW Document]. Meas. Serv. Div. Natl. Inst. Stand. Technol. https://doi.org/10.18434/T4T88K

Navarro, P., Alvarez, R., Vargas, C., Alguacil, F.J., 2004. On the use of zinc for gold cementation from ammoniacal-thiosulphate solutions. Miner. Eng. 17, 825–831. https://doi.org/10.1016/j.mineng.2004.02.001

Nekouei, F., Nekouei, S., Tyagi, I., Gupta, V.K., 2015. Kinetic, thermodynamic and isotherm studies for acid blue 129 removal from liquids using copper oxide nanoparticle-modified activated carbon as a novel adsorbent. J. Mol. Liq. 201, 124–133. https://doi.org/10.1016/j.molliq.2014.09.027

Nelson, A., Wang, W., Demopoulos, G.P., Houlachi, G., 2000. Removal of cobalt from zinc electrolyte by cementation: A critical review. Miner. Process. Extr. Metall. Rev. 20, 325–356. https://doi.org/10.1080/08827500008547436

Park, I., Higuchi, K., Tabelin, C.B., Jeon, S., Ito, M., Hiroyoshi, N., 2021. Suppression of arsenopyrite oxidation by microencapsulation using ferric-catecholate complexes and phosphate. Chemosphere

269, 129413. https://doi.org/10.1016/j.chemosphere.2020.129413

Park, I., Tabelin, C.B., Seno, K., Jeon, S., Inano, H., Ito, M., Hiroyoshi, N., 2020. Carrier-microencapsulation of arsenopyrite using Al-catecholate complex: nature of oxidation products, effects on anodic and cathodic reactions, and coating stability under simulated weathering conditions. Heliyon 6, e03189. https://doi.org/10.1016/j.heliyon.2020.e03189

Peeters, N., Binnemans, K., Riaño, S., 2020. Solvometallurgical recovery of cobalt from lithium-ion battery cathode materials using deep-eutectic solvents. Green Chem. 22, 4210–4221. https://doi.org/10.1039/d0gc00940g

Recéndiz, A., González, I., Nava, J.L., 2007. Current efficiency studies of the zinc electrowinning process on aluminum rotating cylinder electrode (RCE) in sulfuric acid medium: Influence of different additives. Electrochim. Acta 52, 6880–6887. https://doi.org/10.1016/j.electacta.2007.04.112

Saleh, T.A., Gupta, V.K., 2014. Processing methods, characteristics and adsorption behavior of tire derived carbons: A review. Adv. Colloid Interface Sci. 211, 93–101. https://doi.org/10.1016/j.cis.2014.06.006

Shi, Q., Huang, Y., Jing, C., 2013. Synthesis, characterization and application of lanthanum-impregnated activated alumina for F removal. J. Mater. Chem. A 1, 12797–12803. https://doi.org/10.1039/c3ta12548c

Shirley, D.A., 1972. High-resolution x-ray photoemission spectrum of the valence bands of gold. Phys. Rev. B 5, 4709–4714. https://doi.org/10.1103/PhysRevB.5.4709

Silwamba, M., Ito, M., Hiroyoshi, N., Tabelin, C.B., 2020a. Recovery of Lead and Zinc from Zinc Plant Leach Residues by Concurrent Dissolution-Cementation. Metals (Basel). 10, 531. https://doi.org/10.3390/met10040531

Silwamba, M., Ito, M., Hiroyoshi, N., Tabelin, C.B., Fukushima, T., Park, I., Jeon, S., Igarashi, T., Sato, T., Nyambe, I., Chirwa, M., Banda, K., Nakata, H., Nakayama, S., Ishizuka, M., 2020b. Detoxification of lead-bearing zinc plant leach residues from Kabwe, Zambia by coupled extraction-cementation method. J. Environ. Chem. Eng. 8, 104197. https://doi.org/10.1016/j.jece.2020.104197

Suhas, Gupta, V.K., Carrott, P.J.M., Singh, R., Chaudhary, M., Kushwaha, S., 2016. Cellulose: A review as natural, modified and activated carbon adsorbent. Bioresour. Technol. 216, 1066–1076. https://doi.org/10.1016/j.biortech.2016.05.106

Sulyman, M., Namiesnik, J., Gierak, A., 2017. Low-cost adsorbents derived from agricultural by-

products/wastes for enhancing contaminant uptakes from wastewater: A review. Polish J. Environ. Stud. 26, 479–510. https://doi.org/10.15244/pjoes/66769

Tabelin, C.B., Corpuz, R.D., Igarashi, T., Villacorte-Tabelin, M., Alorro, R.D., Yoo, K., Raval, S., Ito, M., Hiroyoshi, N., 2020a. Acid mine drainage formation and arsenic mobility under strongly acidic conditions: Importance of soluble phases, iron oxyhydroxides/oxides and nature of oxidation layer on pyrite. J. Hazard. Mater. 399, 122844. https://doi.org/10.1016/j.jhazmat.2020.122844

Tabelin, C.B., Dallas, J., Casanova, S., Pelech, T., Bournival, G., Saydam, S., Canbulat, I., 2021. Towards a low-carbon society : A review of lithium resource availability , challenges and innovations in mining , extraction and recycling , and future perspectives. Miner. Eng. 163, 106743. https://doi.org/10.1016/j.mineng.2020.106743

Tabelin, C.B., Silwamba, M., Paglinawan, F.C., Mondejar, A.J.S., Duc, H.G., Resabal, V.J., Opiso, E.M., Igarashi, T., Tomiyama, S., Ito, M., Hiroyoshi, N., Villacorte-Tabelin, M., 2020b. Solid-phase partitioning and release-retention mechanisms of copper, lead, zinc and arsenic in soils impacted by artisanal and small-scale gold mining (ASGM) activities. Chemosphere 260, 127574. https://doi.org/10.1016/j.chemosphere.2020.127574

Tabelin, C.B., Veerawattananun, S., Ito, M., Hiroyoshi, N., Igarashi, T., 2017a. Pyrite oxidation in the presence of hematite and alumina: II. Effects on the cathodic and anodic half-cell reactions. Sci. Total Environ. 581–582, 126–135. https://doi.org/10.1016/j.scitotenv.2016.12.050

Tabelin, C.B., Veerawattananun, S., Ito, M., Hiroyoshi, N., Igarashi, T., 2017b. Pyrite oxidation in the presence of hematite and alumina: I. Batch leaching experiments and kinetic modeling calculations. Sci. Total Environ. 580, 687–698. https://doi.org/10.1016/j.scitotenv.2016.12.015

Tables, V.K., Electrode, S., Dekker, M., York, N., 2018. Electrochemical Series. Corros. Mater. 665–671. https://doi.org/10.31399/asm.hb.v13b.a0006542

Uhlig, H.H., Revie, R.W., 1985. Corrosion and corrosion control: and introduction of corrosion science and engineering, 4th ed. A john wiley & sons, New York.

Wernick, S., 1932. The Electrodeposition of Cadmium from Cadmium Sulfate Solutions : Part I . The Effect of pH , Current Density , and Temperature on the Crystal Size of the Deposit , the Current Efficiency , and the Electrode Efficiency Ratio. Trans. Electrochem. Soc. 62, 27–38.

Zähr, J., Oswald, S., Türpe, M., Ullrich, H.J., Füssel, U., 2012. Characterisation of oxide and hydroxide layers on technical aluminum materials using XPS. Vacuum 86, 1216–1219. https://doi.org/10.1016/j.vacuum.2011.04.004

Zhang, P., Yokoyama, T., Itabashi, O., Wakui, Y., Suzuki, T.M., Inoue, K., 1998. Hydrometallurgical process for recovery of metal values from spent nickel-metal hydride secondary batteries. Hydrometallurgy 50, 61–75. https://doi.org/10.1016/S0304-386X(98)00046-2

This chapter was based on a research paper published under the following details: -

Choi, S., Jeon, S., Park, I., Tabelin, C.B., Ito, M., Hiroyoshi, N., 2021. Enhanced cementation of Cd^{2+}, Co^{2+}, Ni^{2+}, and Zn^{2+} on Al from sulfate solutions by activated carbon addition. Hydrometallurgy 201, 105580. https://doi.org/10.1016/j.hydromet.2021.105580

CHAPTER 3 – Removal of Pb^{2+}, Cd^{2+}, Co^{2+}, Ni^{2+}, and Zn^{2+} from chloride solutions by cementation using aluminum as electron donor and the effect of activated carbon addition

3.1 Introduction

In the previous chapter 2, Cd^{2+}, Co^{2+}, Ni^{2+}, and Zn^{2+} could be successfully removed via cementation from acidic sulfate solutions by the concurrent use of Al and AC even without Al_2O_3 removal. To date, AC/Al cementation has been already widely studied in the situation where Al_2O_3 layer is present on Al^0 surface like sulfate and thiosulfate solutions (Jeon et al., 2020), but it remains unclear how the absence of Al_2O_3 layer affects the removal of heavy metals during AC/Al cementation process.

In this chapter, thus, AC/Al cementation technique for recovering/removing heavy metals (e.g., Pb^{2+}, Cd^{2+}, Co^{2+}, Ni^{2+}, and Zn^{2+}) from acidic chloride media where Al_2O_3 layer present on the surface of Al^0 is known to be dissolved was investigated. Specifically, the objectives of this chapter are to: (1) investigate how effective AC/Al-cementation technique is for recovering/removing heavy metal ions from chloride solutions and (2) elucidate the possible mechanisms involved in this technique. The first objective was accomplished by the batch-type cementation experiments using AC and/or Al while the second objective was achieved by electrochemical studies (e.g., open circuit potential (OCP), linear sweep voltammetry (LSV)) and solid-phase analyses (e.g., Brunauer-Emmett-Teller (BET) analysis, and scanning electron microscopy with energy-dispersive X-ray spectroscopy (SEM-EDS)).

3.2 Materials and methods

3.2.1 Cementation experiments

3.2.1.1 Cementation methods

Chloride solutions containing 1 mM of metal ions were prepared by separately dissolving $PbCl_2$ (99.0%, Wako Pure Chemical Industries, Ltd., Japan), $CdCl_2 \cdot 2.5H_2O$ (98.0%, Wako Pure Chemical Industries, Ltd., Japan), $CoCl_2 \cdot 6H_2O$ (99.0%, Kishida Chemical Co., Ltd., Japan), $NiCl_2 \cdot 6H_2O$ (98.0%, Kishida Chemical Co., Ltd., Japan), and $ZnCl_2$ (99.0%, Wako Pure Chemical Industries, Ltd., Japan) in deionized (DI) water (18 MΩ·cm, Mill-Q® Integral Water Purification System, Merck Millipore, USA). The initial pH was fixed to 4.0 with 1 M HCl (Wako Pure Chemical Industries, Ltd., Japan) to avoid an undesired side reaction between Al and protons (H^+) at low pH (MacKinnon and Ingraham, 1971), and total Cl^- concentration was maintained to 0.1 M using 1 M NaCl (99.0 %, Wako Pure Chemical Industries, Ltd., Japan) to normalize the effects of Cl^- on cementation experiment.

For the cementation experiment, 10 mL of prepared solution was added into a 50-mL Erlenmeyer flask, and the solution was deoxygenated by bubbling ultrapure N_2 gas (99.99%) for 15 min before each experiment. Afterward, 0.1 g of Al and/or 0.1 g of AC was added into the flask, and then the N_2 gas was re-introduced for 5 min. The top of the flask was tightly capped by a rubber stopper and sealed with parafilm to prevent evaporation as well as air introduction. The flask was shaken by a thermostat water bath shaker (Cool bath shaker, ML-10F, Taitec Corporation, Japan) with 40 mm of shaking amplitude and 120 min^{-1} of shaking frequency at 25 °C for up to 24 h.

The flask was collected at designated time intervals, the suspension was filtered by a syringe-driven membrane filter (pore size: 0.2 μm, LMS Co., Ltd., Tokyo, Japan), the final pH of filtrate was measured. The metal ion concentrations in the filtrate were analyzed by inductively coupled plasma atomic emission spectroscopy (ICP-AES, ICPE-9820, Shimadzu Corporation, Japan) (margin of error = ± 2%).

The removal efficiency (R) of metal ions from chloride solution was calculated using the following equation:

$$R = \frac{C_i - C_f}{C_i} \, x \, 100 \qquad (3\text{-}1)$$

where C_i and C_f were the initial and final concentrations of metal ions, respectively.

3.2.1.2 Electrochemical measurements

The cementation products were collected by vacuum filtration (pore size: 0.2 μm, Merck Millipore, USA), rinsed using DI water thoroughly, dried in a vacuum oven at 40 °C for 24 h, and analyzed by scanning electron microscopy with energy-dispersive X-ray spectroscopy (SEM-EDS, JSM-IT200^{TM}, JEOL Co., Ltd., Japan).

3.2.2 Cementation methods

3.2.2.1 Open circuit potential (OCP)

To understand the reduction reactions of Pb^{2+}, Cd^{2+}, Co^{2+}, Ni^{2+}, and Zn^{2+} occurring on the surface of Al, open circuit potential (OCP) was measured using a potentiostat (SP-300, Biologic, France). For this, Al rod (99.999%, 10 mm φ, Nilaco Corp.), Ag/AgCl electrode filled with saturated KCl were used as working and reference electrodes, respectively. The Al working electrode was polished via 1200-grit silicon carbide papers followed by a 1 μm diamond paste on a polishing cloth plate using a polishing machine (Saphir 250 M1, ATM, Germany). After this, the polished electrode was ultrasonically cleaned for 3 min in DI water to remove impurities attached on Al surface, and rinsed

with DI water. Two electrodes were immersed into the prepared solution (e.g., 1 mM Pb^{2+}, Cd^{2+}, Co^{2+}, Ni^{2+}, or Zn^{2+} at pH 4.0 with 0.1 M Cl^- as a supporting electrolyte), deoxygenated by N_2 purging, and then OCP was measured at 25 °C for 10 min.

3.2.2.2 Linear sweep voltammetry (LSV)

The hydrogen evolution overpotential (i.e., hydrogen overpotential) on Pb, Cd, Co, Ni, and Zn metal surface was investigated by linear sweep voltammetry (LSV) using a potentiostat with a conventional three-electrode system in acidic chloride solution (pH, 4; [Cl^-], 0.1 M). The working electrodes were prepared using Pb rod (99.999%, 8 mm φ, Nilaco Corp.), Cd rod (99.99%, 8 mm φ, Nilaco Corp.), Co rod (99.995%, 5 mm φ, Nilaco Corp.), Ni rod (99.99%, 5 mm φ, Nilaco Corp.), and Zn rod (99.99%, 10 mm φ, Nilaco Corp.). The reference electrode was an Ag/AgCl electrode filled with saturated KCl, and the counter electrode was a platinum (Pt) electrode. Before the experiments, the working electrode was polished in the same manner as described in section 2.3.1. Dissolved oxygen was removed by N_2 purging for 30 min. Then three electrodes were immersed into the prepared solution, and equilibrated at 25 °C for 15 min. After measuring OCP, LSV was measured starting from OCP to –1.8 V vs. Ag/AgCl for Pb, Cd, Zn, Co, and Ni at the scan rate of 1 mV/s.

3.3 Results and discussion

3.3.1 BET surface area of Al and AC

The surface area of Al (D_{50}: 21.3 μm, 99.99%, Wako Chemical Co., Ltd., Japan) and AC (D_{50}: 38.1 μm, Wako pure Chemical Industries, Ltd., Japan) was characterized by the BET method using a surface area analyzer (NOVA 2200e, Quantachrome, USA). Degassing of an adequate amount of Al or AC was conducted in the sample cell under the nitrogen (N_2, 99.99%) flow at 200 °C for 2 h. After degassing, the multipoint BET surface area was determined via N_2 sorption at –196 °C in the relative pressure (P/P_0) range of 0.05 to 0.3, where P and P_0 represent the equilibrium and saturation pressure of the adsorbate N_2 gas, respectively.

The BET surface area of Al and AC was measured by the N_2 adsorption-desorption method. Figures 3-1(a) and (b) show the N_2 adsorption-desorption isotherm of Al and AC, respectively. The specific surface areas determined by the BET method of AC and Al were 1,484.6 m^2/g and 1.3 m^2/g, respectively, indicating that the specific surface area of the former was obviously larger than that of the latter.

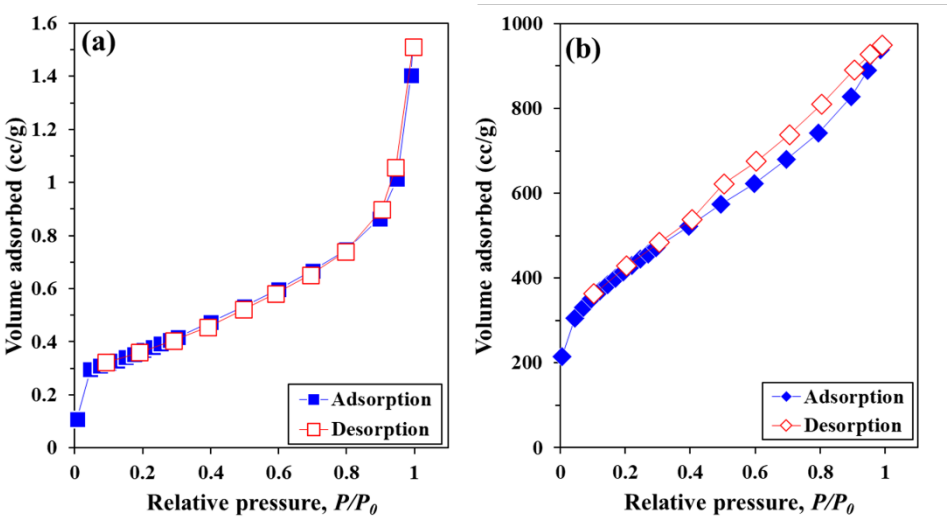


Fig. 3-1 BET nitrogen adsorption-desorption isotherm plot of (a) aluminum (Al) and (b) activated carbon (AC).

3.3.2 Removal of metal ions from chloride solutions

3.3.2.1 Addition of only Al

Figures 3-2(a), (b), and (c) show the removal efficiencies of Pb^{2+}, Cd^{2+}, Co^{2+}, Ni^{2+}, and Zn^{2+}, changes in pH, and Al concentrations during cementation using Al as a function of time, respectively. The results showed that the removal efficiencies of Pb^{2+} and Cd^{2+} were around 99% within 1 and 2 h, respectively, indicating that Al oxide layer was removed. However, Co^{2+}, Ni^{2+}, and Zn^{2+} were about 0% for 24 h, suggesting that the cementation of Co^{2+}, Ni^{2+}, and Zn^{2+} were impossible to occur when using Al even in the absence of Al oxide layer. After cementation for 24 h, the pH observed in Pb^{2+}, Cd^{2+}, Co^{2+}, Ni^{2+}, and Zn^{2+} solutions increased to 4.6, 4.8, 4.6, 4.7, and 4.6, respectively (Fig. 3-2(b)), and this can be elucidated by the fact that the protons (H^+) in solutions were consumed by dissolution of Al oxide layer and/or Al metal as described in Eqs. 3-2 and 3-3 (Reboul, et al., 1997; Tak et al., 2006).

$$Al_2O_{3(s)} + 6\ HCl_{(aq)} \rightarrow 2\ AlCl_{3(aq)} + 3\ H_2O \quad (3\text{-}2)$$

$$2\ Al_{(s)} + 6\ HCl_{(aq)} \rightarrow 2\ AlCl_{3(aq)} + 3\ H_{2(g)} \quad (3\text{-}3)$$

Once the insulating Al oxide layer is removed, the reduction of metal ions having a higher standard reduction potential than Al (Al^{3+}/Al; –1.67 V vs. SHE) is expected to occur. Moreover, the Gibbs free energy values for each metal ion reaction with Al^0 are all negative (Table 3-1) (Tables et al., 2018), indicating that cementation of those metal ions should spontaneously occur as described in

Eq. 3-4; however, the results showed that only Pb^{2+} and Cd^{2+} could be cemented on Al^0. As cementation of Pb^{2+} and Cd^{2+} progressed, dissolved Al concentration increased to about 78 to 83 mg/L, whereas its concentration was very low (<5 mg/L) for the cases of Co^{2+}, Ni^{2+}, and Zn^{2+}, which supports that the latter three metal ions were not cemented (Figs. 3-2(a) and (c)).

$$3\ Me^{2+}_{(aq)} + 2\ Al^{0}_{(s)} \rightarrow 3\ Me^{0}_{(s)} + 2\ Al^{3+}_{(aq)} \quad (3\text{-}4)$$

Considering this, there would be another reason for the limited cementation of Co^{2+}, Ni^{2+}, and Zn^{2+} using Al, which will be discussed in the following sub-section.

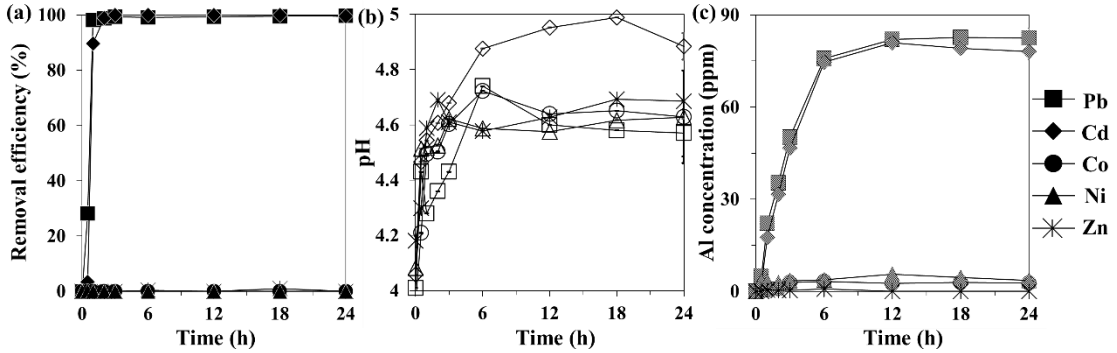


Fig. 3-2 (a) The removal efficiencies of Pb^{2+}, Cd^{2+}, Co^{2+}, Ni^{2+}, and Zn^{2+}, (b) the changes in pH and (c) Al concentration during the cementation using Al with time at initial pH 4.0 and 0.1 M Cl^{-}.

Table 3-1 Standard electrode potential of each metal and Gibbs free energy changes of cementation reaction using only aluminum at 25 °C.

Half reaction	E^0 (V)	$E^0_{cell} = E^0_{Me2+/Me} - E^0_{Al3+/Al0}$ (V)	G^0 (kJ/mol)
Pb^{2+}/Pb^0	–0.13	1.53	–885.73
Cd^{2+}/Cd^0	–0.40	1.26	–729.43
Co^{2+}/Co^0	–0.28	1.38	–798.90
Ni^{2+}/Ni^0	–0.26	1.40	–810.47
Zn^{2+}/Zn^0	–0.76	0.90	–521.02
Al^{3+}/Al^0	–1.66	–	–

3.3.2.2 OCP behaviors of metal ions on Al

During cementation of metal ions with Al, anodic half-cell ($Al = Al^{3+} + 3e^{-}$) and cathodic ($Me^{2+} + 2e^{-} = Me^0$; $2H^{+} + 2e^{-} = H_2$) reactions occur on the surface of Al, and thus open circuit potential (OCP), a mixed potential of anodic and cathodic reactions occurring on the electrode surface, is affected by types of metal ions present in the system (Gros et al., 2011; Hiromoto et al., 2008; Ramdani et al., 2007). As shown in Fig. 3-3, the E_{OCP} of Al electrode in the absence of any metal ions was –1.0

V at 0 s and decreased with time to reach –1.2 V at 600 s. In this case, Al dissolution (i.e., $Al = Al^{3+} + 3e^-$) and H_2 evolution (Eq. 3-5) are main anodic and cathodic reactions, respectively.

$$2\ H^+_{(aq)} + 2\ e^- \rightarrow H_{2(g)} \qquad (3\text{-}5)$$

Since H^+ is consumed by the cathodic reaction, H^+ concentration near the surface of the Al electrode is reduced with time, causing the decrease in the cathodic current and shift of E_{OCP} to a negative direction. When metal ions were present in the solution, not only the H_2 evolution but also the reduction of those ions (i.e., $Me^{2+} + 2e^- = Me^0$) were also considered as cathodic reactions. When the reduction of metal ions occurs, the total cathodic currents increase and finally cause the positive shift of E_{OCP}. With Co^{2+} and Ni^{2+} in the solution, E_{OCP} at 0 s was around –0.98 V, which was very close to that without metal ions, suggesting that reduction of these metal ions on the surface of Al electrode was not so significant. With Pb^{2+} and Cd^{2+}, however, E_{OCP} at 0 s was much higher than that without metal ions (i.e., –0.65 V with Pb^{2+}; –0.75 V with Cd^{2+}), and this may be due to the reduction of Pb^{2+} and Cd^{2+} on the Al surface. On the other hand, E_{OCP} with Zn^{2+} was more negative than that without metal ions at 0 s and slightly decreased with time. Similar to the cases of Co^{2+} and Ni^{2+}, E_{OCP} with Zn^{2+} measured for 100 s was within E_{OCP} without metal ions, implying that the reduction of Zn^{2+} hardly occurred. Summing up the results of OCP measurements (Fig. 3-3), Pb^{2+} and Cd^{2+} were much easier to be reduced on the surface of Al than Co^{2+}, Ni^{2+}, and Zn^{2+} in the chloride system, and these results were in good agreement with the cementation results shown in Fig. 3-2(a).

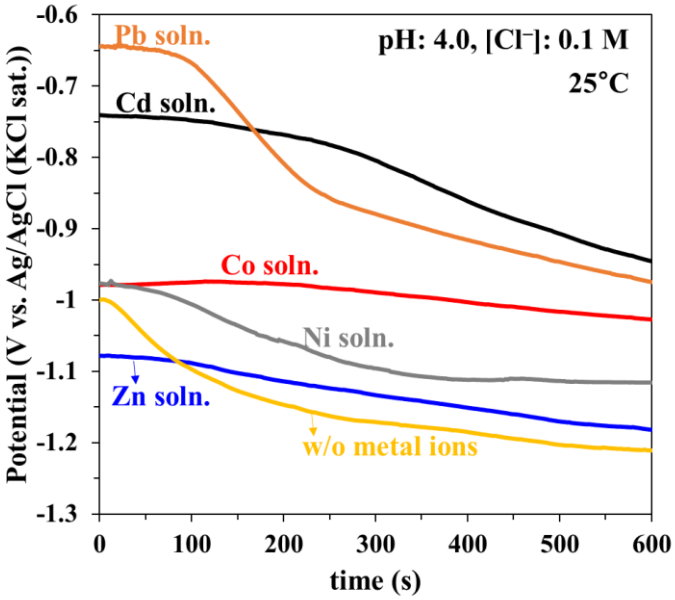


Fig. 3-3 The open circuit potential (OCP) of Al electrode in chloride solutions at 25 °C for 10 min (solutions: 1 mM Pb^{2+}, Cd^{2+}, Co^{2+}, Ni^{2+}, Zn^{2+} and without metal ions in 0.1 M Cl^- at initial pH 4.0).

3.3.2.3 Hydrogen evolution overpotential on Pb, Cd, Co, Ni, and Zn

When metal ions are cemented on the Al surface, HER occurs on the cemented metal surface, and the rate of HER varies depending on the type of metals (Beyene et al., 2018; Ezaki et al., 1993; Hickling and Salt, 1940; Uhlig and Revie, 1985). To evaluate the HER on each metal surface in the studied system (i.e., acidic chloride solution (pH 4)), linear sweep voltammetry (LSV) was conducted using Pb, Cd, Co, Ni, and Zn electrodes.

Figure 3-4 shows the cathodic linear sweep voltammograms for Pb, Cd, Co, Ni, and Zn electrodes in the solutions containing 0.1 M Cl^- at pH 4 without metal ions. The results showed that the current densities measured using Co and Ni electrodes were significantly larger than using Pb, Cd, and Zn electrodes; that is, at an applied potential of –1.8 V, the current densities for hydrogen evolution were around –22.9, –28.2, –1.9, –2.8, and –3.5 mV/cm^2 on Co, Ni, Cd, Zn, and Pb electrodes, respectively, indicating that hydrogen evolution occurred more actively on Co and Ni electrodes than the other cases (Ezaki et al., 1993; Hickling and Salt, 1940; Nelson et al., 2000; Uhlig and Revie, 1985). During the cementation of Co^{2+} and Ni^{2+}, a limited amount of these metal ions can be cemented on the surface of Al (Eq. 3-4), but their further deposition would be stopped because of the active hydrogen evaluation on the cemented metals competing with the reduction of metal ions in the solution. On the other hand, Pb^{2+} and Cd^{2+} cementation can occur since the HER does not actively take place on the surface of metals. In the case of Zn, although the HER is inactive like Pb and Cd (Fig. 3-4), the cementation of Zn^{2+} was suppressed (Fig. 3-2(a)), which means that the competition between HER and metal reduction is not the main reason for the suppressed cementation of Zn^{2+} in the system. This can be elucidated by the fact that the reduction rate of Zn^{2+} on Al is slower than those of Pb^{2+} and Cd^{2+} (Gabe, 1997; Ivanov, 2004; Recéndiz et al., 2007; Wernick, 1932). As shown in Table 1, the standard reduction potential for Zn^{2+} is much lower than Pb^{2+} and Cd^{2+}, and this lower reduction potential may be a reason for the slower reduction rate of Zn^{2+}.

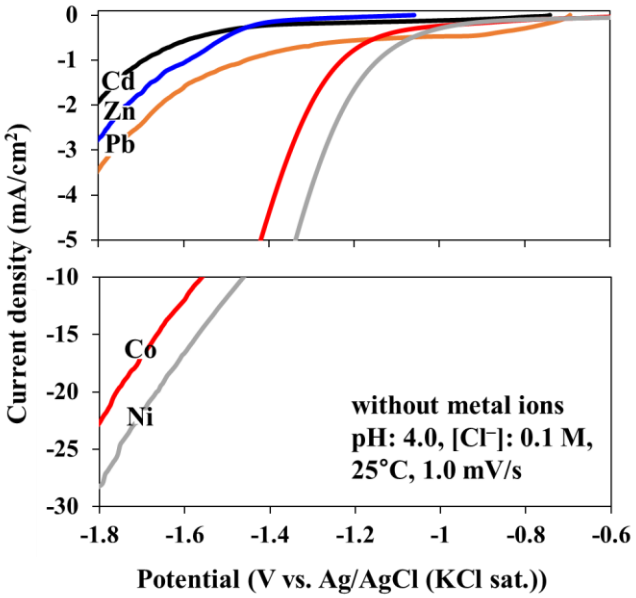


Fig. 3-4 The linear sweep voltammograms of Pb, Cd, Co, Ni and Zn electrodes in chloride solutions at 25 °C (solutions: without metal ions in 0.1 M Cl^- at initial pH 4.0; sweep rate: 1.0 mV/s).

3.3.2.3 Effects of AC for cementation using Al

The results of cementation experiments using Al and/or AC powder (i.e., removal efficiency of each metal ion, changes in pH and Al concentration) were summarized in Table 3-2. The maximum pH values observed after cementation experiments were less than 5.1, below which the precipitation of metal ions as hydroxides was neglected as shown in the activity – pH diagrams for Pb^{2+}, Cd^{2+}, Co^{2+}, Ni^{2+}, and Zn^{2+} (Fig. 3-5), indicating that the removal of metal ions resulted from cementation reactions, not their precipitation.

Results of experiments using only AC showed removal efficiency of each metal ions increased rapidly within 30 min, then it became constant until 24 h (Table 3-2). The rapid increase in removal efficiency is most likely caused by the adsorption of metal ions onto the AC surface. The surface functional groups like carboxyl group act as adsorption sites where metal ions are attracted (Gao et al., 2018; Iida et al., 2013; Kadirvelu et al., 2001; Karnib et al., 2014; Sulyman et al., 2017). Because adsorption sites were saturated within 30 min (Karnib et al., 2014; Sulyman et al., 2017), and thus the removal efficiency was maintained at an almost constant value.

Removal efficiencies of metal ions with AC/Al-mixture by 3 h were almost the same as that with only AC, suggesting that the metal removal until 3 h was mainly due to the adsorption of metal ions on AC. However, it is important to note that after 3h, the removal efficiencies of metal ions were continuously increased by 12 h when using AC/Al-mixture, which indicates that the removal of metal ions was achieved by not only adsorption but also relatively slow chemical process like cementation.

Table 3-2 The removal efficiency of metal ions (Pb^{2+}, Cd^{2+}, Co^{2+}, Ni^{2+}, and Zn^{2+}), and the changes in pH and Al concentration during cementation using Al, AC, and Al/AC mixture in chloride solutions at initial pH 4.0 for 24 h.

		Al			AC		Al+AC (1:1)		
Elem.	**Time (h)**	**pH**	**Al conc. (mg/L)**	**Removal efficiency (%)**	**pH**	**Removal efficiency (%)**	**pH**	**Al conc. (mg/L)**	**Removal efficiency (%)**
Pb^{2+}	0	4.0	-	**-**	4.0	**-**	4.0	-	**-**
	0.5	4.4	5.0	**28.3**	4.3	**69.5**	4.4	< 0.1	**58.7**
	1	4.3	22.2	**98.1**	4.3	**67.8**	4.4	< 0.1	**69.2**
	2	4.4	35.3	**98.8**	4.3	**70.3**	4.5	< 0.1	**72.3**
	3	4.4	50.2	**99.4**	4.3	**70.9**	4.6	< 0.1	**75.3**
	6	4.7	75.8	**99.1**	4.3	**70.7**	4.8	< 0.1	**85.3**
	12	4.6	82.0	**99.3**	4.3	**71.7**	4.8	1.9	**91.5**
	18	4.6	82.7	**99.6**	4.4	**73.4**	4.8	2.2	**92.1**
	24	4.6	82.5	**99.7**	4.4	**72.0**	4.8	2.1	**92.8**
Cd^{2+}	0	4.1	-	**-**	4.1	**-**	4.1	-	**-**
	0.5	4.5	2.4	**3.4**	4.7	**25.2**	4.7	< 0.1	**26.2**
	1	4.5	17.6	**89.6**	4.8	**26.7**	4.7	< 0.1	**27.1**
	2	4.6	31.6	**98.9**	4.7	**28.4**	4.7	< 0.1	**28.3**
	3	4.7	46.6	**100**	4.7	**30.1**	4.8	< 0.1	**32.0**
	6	4.9	74.6	**100**	4.8	**32.7**	4.9	< 0.1	**43.8**
	12	5.0	80.9	**100**	4.8	**35.0**	5.1	2.2	**45.4**
	18	5.0	79.1	**100**	4.8	**33.4**	5.1	2.1	**45.5**
	24	4.9	78.1	**100**	4.7	**35.0**	5.1	2.2	**45.4**
Co^{2+}	0	4.0	-	**-**	4.0	**-**	4.0	-	**-**
	0.5	4.2	< 0.1	**0**	4.5	**43.4**	4.5	< 0.1	**42.8**
	1	4.5	0.5	**0**	4.5	**42.8**	4.4	< 0.1	**42.8**
	2	4.5	0.9	**0**	4.5	**42.6**	4.5	< 0.1	**42.8**
	3	4.6	2.9	**0**	4.6	**45.3**	4.6	< 0.1	**45.8**
	6	4.7	3.2	**0**	4.5	**46.2**	4.8	< 0.1	**79.5**
	12	4.6	2.6	**0**	4.6	**43.9**	4.9	< 0.1	**77.5**
	18	4.7	2.9	**0**	4.6	**43.6**	4.9	< 0.1	**76.9**
	24	4.6	2.7	**0**	4.5	**42.8**	4.9	< 0.1	**76.4**
Ni^{2+}	0	4.1	-	**-**	4.1	**-**	4.1	-	**-**
	0.5	4.5	3.5	**0**	4.6	**55.1**	4.6	< 0.1	**55.1**
	1	4.5	3.2	**0**	4.5	**54.7**	4.5	< 0.1	**55.3**
	2	4.5	2.8	**0**	4.5	**53.3**	4.5	< 0.1	**53.7**
	3	4.6	3.5	**0**	4.5	**53.9**	4.5	< 0.1	**55.1**
	6	4.6	3.8	**0**	4.5	**55.5**	4.7	< 0.1	**78.1**
	12	4.6	5.0	**0**	4.4	**54.5**	4.9	< 0.1	**80.8**
	18	4.6	4.5	**0**	4.5	**56.3**	5.0	< 0.1	**78.7**
	24	4.6	3.6	**0**	4.4	**55.3**	5.0	< 0.1	**79.1**
Zn^{2+}	0	4.2	-	**-**	4.2	**-**	4.2	-	**-**
	0.5	4.3	< 0.1	**0**	4.6	**44.3**	4.6	< 0.1	**44**
	1	4.6	0.4	**0**	4.6	**44.9**	4.7	< 0.1	**44.3**
	2	4.7	0.4	**0**	4.6	**45.5**	4.6	< 0.1	**46.1**
	3	4.6	0.3	**0**	4.6	**46.4**	4.6	< 0.1	**45.1**
	6	4.6	0.8	**0**	4.5	**46.6**	4.8	< 0.1	**70.6**
	12	4.6	< 0.1	**0**	4.6	**47.6**	5.0	< 0.1	**86.4**
	18	4.7	< 0.1	**0**	4.5	**48.9**	5.0	< 0.1	**81.5**
	24	4.7	< 0.1	**0**	4.6	**48.8**	5.0	< 0.1	**80.0**

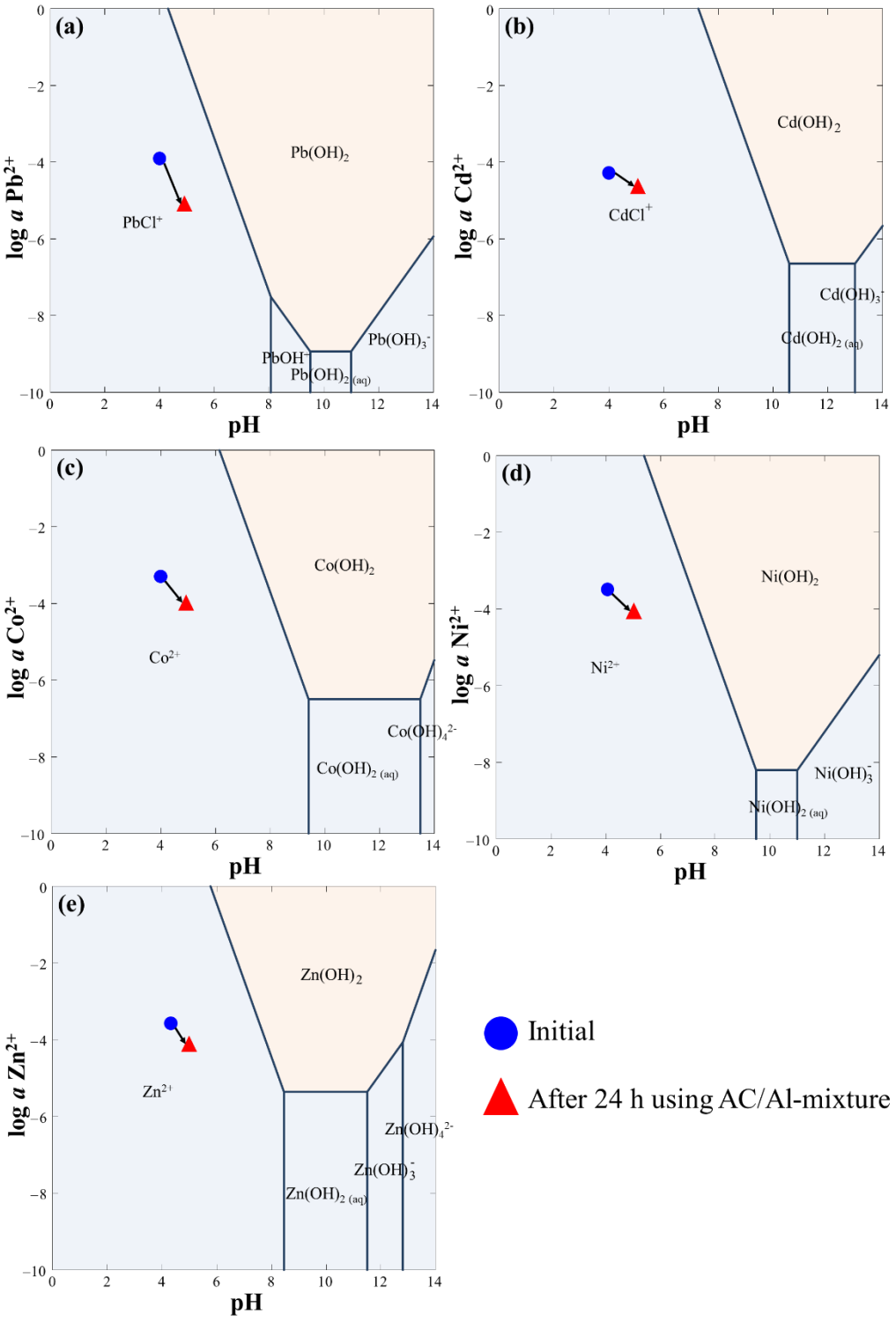


Fig. 3-5 The activity – pH diagram for 1 mM (a) Pb^{2+}, (b) Cd^{2+}, (c) Co^{2+}, (d) Ni^{2+} and (e) Zn^{2+} species with 0.1 M Cl^- at 25°C (created using the GWB Professional Ver. 12.0.3 software).

3.3.3 Surface analysis of Pb^{2+}, Cd^{2+}, Co^{2+}, Ni^{2+}, and Zn^{2+} cementation products (AC/Al-mixture)

To investigate the effects of AC on cementation of Pb^{2+}, Cd^{2+}, Co^{2+}, Ni^{2+}, and Zn^{2+}, the residues obtained from the cementation experiments using AC/Al-mixture were analyzed by SEM-EDS. As shown in Fig. 3-6, SEM photomicrographs for all cases showed small bright particles attached to the surface of large and dark particles. Strong signals of Al and O were detected on the spectra of "points a-1, b-1, c-1, d-1, and e-1", confirming that the dark particles were Al. Meanwhile, the spectra of the points a-2, b-2, c-2, d-2, and e-2 showed strong signals of Pb, Cd, Co, Ni, and Zn, respectively, indicating that bright particles attached on Al particles are cemented metals. In the spectra of the points a-2, b-2, c-2, d-2, and e-2, C signal was detected together with cemented metals (Pb, Cd, Co, Ni, and Zn), confirming that AC coexists with cemented metals. The results of SEM-EDS observation for cementation products suggest that AC act as an electron mediator from Al to metal ions (Pb^{2+}, Cd^{2+}, Co^{2+}, Ni^{2+}, and Zn^{2+}), and thus the efficiency of cementation of these metal ions was enhanced.

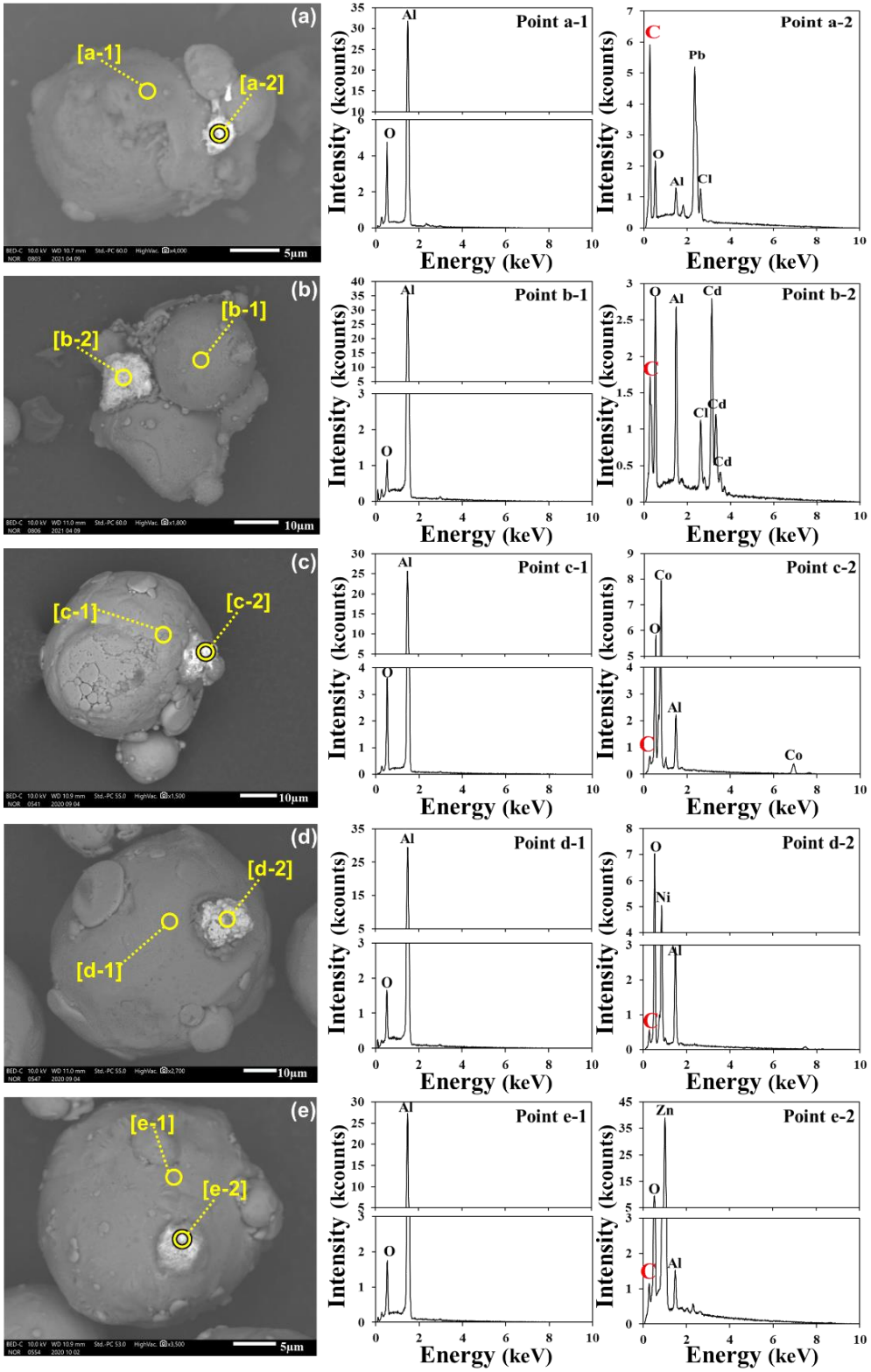


Fig. 3-6 SEM photomicrograph of cementation products using AC/Al-mixture (a) Pb, (b) Cd, (c) Co, (d) Ni and (e) Zn, and EDS point analysis of each point (1 and 2).

3.3 Comparison of cementation of metal ions using AC/Al mixture in sulfate and chloride solutions

In a previous chapter 2, the cementation of various metal ions (Cd^{2+}, Co^{2+}, Ni^{2+}, and Zn^{2+}) using AC/Al mixture in sulfate solutions was investigated, and it was reported that AC act as an electron mediator from Al to metal ions, leading to the enhanced cementation. Similarly, AC acted as an electron mediator during cementation of metal ions (Pb^{2+}, Cd^{2+}, Co^{2+}, Ni^{2+}, and Zn^{2+}) using AC/Al mixture in chloride solutions as confirmed by Fig. 3-6; however, the cementation efficiency was enhanced only for Co^{2+}, Ni^{2+}, and Zn^{2+}. In other words, the addition of AC suppressed the cementation of Pb^{2+} and Cd^{2+} on Al.

An important difference between sulfate and chloride system is the presence of insulating Al_2O_3 layer on Al surface; that is, Al_2O_3 layer covers Al surface in sulfate solutions while it is removed in chloride solutions (Malik, 1991; Reboul, et al., 1997). Because of the presence of insulating Al_2O_3 layer in sulfate solutions, cementation of metal ions using only Al powder did not occur, while the addition of AC enhanced metal cementation using Al. In chloride solutions, there was no Al_2O_3 layer on Al, and this allowed the cementation of Pb^{2+} and Cd^{2+} on Al, but other metal ions like Co^{2+}, Ni^{2+}, and Zn^{2+} were not cemented.

For the cases of Co^{2+} and Ni^{2+}, the amounts of metal deposition are limited due to the competition with HER. Once Co^{2+} and Ni^{2+} are reductively cemented on Al, hydrogen evolution occurs with high reaction rates on the surface of cemented metals (e.g., Co and Ni), suppressing further deposition of these metal ions (Fig. 3-7(a)). Moreover, the surface area of Al is relatively small, which causes limited sites for Co and Ni deposition. Activated carbon, acting as an electron mediator, provides very large surface area for metal deposition (Fig. 3-7(b)), and this may cause larger amounts of Co and Ni deposition even with HER as shown in Table 3-2 and Fig. 3-7(b). As a result, the cementation of Ni^{2+} and Co^{2+} using Al as electron donor is enhanced with AC.

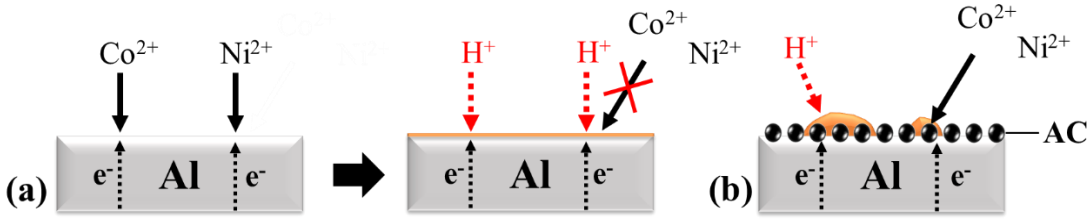


Fig. 3-7 Schematic diagram of Co^{2+} and Ni^{2+} cementation using (a) only Al and (b) AC/Al-mixture.

In the cases of Pb^{2+} and Cd^{2+}, metal deposition is not limited by the competition with HER, as the rate of HER on Pb and Cd is very slow as shown in Fig. 3-4. Because of this, Pb and Cd can be continuously cemented on Al surface without AC (Fig. 3-8(a)). With AC, however, HER occurs on AC surface with a higher rate (Moseley et al., 2018). As a result, electrons for cementing metal ions are

consumed by HER, thus suppressing metal deposition (Fig. 3-8(b)).

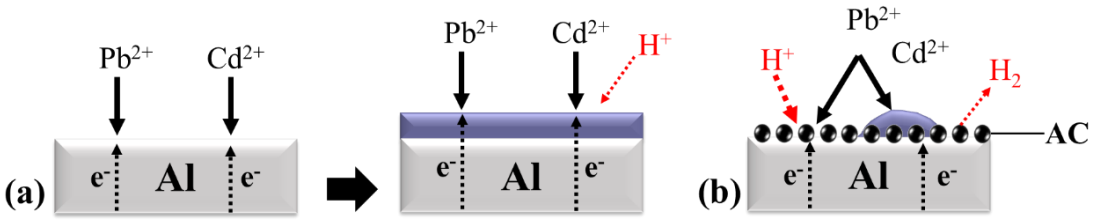


Fig. 3-8 Schematic diagram of Pb^{2+} and Cd^{2+} cementation using (a) only Al and (b) AC/Al-mixture.

In the case of Zn^{2+}, as discussed in a previous section, the limited cementation of Zn^{2+} is not due to the competition with HER but its slow reduction rate (Fig. 3-9(a)). When AC is added, AC attached on Al acts as sites for metal deposition. As a result, with AC, although HER occurs on AC surface, a larger surface area can be used for metal deposition (Fig. 3-9(b)), and this causes the enhancement of Zn cementation with AC.

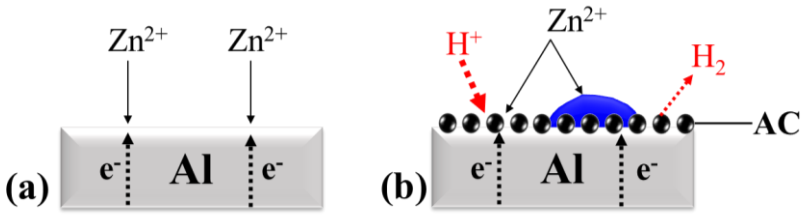


Fig. 3-9 Schematic diagram of Zn^{2+} cementation using (a) only Al and (b) AC/Al-mixture.

The results of the present chapter show that in both sulfate and chloride solutions, AC acts as an electron mediator from Al to metal ions, while its effects on metal cementation are depending on metal species and solutions. In sulfate solutions, metal cementation is enhanced by AC addition. On the other hand, in chloride solutions, AC suppressed the cementation of Pb and Cd, while it enhanced Co, Ni, and Zn cementation. When using only Al, Co^{2+}, Ni^{2+}, and Zn^{2+} cannot be recovered by cementation, while they can be recovered by applying AC/Al-mixture.

3.4 Summary

In this chapter, cementation experiments for Pb^{2+}, Cd^{2+}, Co^{2+}, Ni^{2+}, and Zn^{2+} using Al as an electron donor were carried out in chloride solutions and the effects of AC addition on the cementation were investigated. The results of SEM-EDS analysis for the solid products showed that metals were cemented on AC attached on Al, suggesting that AC act as electron mediator from Al to metal ions. The results of solution analysis showed that AC addition suppressed the cementation of Pb^{2+} and Cd^{2+}, while enhanced the cementation of Co^{2+}, Ni^{2+}, and Zn^{2+}.

References

Abdel-Aziz, M.H., El-Ashtoukhy, E.S.Z., Bassyouni, M., 2016. Recovery of Copper from Effluents by Cementation on Aluminum in a Multirotating Cylinder-Agitated Vessel. Metall. Mater. Trans. B Process Metall. Mater. Process. Sci. 47, 657–665. https://doi.org/10.1007/s11663-015-0467-y

Abdollahi, P., Yoozbashizadeh, H., Moradkhani, D., Behnian, D., 2015. A Study on Cementation Process of Lead from Brine Leaching Solution by Aluminum Powder. OALib 02, 1–6. https://doi.org/10.4236/oalib.1100990

Anacleto, A.L., Carvalho, J.R., 1996. Mercury cementation from chloride solutions using iron, zinc and aluminium. Miner. Eng. 9, 385–397. https://doi.org/10.1016/0892-6875(96)00025-8

Annamalai, V., Hiskey, J.B., Murr, L.E., 1978. The effects of kinetic variables on the structure of copper deposits cemented on pure aluminum discs: A scanning electron microscopic study. Hydrometallurgy 3, 163–180. https://doi.org/10.1016/0304-386X(78)90018-X

Annamalai, V., Murr, L.E., 1978. Effects of the source of chloride ion and surface corrosion patterns on the kinetics of the copper-aluminum cementation system. Hydrometallurgy 3, 249–263. https://doi.org/10.1016/0304-386X(78)90026-9

Artamonov, V. V., Moroz, D.R., Bykov, A.O., Artamonov, V.P., 2013. Experimental studies of cementation of tin in a dispersed form. Russ. J. Non-Ferrous Met. 54, 128–131. https://doi.org/10.3103/S1067821213020041

Beyene, B.B., Mane, S.B., Hung, C.H., 2018. Electrochemical Hydrogen Evolution by Cobalt (II) Porphyrins: Effects of Ligand Modification on Catalytica Activity, Efficiency and Overpotential. J. Electrochem. Soc. 165, H481–H487. https://doi.org/10.1149/2.0481809jes

Boyanov, B.S., Konareva, V. V., Kolev, N.K., 2004. Purification of zinc sulfate solutions from cobalt and nickel through activated cementation. Hydrometallurgy 73, 163–168. https://doi.org/10.1016/j.hydromet.2003.09.002

Chen, H.J., Lee, C., 1994. Effects of the Type of Chelating Agent and Deposit Morphology on the Kinetics of the Copper-Aluminum Cementation System. Langmuir 10, 3880–3886. https://doi.org/10.1021/la00022a079

Choi, S., Yoo, K., Alorro, R.D., Tabelin, C.B., 2020. Cementation of Co ion in leach solution using Zn powder followed by magnetic separation of cementation-precipitate for recovery of unreacted Zn powder. Miner. Eng. 145. https://doi.org/10.1016/j.mineng.2019.106061

Demirkran, N., Künkül, A., 2011. Recovering of copper with metallic aluminum. Trans. Nonferrous Met.

Soc. China (English Ed. 21, 2778–2782. https://doi.org/10.1016/S1003-6326(11)61123-0

Djokić, S.S., 1996. Cementation of Copper on Aluminum in Alkaline Solutions. J. Electrochem. Soc. 143, 1300–1305. https://doi.org/10.1149/1.1836634

Dönmez, B., Sevim, F., Saraç, H., 1999. Kinetic study of the cementation of copper from sulphate solutions onto a rotating aluminum disc. Hydrometallurgy 53, 145–154. https://doi.org/10.1016/S0304-386X(99)00042-0

Ekmekyapar, A., Tanaydin, M., Demirkiran, N., 2012. Investigation of copper cementation kinetics by rotating aluminum disc from the leach solutions containing copperions. Physicochem. Probl. Miner. Process. 48, 355–367. https://doi.org/10.5277/ppmp120203

Ezaki, H., Morinaga, M., Watanabe, S., 1993. Hydrogen overpotential for transition metals and alloys, and its interpretation using an electronic model. Electrochim. Acta 38, 557–564. https://doi.org/10.1016/0013-4686(93)85012-N

Farahmand, F., Moradkhani, D., Sadegh Safarzadeh, M., Rashchi, F., 2009. Optimization and kinetics of the cementation of lead with aluminum powder. Hydrometallurgy 98, 81–85. https://doi.org/10.1016/j.hydromet.2009.04.001

Gabe, D.R., 1997. The role of hydrogen in metal electrodeposition processes. J. Appl. Electrochem. 27, 908–915. https://doi.org/10.1023/A:1018497401365

Gao, X., Wu, L., Xu, Q., Tian, W., Li, Z., Kobayashi, N., 2018. Adsorption kinetics and mechanisms of copper ions on activated carbons derived from pinewood sawdust by fast H3PO4 activation. Environ. Sci. Pollut. Res. 25, 7907–7915. https://doi.org/10.1007/s11356-017-1079-7

Gouvea, L.R., Morais, C.A., 2007. Recovery of zinc and cadmium from industrial waste by leaching/cementation. Miner. Eng. 20, 956–958. https://doi.org/10.1016/j.mineng.2007.04.016

Gros, F., Baup, S., Aurousseau, M., 2011. Copper cementation on zinc and iron mixtures: Part 1: Results on rotating disc electrode. Hydrometallurgy 106, 119–126. https://doi.org/10.1016/j.hydromet.2010.12.011

Hickling, A., Salt, F.W., 1940. Studies in hydrogen overvoltage at high current densities: Part 1 - The influence of electrode material, current density, and time, in aqueous solution. Trans. Faraday Soc. 36, 1226–1235. https://doi.org/10.1039/TF9403601226

Hiromoto, S., Yamamoto, A., Maruyama, N., Somekawa, H., Mukai, T., 2008. Polarization behavior of pure magnesium under a controlled flow in a NaCl solution. Mater. Trans. 49, 1456–1461. https://doi.org/10.2320/matertrans.MRA2008011

Hong, H.S., Kim, G.H., Hong, M.H., Lee, S., Lee, J.C., 2014. Indium ion cementation onto aluminum plates in hydrochloric acid solutions: A kinetic perspective. Int. J. Mater. Res. 105, 177–182. https://doi.org/10.3139/146.111004

Hsu, Y.J., Tran, T., 1996. Selective removal of gold from copper-gold cyanide liquors by cementation using zinc. Miner. Eng. 9, 1–13. https://doi.org/10.1016/0892-6875(95)00127-1

Iida, T., Amano, Y., Machida, M., Imazeki, F., 2013. Effect of surface property of activated carbon on adsorption of nitrate ion. Chem. Pharm. Bull. 61, 1173–1177. https://doi.org/10.1248/cpb.c13-00422

Ivanov, I., 2004. Increased current efficiency of zinc electrowinning in the presence of metal impurities by addition of organic inhibitors. Hydrometallurgy 72, 73–78. https://doi.org/10.1016/S0304-386X(03)00129-4

Jeon, S., Tabelin, C.B., Takahashi, H., Park, I., Ito, M., Hiroyoshi, N., 2020. Enhanced cementation of gold via galvanic interactions using activated carbon and zero-valent aluminum: A novel approach to recover gold ions from ammonium thiosulfate medium. Hydrometallurgy 191, 105165. https://doi.org/10.1016/j.hydromet.2019.105165

Kadirvelu, K., Thamaraiselvi, K., Namasivayam, C., 2001. Removal of heavy metals from industrial wastewaters by adsorption onto activated carbon prepared from an agricultural solid waste. Bioresour. Technol. 76, 63–65. https://doi.org/10.1016/S0960-8524(00)00072-9

Karnib, M., Kabbani, A., Holail, H., Olama, Z., 2014. Heavy metals removal using activated carbon, silica and silica activated carbon composite. Energy Procedia 50, 113–120. https://doi.org/10.1016/j.egypro.2014.06.014

Ku, Y., Chen, C.H., 1992. Kinetic Study of Copper Deposition on Iron by Cementation Reaction. Sep. Sci. Technol. 27, 1259–1275. https://doi.org/10.1080/01496399208019424

Lee, H.Y., Kim, S.G., Oh, J.K., 1997. Cementation behavior of gold and silver onto Zn, Al, and Fe powders from acid thiourea solutions. Can. Metall. Q. 36, 149–155. https://doi.org/10.1179/cmq.1997.36.3.149

Li, W., Cochell, T., Manthiram, A., 2013. Activation of aluminum as an effective reducing agent by pitting corrosion for wet-chemical synthesis. Sci. Rep. 3, 1–7. https://doi.org/10.1038/srep01229

MacKinnon, D.J., Ingraham, T.R., 1971. Copper cementation on aluminum canning sheet. Can. Metall. Q. 10, 197–201. https://doi.org/10.1179/cmq.1971.10.3.197

MacKinnon, D.J., Ingraham, T.R., 1970. Kinetics of Cu(ll) cementation on a pure aluminum disc in acidic

sulphate solutions. Can. Metall. Q. 9, 443–448. https://doi.org/10.1179/cmq.1970.9.3.443

Makhloufi, L., Saidani, B., Hammache, H., 2000. Removal of lead ions from acidic aqueous solutions by cementation on iron. Water Res. 34, 2517–2524. https://doi.org/10.1016/S0043-1354(99)00405-4

Malik, F., 1991. A study of passive films on valve metals. Thin Solid Films 206, 345–348. https://doi.org/10.1016/0040-6090(91)90448-7

McCafferty, E., 2003. Sequence of steps in the pitting of aluminum by chloride ions. Corros. Sci. 45, 1421–1438. https://doi.org/10.1016/S0010-938X(02)00231-7

Moseley, P.T., Rand, D.A.J., Davidson, A., Monahov, B., 2018. Understanding the functions of carbon in the negative active-mass of the lead–acid battery: A review of progress. J. Energy Storage 19, 272–290. https://doi.org/10.1016/j.est.2018.08.003

Murr, L.E., Annamalai, V., 1978a. Characterization of copper nucleation and growth from aqueous solution on aluminum: A transmission electron microscopy study of copper cementation. Thin Solid Films 54, 189–195. https://doi.org/10.1016/0040-6090(78)90198-0

Murr, L.E., Annamalai, V., 1978b. An Electron Microscopic Study of Nucleation and Growth in Electrochemical Displacement Reactions: A Comparison of the Cu/Fe and Cu/AI Cementation Systems. Metall. Trans. B 9, 515–525. https://doi.org/10.1007/BF03257198

Natishan, P.M., O'Grady, W.E., 2014. Chloride Ion Interactions with Oxide-Covered Aluminum Leading to Pitting Corrosion: A Review. J. Electrochem. Soc. 161, C421–C432. https://doi.org/10.1149/2.1011409jes

Navarro, P., Alvarez, R., Vargas, C., Alguacil, F.J., 2004. On the use of zinc for gold cementation from ammoniacal-thiosulphate solutions. Miner. Eng. 17, 825–831. https://doi.org/10.1016/j.mineng.2004.02.001

Nelson, A., Wang, W., Demopoulos, G.P., Houlachi, G., 2000. Removal of cobalt from zinc electrolyte by cementation: A critical review. Miner. Process. Extr. Metall. Rev. 20, 325–356. https://doi.org/10.1080/08827500008547436

Ramdani, O., Chassaing, E., Canava, B., Grand, P.-P., Roussel, O., Lamirand, M., Rzepka, E., Etcheberry, A., Guillemoles, J.-F., Lincot, D., Kerrec, O., 2007. Electrochemical Cementation Phenomena on Polycrystalline Molybdenum Thin Films from Cu(II)–In(III)–Se(IV) Acidic Solutions. J. Electrochem. Soc. 154, D383. https://doi.org/10.1149/1.2740041

Reboul, M.C., Warner, T.J., Mayer, H., Barouk, B., 1997. A Ten Step Mechanism for the Pitting Corrosion of Aluminium Alloys. Corros. Rev. 15, 471–496.

https://doi.org/10.1515/CORRREV.1997.15.3-4.471

Recéndiz, A., González, I., Nava, J.L., 2007. Current efficiency studies of the zinc electrowinning process on aluminum rotating cylinder electrode (RCE) in sulfuric acid medium: Influence of different additives. Electrochim. Acta 52, 6880–6887. https://doi.org/10.1016/j.electacta.2007.04.112

Silwamba, M., Ito, M., Hiroyoshi, N., Tabelin, C.B., 2020a. Recovery of Lead and Zinc from Zinc Plant Leach Residues by Concurrent Dissolution-Cementation. Metals (Basel). 10, 531. https://doi.org/10.3390/met10040531

Silwamba, M., Ito, M., Hiroyoshi, N., Tabelin, C.B., Fukushima, T., Park, I., Jeon, S., Igarashi, T., Sato, T., Nyambe, I., Chirwa, M., Banda, K., Nakata, H., Nakayama, S., Ishizuka, M., 2020b. Detoxification of lead-bearing zinc plant leach residues from Kabwe, Zambia by coupled extraction-cementation method. J. Environ. Chem. Eng. 8, 104197. https://doi.org/10.1016/j.jece.2020.104197

Sulyman, M., Namiesnik, J., Gierak, A., 2017. Low-cost adsorbents derived from agricultural by-products/wastes for enhancing contaminant uptakes from wastewater: A review. Polish J. Environ. Stud. 26, 479–510. https://doi.org/10.15244/pjoes/66769

Tables, V.K., Electrode, S., Dekker, M., York, N., 2018. Electrochemical Series. Corros. Mater. 665–671. https://doi.org/10.31399/asm.hb.v13b.a0006542

Tak, Y., Kang, J., Choi, J., 2006. Electrochemical Properties of Metal Aluminum and Its Application. J. Korean Ind. Eng. Chem. 17, 335–342.

Uhlig, H.H., Revie, R.W., 1985. Corrosion and corrosion control: and introduction of corrosion science and engineering, 4th ed. A john wiley & sons, New York.

Vasil'ev, E.A., Darintseva, A.B., Naboichenko, S.S., 2010. Experimental investigations of cementation of indium. Russ. J. Non-Ferrous Met. 51, 268–272. https://doi.org/10.3103/S1067821210040024

Wang, Z., Chen, D., Chen, L., 2007. Application of fluoride to enhance aluminum cementation of gold from acidic thiocyanate solution. Hydrometallurgy 89, 196–206. https://doi.org/10.1016/j.hydromet.2007.07.005

Wei, W.Y., Lee, C., Chen, H.J., 1994. Modeling and Analysis of the Cementation Process on a Rotating Disk. Langmuir 10, 1980–1986. https://doi.org/10.1021/la00018a058

Wernick, S., 1932. The Electrodeposition of Cadmium from Cadmium Sulfate Solutions : Part I . The Effect of pH , Current Density , and Temperature on the Crystal Size of the Deposit , the Current Efficiency , and the Electrode Efficiency Ratio. Trans. Electrochem. Soc. 62, 27–38.

CHAPTER 4 – Enhanced cementation of Co^{2+} and Ni^{2+} from sulfate and chloride solutions using aluminum as electron donor and electron-conductive particles as electron mediator

4.1 Introduction

In previous chapters 2 and 3, cementation of Cd^{2+}, Co^{2+}, Ni^{2+}, and Zn^{2+} from sulfate solutions and Pb^{2+}, Cd^{2+}, Co^{2+}, Ni^{2+}, and Zn^{2+} from chloride solutions using Al and AC were investigated. The results of surface analysis for the cementation products have suggested that AC attached on the Al surface acted as an electron mediator from Al to noble metal ions, even in the presence of a surface Al_2O_3 layer (Jeon et al., 2020b). If this is the case and the essential role of AC is just as an electron mediator, enhanced cementation would occur even when AC is replaced by other (semi)conductors. On the other hand, as AC is a porous material and has a very large specific surface area, not only the electroconductivity but also large adsorption capacity of AC for metal ions may play an important role in the enhanced cementation using the AC/Al-mixture. If this is the case, replacing AC to another conductor with a low specific surface area cannot enhance the cementation using Al as an electron donor.

Cobalt (Co) and nickel (Ni) represent important strategic resources in the world market and their use is rapidly growing for renewable energy technologies and rechargeable battery productions, and the importance of the development of technologies for recovering and purifying Co and Ni is continuously increasing (*Global EV Outlook 2020*, 2020; Lee et al., 2011; Liu et al., 2014; Negem et al., 2019; Zeng et al., 2014; R. Zhang et al., 2018). Therefore, this chapter aims to investigate whether the AC could be replaced with other (semi)conductors for recovery of Co and Ni from sulfate and chloride solutions. Titanium dioxide (TiO_2) was selected for a semiconductor because of its nontoxic, nonreactive, and high chemical stability, while silicon dioxide (SiO_2) was chosen for a nonconductor to clarify the mechanism(s) of the enhanced cementation using the mixture of conductor and Al (Hext et al., 2005; Nesbitt et al., 2004).

In this chapter, batch-type cementation experiments were conducted using Al as an electron donor to recover Co^{2+} and Ni^{2+} from sulfate and chloride solutions and the effects of the addition of AC, TiO_2, or SiO_2 on the recoveries of these metal ions were investigated. Surface analysis (Auger electron spectroscopy (AES)) for the cementation products was also conducted to elucidate the cementation mechanism.

4.2 Materials and methods

4.2.1 Materials (Al, AC, TiO_2, and SiO_2)

As an electron donor, Al powder (99.99%, Wako Pure Chemical Industries, Ltd., Osaka, Japan) was used, and AC powder (99.99%, Wako Pure Chemical Industries, Ltd., Osaka, Japan), TiO_2 powder (99.0%, rutile form, Wako Pure Chemical Industries, Ltd., Osaka, Japan), and SiO_2 powder (99.0%, Wako pure Chemical Industries, Ltd., Osaka, Japan) were used as an electron mediator. Particle size distribution of these materials, measured by laser diffraction (Microtrac® MT3300SX, Nikkiso Co. Ltd., Osaka, Japan), is shown in Fig. 4-1. The median diameters (D_{50}) of Al, AC, TiO_2, and SiO_2 were 21.3, 38.1, 8.5, and 21.2 µm, respectively.

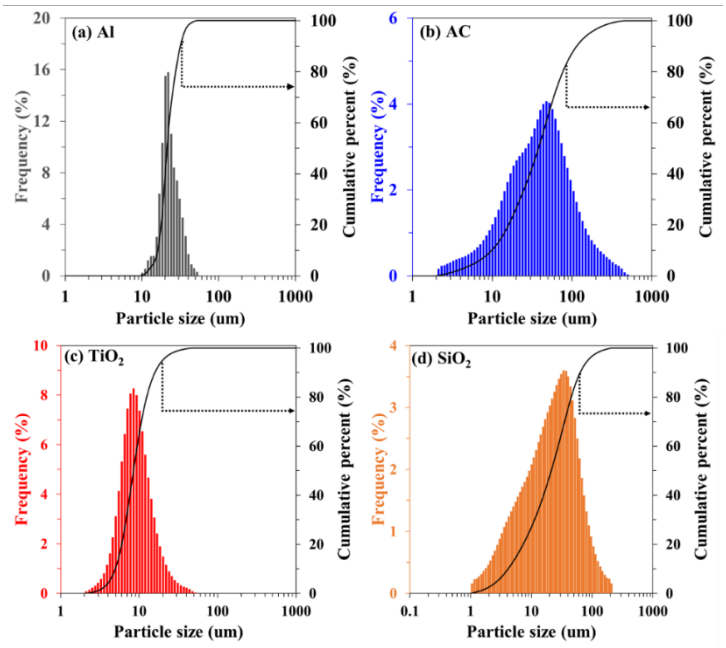


Fig. 4-1 Particle size distribution for (a) aluminum (Al), (b) activated carbon (AC), (c) titanium dioxide (TiO_2), and (d) silicon dioxide (SiO_2) used in this chapter.

4.2.2 Recovery of Co^{2+} and Ni^{2+} from sulfate and chloride solutions

4.2.2.1 Preparation of Co^{2+} and Ni^{2+} solutions

The cementation products were collected by vacuum filtration (pore size: 0.2 µm, Merck Millipore, USA), rinsed using DI water thoroughly, dried in a vacuum oven at 40 °C for 24 h, and analyzed by scanning electron microscopy with energy-dispersive X-ray spectroscopy (SEM-EDS, JSM-IT200^{TM}, JEOL Co., Ltd., Japan). The sulfate solutions containing 1 mM metal ions were

prepared by dissolving $CoSO_4 \cdot 7H_2O$ (99.0%, Wako Pure Chemical Industries, Ltd., Osaka, Japan) or $NiSO_4 \cdot 6H_2O$ (99.0%, Wako Pure Chemical Industries, Ltd., Osaka, Japan) in deionized (DI) water (18 MΩ·cm, Mill-Q® Integral Water Purification System, Merck Millipore, USA). For the preparation of 1 mM metal chloride solutions, $CoCl_2 \cdot 6H_2O$ (99.0%, Kishida Chemical Co., Ltd., Osaka, Japan), or NiCl2·6H2O (98.0%, Kishida Chemical Co., Ltd., Osaka, Japan) was dissolved in DI water. The initial pH of sulfate and chloride solutions was adjusted to 4.0 using 1 M H_2SO_4 and HCl (Wako Pure Chemical Industries, Ltd., Osaka, Japan), respectively. The total concentration of SO_4^{2-} and Cl^- were fixed to 0.1 M using Na_2SO_4 (99.0%, Wako Pure Chemical Industries, Ltd., Osaka, Japan) and NaCl (99.5%, Wako Pure Chemical Industries, Ltd., Osaka, Japan) to normalize their effects on experiments.

4.2.2.2 Cementation tests

The cementation tests were carried out in a 50 mL Erlenmeyer flask using a thermostat water bath shaker (Cool bath shaker, ML-10F, Taitec Corporation, Saitama, Japan) with 40 mm of shaking amplitude and 120 min^{-1} of shaking frequency at 25 °C for 24 h. (Note that these parameters were selected based on our preliminary experiments). Ten milliliters of the prepared solution were added to the flask, then ultrapure nitrogen gas (99.9%) was introduced for 15 min before experiments to maintain an oxygen-free environment. One-tenth gram of Al powder and/or a predetermined amount (0.01, 0.05, 0.1, 0.2, 0.4 g) of electron mediators (i.e., AC, TiO_2, and SiO_2) were added to the solution. Ultrapure nitrogen gas (99.9%) was further introduced to the flask for 5 min, then the flask was tightly capped with a rubber cap and sealed with parafilm, and an experiment was conducted. After 24 h, the suspension was filtered using a syringe-driven membrane filter (pore size: 0.2 μm, LMS Co., Ltd., Tokyo, Japan); final pH of the filtrate was measured. The filtrate was diluted with 0.1 M HNO_3, and the concentrations of metal ions were analyzed by inductively coupled plasma atomic emission spectroscopy (ICP-AES, ICPE-9820, Shimadzu Corporation, Kyoto, Japan). The recovery efficiency of Co^{2+} and Ni^{2+} was calculated based on Eq. 4-1:

$$R = \frac{C_i - C_f}{C_i} x\ 100 \qquad (4\text{-}1)$$

where Ci and Cf are the initial and final concentrations of metal ions, respectively.

4.2.2.3 Surface analysis

The solid products obtained by filtration were washed 5 times with DI water, dried in a vacuum oven at 40 °C for 24 h, and then analyzed by Auger electron spectroscopy (AES) using JAMP-9500F (JEOL Co., Ltd., Tokyo, Japan). The dried residue was mounted on an AES holder using conductive carbon tape. The analysis was conducted under the following conditions: ultrahigh vacuum condition, ~1×10^{-7} Pa; probe energy, 10 kV; and probe current, 19.7 nA. The spectra were analyzed by using Spectra Investigator AES software.

4.3 Results and discussion

4.3.1 Recovery of Co^{2+} and Ni^{2+}

4.3.1.1 Recovery of Co^{2+} and Ni^{2+} from sulfate solutions

Cementation experiments for recovering Co^{2+} and Ni^{2+} from sulfate solutions (initial pH = 4) were conducted for 24 h using Al powder as an electron donor, and the effects of the dosage of electron mediators (AC, TiO_2, and SiO_2) on the efficiency of Co and Ni recoveries were investigated. To access the adsorption of Co^{2+} and Ni^{2+} on the electron mediators, experiments without Al were also conducted.

Figures 4-2(a) – (c) and 4-3(a) – (c) show the Co and Ni recovery efficiencies and final pH as a function of SiO_2, AC, and TiO_2 dosages, respectively. In all experiments, final pH was in the range from 5.1 to 5.6, at which Co^{2+} and Ni^{2+} do not precipitate as their hydroxide (Fig. 4-4).

As shown in Figs. 4-2(a) and 4-3(a), without Al, the efficiencies of Co and Ni recovery were almost 0% at any dosage of SiO_2, suggesting that there was no adsorption of Co^{2+} and Ni^{2+} on the SiO_2 surface. Even with Al, the Co and Ni recovery efficiencies were also almost 0% regardless of SiO_2 dosage, suggesting that cementation of Co^{2+} and Ni^{2+} using Al as an electron donor did not occur. This may be due to the presence of an Al_2O_3 layer covering the Al surface, which inhibits the electron transportation from Al to Co^{2+} and Ni^{2+} (Chen and Lee, 1994; Demirkran and Künkül, 2011). Because the cementation did not occur regardless of SiO_2 addition, the results also confirm that physical breakage of the Al_2O_3 layer due to the collision of SiO_2 to Al powder in the shaking flask did not cause enhanced cementation. As shown in Figs. 4-2(b) and 4-3(b), even without Al, the recovery efficiency of Co^{2+} and Ni^{2+} increased with increasing AC dosage, suggesting that these metal ions adsorbed on the AC surface. It has been reported that there are functional groups such as carboxyl and carbonyl groups on the surface of the activated carbon and they act as adsorption sites to metal ions through the reaction described by Eq. 4-2 (Gao et al., 2018; Karnib et al., 2014; Sulyman et al., 2017). Increase in final pH indicates that not only Co^{2+} and Ni^{2+}, but also proton (H^+) adsorbed on AC (Burakov et al., 2018; Dil et al., 2016).

$$M^{n+} + n(\text{–COOH}) \leftrightarrow (\text{–COO})nM + nH^+ \quad (4\text{-}2)$$

In the range between 0.05 to 0.2 g AC dosage, recovery efficiency was much higher with Al than without Al; at 0.1 g AC dosage, the efficiency was 56% for Co and 61% for Ni with Al, while it was 31% for Co and 43% for Ni without Al. The difference of metal recovery efficiency between either with or without Al was 25% for Co and 18% for Ni, which cannot be ignored as an experimental error. This suggests that the addition of AC enhances Co and Ni cementation using Al as an electron donor (Eqs. 4-3 and 4-4), even though the Al_2O_3 layer remained on the Al surface.

$$3\ Co^{2+}_{(aq)} + 2Al^{0}_{(s)} \rightarrow 3\ Co^{0}_{(s)} + 2Al^{3+}_{(aq)} \quad (4\text{-}3)$$

$$3\ Ni^{2+}_{(aq)} + 2Al^{0}_{(s)} \rightarrow 3\ Ni^{0}_{(s)} + 2Al^{3+}_{(aq)} \quad (4\text{-}4)$$

Following these equations, it is expected that the stoichiometric amount of Al dissolves when cementation occurs; however, the dissolved Al concentration after cementation was less than 3 ppm, which means that most of the Al^{3+} were precipitated as Al-(oxy)hydroxide (Abdollahi et al., 2015; Park et al., 2020).

As shown in Figs. 4-2(c) and 4-3(c), the recovery efficiency of Co^{2+} and Ni^{2+} without Al was almost 0% regardless of TiO_2 dosage, indicating that TiO_2 has no ability to adsorb Co^{2+} and Ni^{2+}. When 0.1 g of Al was used together with TiO_2, the recovery efficiency continuously increased with increasing TiO_2 dosage and reached the maximum value of 52% for Co and 71% for Ni with 0.4 g TiO_2. As already discussed, Co^{2+} and Ni^{2+} do not precipitate as hydroxides at the pH ranges observed in this series of experiments; the enhanced recovery of Co^{2+} and Ni^{2+} with TiO_2 and Al suggests that the addition of TiO_2 enhanced the cementation of Co^{2+} and Ni^{2+} by Al (Eqs. 4-3 and 4-4). It was also confirmed that the dissolved Ti concentrations were below detection limit, indicating that TiO_2 is stable enough to be used as an agent to enhance cementation of Co^{2+} and Ni^{2+} with Al in the sulfate solution.

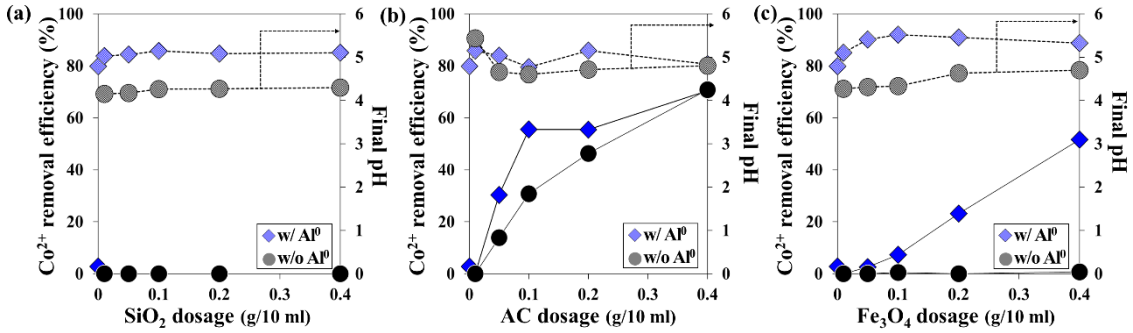


Fig. 4-2 The effects of (a) SiO_2, (b) AC, and (c) TiO_2 dosages on the recovery efficiency of Co^{2+} and final pH in sulfate solutions at initial pH 4.0 for 24 h.

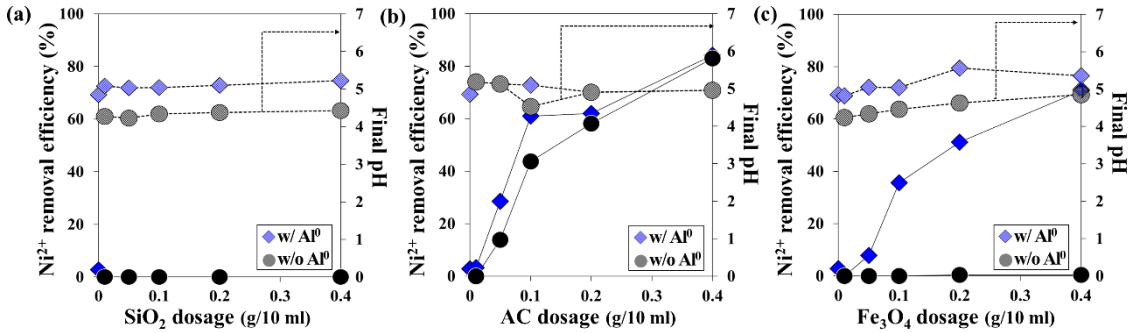


Fig. 4-3 The effects of (a) SiO_2, (b) AC, and (c) TiO_2 dosages on the recovery efficiency of Ni^{2+} and final pH in sulfate solutions at initial pH 4.0 for 24 h.

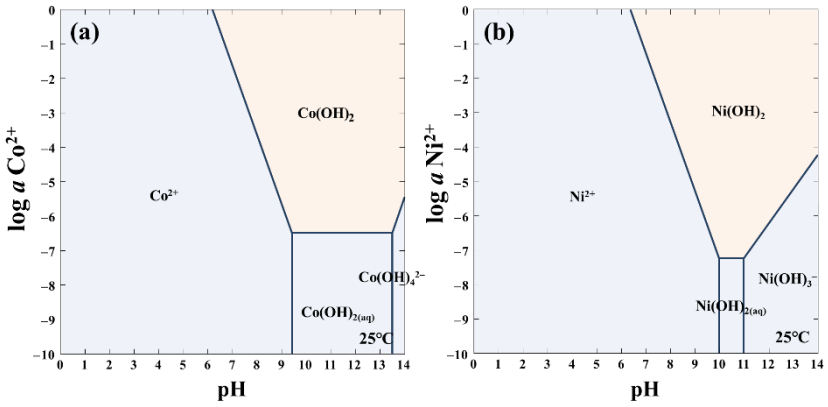


Fig. 4-4 The activity–pH diagram for 1 mM (a) Co^{2+} and (b) Ni^{2+} species with 0.1 M SO_4^{2-} at 25 °C (created using the GWB Professional Ver. 12.0.3 software).

4.3.2 Removal of metal ions from chloride solutions

4.3.1.1 Recovery of Co^{2+} and Ni^{2+} from chloride solutions

Cementation experiments for recovering Co^{2+} and Ni^{2+} from chloride solutions (initial pH = 4) were conducted for 24 h using Al powder as an electron donor, and the effects of the dosage of electron mediators (AC, TiO_2, and SiO_2) on the efficiency of Co and Ni recovery were investigated. To access the adsorption of Co^{2+} and Ni^{2+} on the mediators, experiments without Al were also conducted. Figures 4-5(a) – (c) and 4-6(a) – (c) show the Co and Ni recovery efficiencies and final pH as a function of AC, TiO_2, and SiO_2 dosages, respectively.

As discussed in previous chapter 3, with only Al, the recovery efficiency of Co^{2+} and Ni^{2+} was 0% due to the low hydrogen overpotential on Co and Ni. Hydrogen overpotential is the voltage required for hydrogen evolution reaction (HER) on a metal surface. If hydrogen overpotential is low, the reduction of H^+ to H_2 (Eq. 4-5) occurs easily because the required voltage for HER is low.

$$2\ H^+ + 2\ e^- \rightarrow H_2 \qquad (4\text{-}5)$$

In the case of Co and Ni, the hydrogen overpotential is quite low (i.e., –0.3 to –0.4 V for Co; (Boyanov et al., 2004; Ezaki et al., 1993; Yan et al., 2018; W. Zhang et al., 2018), and –0.3 V for Ni; (Ezaki et al., 1993; Hickling and Salt, 1940)), so it is expected that even if the small amount of Co^{2+} and Ni^{2+} is deposited (Eqs. 4-3 and 4-4), the deposited Co and Ni is easily dissolved because of the HER on deposited Co and Ni surface. Therefore, the cementation of Co^{2+} and Ni^{2+} was suppressed even though the standard electrode potential of Al is lower than Co and Ni (redox pair: Co^{2+}/Co (–0.28 V vs. SHE) and redox pair: Ni^{2+}/Ni (–0.26 V vs. SHE) > Al^{3+}/Al (–1.67 V vs. SHE)).

As shown in Figs. 4-5(a) and 4-6(a), when SiO_2 was used as an electron mediator, the recovery

efficiencies of Co^{2+} and Ni^{2+} both with and without Al were almost 0%. This indicates that in chloride solutions, Co^{2+} and Ni^{2+} were not adsorbed on SiO_2, and the cementation of Co and Ni with Al did not occur.

The results shown in Figs. 4-5(b) and 4-6(b) suggest that adsorption of Co^{2+} and Ni^{2+} on AC occurred in chloride solutions, because in the absence of Al, recovery efficiencies of these ions increased with increasing AC dosage. As in sulfate solutions, in the presence of AC, enhancement of metal ion recovery by Al addition was confirmed (Figs. 4-5(b) and 4-6(b)); e.g., at 0.1 g AC dosage, by adding Al, the efficiency increased from 57% to 70% for Co, and it increased from 57% to 70% for Ni. This suggests that enhanced cementation of these metal ions with AC occurred in chloride solutions.

Figures 4-5(c) and 4-6(c) show that the efficiencies of Co^{2+} and Ni^{2+} recovery in the absence of Al were almost 0% at any dosage of TiO_2, suggesting that adsorption of these ions on TiO_2 can be ignored. In the presence of Al, the efficiencies of Co^{2+} and Ni^{2+} recovery increased with increasing TiO_2 dosage; without TiO_2, the efficiencies were almost 0% for both Co and Ni while they increased to 61% for Co^{2+} and 99.9% for Ni^{2+} when 0.4 g TiO_2 was added. These results suggest clearly that addition of TiO_2 enhanced the cementation of Co and Ni by using Al as an electron donor, and indicated that AC can be replaced with TiO_2 even if its surface area is lower than AC (Andersson et al., 2007; Inada et al., 2009; Sulyman et al., 2017).

Compared to the result obtained in sulfate solution, the recovery efficiency was about 10–20% for Co and about 30–50% for Ni higher in chloride solution, which is presumed as the following reasons: (1) the more active electron transfer occurs through TiO_2 attached on Al surface because of the removal of Al_2O_3 layer (Annamalai and Murr, 1978; Hutt et al., 2002; Wei et al., 1994), (2) Cl^- promotes the exchange current between the anode and cathode surfaces and catalyzes the cementation reaction (Hong et al., 2014; Murr and Annamalai, 1978; Vasil'ev et al., 2010), and/or (3) the passivation of cemented Co and Ni surface would be prevented by Cl^- (Annamalai et al., 1978; Hong et al., 2014; Vasil'ev et al., 2010). In the case of Co and Ni, hydrogen overpotential is changed depending on the deposited surface (Xu et al., 2006), so it speculated that the hydrogen overpotential of Co increases on the AC and TiO_2 surfaces, and thus the cementation of Co^{2+} and Ni^{2+} was enhanced when using AC/Al and TiO_2/Al-mixture compared to Al only.

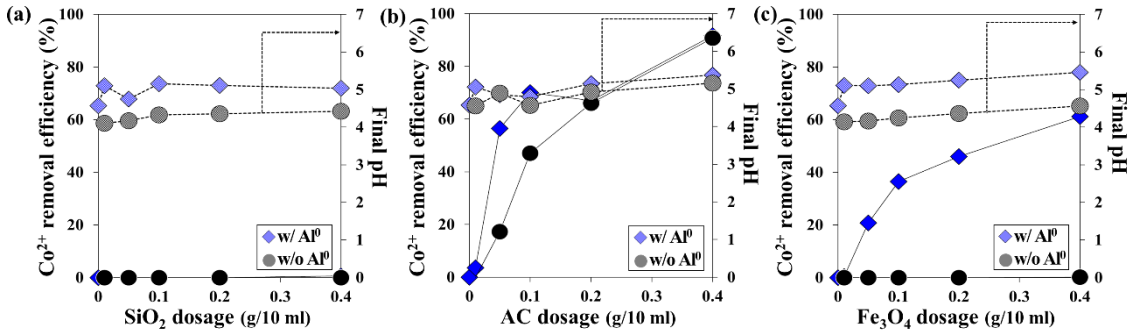


Fig. 4-5 The effects of (a) SiO_2, (b) AC, and (c) TiO_2 dosages on the recovery efficiency of Co^{2+} and final pH in chloride solutions at initial pH 4.0 for 24 h.

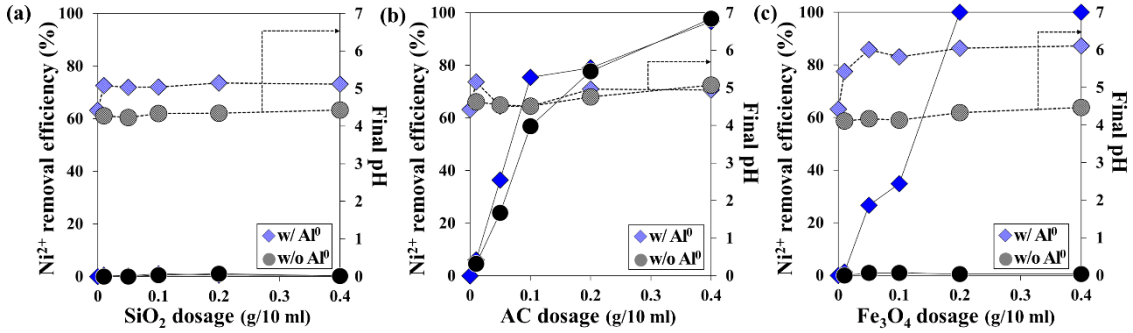


Fig. 4-6 The effects of (a) SiO_2, (b) AC, and (c) TiO_2 dosages on the recovery efficiency of Ni^{2+} and final pH in chloride solutions at initial pH 4.0 for 24 h.

4.3.2 Surface analysis of deposited Co and Ni

To investigate the elemental compositions of the deposited Co and Ni, residues obtained from the Co^{2+} and Ni^{2+} recovery experiment from chloride solutions using 0.4 g of TiO_2 and 0.1 g of Al were analyzed by AES. Figures 4-7 and 4-8 show the AES photomicrographs (Figs. 4-7(a) and 4-8 (a)) and scan results of Co (Figs. 4-7(b) and (c)) and Ni (Figs. 4-8(b) and (c)). In both AES photomicrographs, many small gray particles and light particles are attached together onto the surface of the dark particle. The wide AES spectra of the dark particle (point 1 in Figs 4-7(b) and 8 (b)) show strong signals of Al and O, indicating that these particles are assigned to Al powder. The small gray particles correspond to TiO_2 because of Ti and O signals observed at point 2 in Figs. 4-7(b) and 4-8(b). Meanwhile, light particles are observed at point 3 in Figs. 4-7(b) and 4-8(b) are most likely the deposited Co and Ni, respectively.

To identify the elemental composition of the deposited Co and Ni, the narrow AES spectra in the range of 750–785 eV for Co and 830–858 eV for Ni were analyzed (Figs. 4-7(c) and 4-8(c)). These

spectra were fitted using reference spectra of Co, CoO, and Co3O4 for Co composition, and Ni and NiO for Ni composition. Fitting results indicate that the deposited Co consisted of metallic Co (93.1%) and CoO (6.9%), while the deposited Ni was composed of metallic Ni (86.2%) and NiO (13.8%). The analysis range of Auger is 0.3–5 nm, which is a near-surface analysis (Scherer, 2020), so it is speculated that only the outermost surfaces of deposited Co and Ni were oxidized due to the oxidation of metallic Co and Ni during the dry process. These results suggest that Co and Ni were deposited on TiO_2 particles attached on the Al surface and TiO_2 can act as an electron mediator from Al to Co^{2+} and Ni^{2+}, even if the Al_2O_3 layer remains on the Al surface, and showed that physical separation (i.e., ultra-sonification) could be applied as the post-cementation process for Co/Ni–TiO_2 particle and Al separation. Afterward, it is expected that only Co and Ni would be dissolved in acidic aqueous solutions, while TiO_2 would not be dissolved because TiO_2 is more stable than Co and Ni.

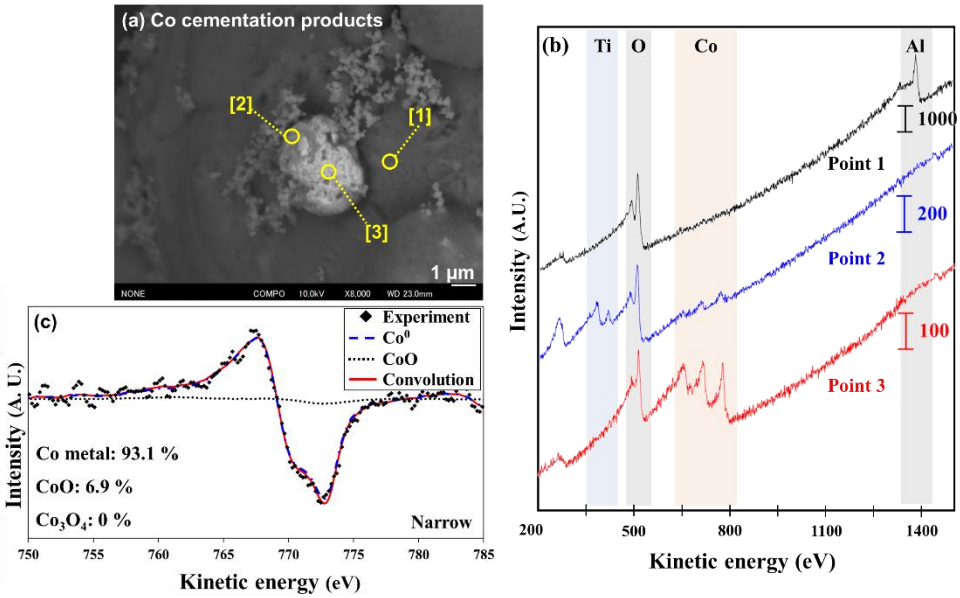


Fig. 4-7 Auger electron spectroscopy (AES) results of the residue obtained after cementation of Co^{2+} from chloride solution using TiO_2/Al: (a) photomicrograph, (b) wide scan energy spectrum of each point, and (c) the narrow scan energy spectrum of the Co peak with fitting spectra of Co, CoO, and Co_3O_4.

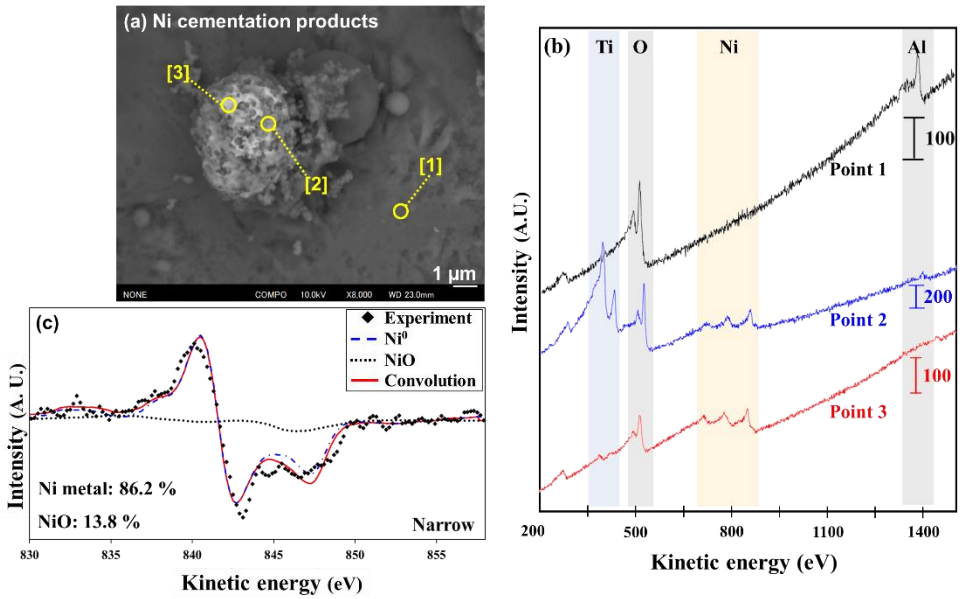


Fig. 4-8 Auger electron spectroscopy (AES) results of the residue obtained after cementation of Ni^{2+} from chloride solution using TiO_2/Al: (a) photomicrograph, (b) wide scan energy spectrum of each points, and (c) the narrow scan energy spectrum of the Ni peak with fitting spectra of Ni and NiO.

4.4 Summary

This chapter investigated whether activated carbon (AC) could be replaced with other electron mediators such as TiO_2 and SiO_2 for the enhanced cementation of Co^{2+} and Ni^{2+} using aluminum (Al) in sulfate and chloride solutions. In summary, the Co^{2+} and Ni^{2+} recovery efficiencies using Al in sulfate and chloride solutions were almost 0% because of the presence of an Al_2O_3 layer on an Al surface and low hydrogen overpotential on Co and Ni.

The adsorption of Co^{2+} and Ni^{2+} occurred when using only AC, while it did not occur when using only TiO_2 and SiO_2. When using an AC/Al-mixture or TiO_2/Al-mixture, the Co^{2+} and Ni^{2+} recovery efficiencies from sulfate and chloride solutions were enhanced compared to using Al, AC, TiO_2, and SiO_2/Al- mixture. From the results of AES analysis, Co and Ni were mostly deposited as zero-valent forms on TiO_2 attached on Al surface. This work establishes that using a conductor (AC) or a semiconductor (TiO_2) could enhance the recovery of Co^{2+} and Ni^{2+} by Al-based cementation even under mild conditions (e.g., low temperature, 25 °C; mild pH conditions, pH 4–5; no Cl^- or a low concentration). Moreover, it is expected that other conductive materials could also be used for the removal and/or recovery of metal ions using Al.

References

Abdel-Aziz, M.H., El-Ashtoukhy, E.S.Z., Bassyouni, M., 2016. Recovery of Copper from Effluents by Cementation on Aluminum in a Multirotating Cylinder-Agitated Vessel. Metall. Mater. Trans. B Process Metall. Mater. Process. Sci. 47, 657–665. https://doi.org/10.1007/s11663-015-0467-y

Abdollahi, P., Yoozbashizadeh, H., Moradkhani, D., Behnian, D., 2015. A Study on Cementation Process of Lead from Brine Leaching Solution by Aluminum Powder. OALib 02, 1–6. https://doi.org/10.4236/oalib.1100990

Andersson, M., Kiselev, A., Österlund, L., Palmqvist, A.E.C., 2007. Microemulsion-mediated room-temperature synthesis of high-surface-area rutile and its photocatalytic performance. J. Phys. Chem. C 111, 6789–6797. https://doi.org/10.1021/jp070284a

Annamalai, V., Hiskey, J.B., Murr, L.E., 1978. The effects of kinetic variables on the structure of copper deposits cemented on pure aluminum discs: A scanning electron microscopic study. Hydrometallurgy 3, 163–180. https://doi.org/10.1016/0304-386X(78)90018-X

Annamalai, V., Murr, L.E., 1978. Effects of the source of chloride ion and surface corrosion patterns on the kinetics of the copper-aluminum cementation system. Hydrometallurgy 3, 249–263. https://doi.org/10.1016/0304-386X(78)90026-9

Artamonov, V. V., Moroz, D.R., Bykov, A.O., Artamonov, V.P., 2013. Experimental studies of cementation of tin in a dispersed form. Russ. J. Non-Ferrous Met. 54, 128–131. https://doi.org/10.3103/S1067821213020041

Boisvert, L., Turgeon, K., Boulanger, J., Bazin, C., Houlachi, G., 2020. Recovery of Cobalt from the Residues of an Industrial Zinc Refinery. Metals (Basel). 10, 1553. https://doi.org/10.3390/met10111553

Boyanov, B., Konareva, V., Kolev, N., 2004. Removal of cobalt and nickel from zinc sulphate solutions using activated cementation. J. Min. Metall. Sect. B Metall. 40, 41–55. https://doi.org/10.2298/jmmb0401041b

Burakov, A.E., Galunin, E. V., Burakova, I. V., Kucherova, A.E., Agarwal, S., Tkachev, A.G., Gupta, V.K., 2018. Adsorption of heavy metals on conventional and nanostructured materials for wastewater treatment purposes: A review. Ecotoxicol. Environ. Saf. 148, 702–712. https://doi.org/10.1016/j.ecoenv.2017.11.034

Chen, H.J., Lee, C., 1994. Effects of the Type of Chelating Agent and Deposit Morphology on the Kinetics of the Copper-Aluminum Cementation System. Langmuir 10, 3880–3886.

https://doi.org/10.1021/la00022a079

Choi, S., Yoo, K., Alorro, R.D., Tabelin, C.B., 2020. Cementation of Co ion in leach solution using Zn powder followed by magnetic separation of cementation-precipitate for recovery of unreacted Zn powder. Miner. Eng. 145. https://doi.org/10.1016/j.mineng.2019.106061

Demirkran, N., Künkül, A., 2011. Recovering of copper with metallic aluminum. Trans. Nonferrous Met. Soc. China (English Ed. 21, 2778–2782. https://doi.org/10.1016/S1003-6326(11)61123-0

Dil, E.A., Ghaedi, M., Ghaedi, A.M., Asfaram, A., Goudarzi, A., Hajati, S., Soylak, M., Agarwal, S., Gupta, V.K., 2016. Modeling of quaternary dyes adsorption onto ZnO-NR-AC artificial neural network: Analysis by derivative spectrophotometry. J. Ind. Eng. Chem. 34, 186–197. https://doi.org/10.1016/j.jiec.2015.11.010

Djokić, S.S., 1996. Cementation of Copper on Aluminum in Alkaline Solutions. J. Electrochem. Soc. 143, 1300–1305. https://doi.org/10.1149/1.1836634

Ekmekyapar, A., Tanaydin, M., Demirkiran, N., 2012. Investigation of copper cementation kinetics by rotating aluminum disc from the leach solutions containing copperions. Physicochem. Probl. Miner. Process. 48, 355–367. https://doi.org/10.5277/ppmp120203

Ezaki, H., Morinaga, M., Watanabe, S., 1993. Hydrogen overpotential for transition metals and alloys, and its interpretation using an electronic model. Electrochim. Acta 38, 557–564. https://doi.org/10.1016/0013-4686(93)85012-N

Farahmand, F., Moradkhani, D., Sadegh Safarzadeh, M., Rashchi, F., 2009. Optimization and kinetics of the cementation of lead with aluminum powder. Hydrometallurgy 98, 81–85. https://doi.org/10.1016/j.hydromet.2009.04.001

Gao, X., Wu, L., Xu, Q., Tian, W., Li, Z., Kobayashi, N., 2018. Adsorption kinetics and mechanisms of copper ions on activated carbons derived from pinewood sawdust by fast H3PO4 activation. Environ. Sci. Pollut. Res. 25, 7907–7915. https://doi.org/10.1007/s11356-017-1079-7

Global EV Outlook 2020, 2020. , International Energy Agency. OECD, Paris, France. https://doi.org/10.1787/d394399e-en

Hext, P.M., Tomenson, J.A., Thompson, P., 2005. Titanium dioxide: Inhalation toxicology and epidemiology. Ann. Occup. Hyg. 49, 461–472. https://doi.org/10.1093/annhyg/mei012

Hickling, A., Salt, F.W., 1940. Studies in hydrogen overvoltage at high current densities: Part 1 - The influence of electrode material, current density, and time, in aqueous solution. Trans. Faraday Soc. 36, 1226–1235. https://doi.org/10.1039/TF9403601226

Hong, H.S., Kim, G.H., Hong, M.H., Lee, S., Lee, J.C., 2014. Indium ion cementation onto aluminum plates in hydrochloric acid solutions: A kinetic perspective. Int. J. Mater. Res. 105, 177–182. https://doi.org/10.3139/146.111004

Hutt, D.A., Liu, C., Conway, P.P., Whalley, D.C., Mannan, S.H., 2002. Electroless nickel bumping of aluminum bondpads - Part II: Electroless nickel plating. IEEE Trans. Components Packag. Technol. 25, 98–105. https://doi.org/10.1109/6144.991181

Inada, M., Mizue, K., Enomoto, N., Hojo, J., 2009. Synthesis of rutile TiO2 with high specific surface area by self-hydrolysis of TiOCl2 in the presence of SDS. J. Ceram. Soc. Japan 117, 819–822. https://doi.org/10.2109/jcersj2.117.819

Jeon, S., Tabelin, C.B., Park, I., Nagata, Y., Ito, M., Hiroyoshi, N., 2020a. Ammonium thiosulfate extraction of gold from printed circuit boards (PCBs) of end-of-life mobile phones and its recovery from pregnant leach solution by cementation. Hydrometallurgy 191, 105214. https://doi.org/10.1016/j.hydromet.2019.105214

Jeon, S., Tabelin, C.B., Takahashi, H., Park, I., Ito, M., Hiroyoshi, N., 2020b. Enhanced cementation of gold via galvanic interactions using activated carbon and zero-valent aluminum: A novel approach to recover gold ions from ammonium thiosulfate medium. Hydrometallurgy 191, 105165. https://doi.org/10.1016/j.hydromet.2019.105165

Karnib, M., Kabbani, A., Holail, H., Olama, Z., 2014. Heavy metals removal using activated carbon, silica and silica activated carbon composite. Energy Procedia 50, 113–120. https://doi.org/10.1016/j.egypro.2014.06.014

Lee, B.-R., Noh, H.-J., Myung, S.-T., Amine, K., Sun, Y.-K., 2011. High-Voltage Performance of Li[Ni[sub 0.55]Co[sub 0.15]Mn[sub 0.30]]O[sub 2] Positive Electrode Material for Rechargeable Li-Ion Batteries. J. Electrochem. Soc. 158, A180. https://doi.org/10.1149/1.3525247

Li, W., Cochell, T., Manthiram, A., 2013. Activation of aluminum as an effective reducing agent by pitting corrosion for wet-chemical synthesis. Sci. Rep. 3, 1–7. https://doi.org/10.1038/srep01229

Liu, S., Xiong, L., He, C., 2014. Long cycle life lithium ion battery with lithium nickel cobalt manganese oxide (NCM) cathode. J. Power Sources 261, 285–291. https://doi.org/10.1016/j.jpowsour.2014.03.083

Murr, L.E., Annamalai, V., 1978. An Electron Microscopic Study of Nucleation and Growth in Electrochemical Displacement Reactions: A Comparison of the Cu/Fe and Cu/AI Cementation Systems. Metall. Trans. B 9, 515–525. https://doi.org/10.1007/BF03257198

Negem, M., Nady, H., El-Rabiei, M.M., 2019. Nanocrystalline nickel–cobalt electrocatalysts to generate hydrogen using alkaline solutions as storage fuel for the renewable energy. Int. J. Hydrogen Energy 44, 11411–11420. https://doi.org/10.1016/j.ijhydene.2019.03.128

Nelson, A., Wang, W., Demopoulos, G.P., Houlachi, G., 2000. Removal of cobalt from zinc electrolyte by cementation: A critical review. Miner. Process. Extr. Metall. Rev. 20, 325–356. https://doi.org/10.1080/08827500008547436

Nesbitt, H.W., Bancroft, G.M., Davidson, R., McIntyre, N.S., Pratt, A.R., 2004. Minimum XPS core-level line widths of insulators, including silicate minerals. Am. Mineral. 89, 878–882. https://doi.org/10.2138/am-2004-5-623

Park, I., Tabelin, C.B., Seno, K., Jeon, S., Inano, H., Ito, M., Hiroyoshi, N., 2020. Carrier-microencapsulation of arsenopyrite using Al-catecholate complex: nature of oxidation products, effects on anodic and cathodic reactions, and coating stability under simulated weathering conditions. Heliyon 6, e03189. https://doi.org/10.1016/j.heliyon.2020.e03189

Park, I., Tabelin, C.B., Seno, K., Jeon, S., Ito, M., Hiroyoshi, N., 2018. Simultaneous suppression of acid mine drainage formation and arsenic release by Carrier-microencapsulation using aluminum-catecholate complexes. Chemosphere 205, 414–425. https://doi.org/10.1016/j.chemosphere.2018.04.088

Scherer, J., 2020. Auger Electron Spectroscopy (AES): A Versatile Microanalysis Technique in the Analyst's Toolbox. Microsc. Microanal. 26, 1564–1565. https://doi.org/10.1017/S143192762001853X

Silwamba, M., Ito, M., Hiroyoshi, N., Tabelin, C.B., 2020a. Recovery of Lead and Zinc from Zinc Plant Leach Residues by Concurrent Dissolution-Cementation. Metals (Basel). 10, 531. https://doi.org/10.3390/met10040531

Silwamba, M., Ito, M., Hiroyoshi, N., Tabelin, C.B., Fukushima, T., Park, I., Jeon, S., Igarashi, T., Sato, T., Nyambe, I., Chirwa, M., Banda, K., Nakata, H., Nakayama, S., Ishizuka, M., 2020b. Detoxification of lead-bearing zinc plant leach residues from Kabwe, Zambia by coupled extraction-cementation method. J. Environ. Chem. Eng. 8, 104197. https://doi.org/10.1016/j.jece.2020.104197

Sulyman, M., Namiesnik, J., Gierak, A., 2017. Low-cost adsorbents derived from agricultural by-products/wastes for enhancing contaminant uptakes from wastewater: A review. Polish J. Environ. Stud. 26, 479–510. https://doi.org/10.15244/pjoes/66769

Vasil'ev, E.A., Darintseva, A.B., Naboichenko, S.S., 2010. Experimental investigations of cementation of

indium. Russ. J. Non-Ferrous Met. 51, 268–272. https://doi.org/10.3103/S1067821210040024

Wei, W.Y., Lee, C., Chen, H.J., 1994. Modeling and Analysis of the Cementation Process on a Rotating Disk. Langmuir 10, 1980–1986. https://doi.org/10.1021/la00018a058

Xu, R., Ma, K., Guo, Z., 2006. Activation mechanism of Sb2O3 during removal of cobalt from zinc sulphate solution. Hydrometallurgy 82, 150–153. https://doi.org/10.1016/j.hydromet.2006.03.009

Yan, Y., Huang, J., Wang, X., Gao, T., Zhang, Y., Yao, T., Song, B., 2018. Ruthenium incorporated cobalt phosphide nanocubes derived from a Prussian blue analog for enhanced hydrogen evolution. Front. Chem. 6, 1–8. https://doi.org/10.3389/fchem.2018.00521

Zeng, X., Li, J., Singh, N., 2014. Recycling of spent lithium-ion battery: A critical review. Crit. Rev. Environ. Sci. Technol. 44, 1129–1165. https://doi.org/10.1080/10643389.2013.763578

Zhang, R., Xia, B., Li, B., Lai, Y., Zheng, W., Wang, H., Wang, W., Wang, M., 2018. Study on the characteristics of a high capacity nickel manganese cobalt oxide (NMC) lithium-ion battery-an experimental investigation. Energies 11. https://doi.org/10.3390/en11092275

Zhang, W., Ma, X., Zhong, C., Ma, T., Deng, Y., Hu, W., Han, X., 2018. Pyrite-type CoS2 nanoparticles supported on nitrogen-doped graphene for enhanced water splitting. Front. Chem. 6, 1–10. https://doi.org/10.3389/fchem.2018.00569

This chapter was based on a research paper published under the following details: -

Choi, S., Jeon, S., Park, I., Ito, M., Hiroyoshi, N., 2021. Enhanced cementation of Co^{2+} and Ni^{2+} from sulfate and chloride solutions using aluminum as electron donor and conductive particles as an electron pathway. Metals 11, 248. https://doi.org/10.3390/met11020248

CHAPTER 5 – Enhanced cementation of Cd^{2+} and Zn^{2+} from sulfate solutions using aluminum powder and Fe_3O_4 as an electron mediator and application of magnetic separation to concentrate cementation products

5.1 Introduction

The cementation method using Al as electron donor and electro-conductive materials as electron mediator could be widely applicable for environmental remediation because a wide variety of metal ions can be removed under mild conditions where Al_2O_3 layer remains on the surface of Al; however, it is important to note that cementation product is a mixture of a small amount of toxic metals deposited on electron mediator and a large amount of clean Al (i.e., unreacted Al). Because of this, the cementation products should be disposed of in special landfills to prevent a recurrence of environmental pollution in the surrounding areas (Tabelin et al., 2018). If cemented metals (i.e., deposited metals) can be recovered/separated from the product (i.e., clean Al and electron mediator), it has two major advantages: (1) the amount of waste disposed of in landfills can be dramatically reduced, and (2) the separated clean Al and electron mediator can be re-utilized for cementation process. However, there is no suitable separation technique because the currently used electron mediators (e.g., AC and TiO_2) have no distinct features.

In this chapter, thus, magnetite (Fe_3O_4) was used as an alternative electron mediator. Magnetite is classified as a semiconductor (Alorro et al., 2010), so it has the potential of acting as an electron mediator for improving the efficiency of cementation using Al. Moreover, Fe_3O_4 is a ferromagnetic material, which facilitates the application of magnetic separation as a post-cementation process to separate heavy metal-loaded Fe_3O_4 from Al. Specifically, this chapter attempted to remove Zn^{2+} and Cd^{2+} via cementation using Fe_3O_4 and Al. In Zn hydrometallurgy process, a huge amount of zinc leach residues (ZLRs) are generated after leaching of calcined ores and cementation-based purification process to remove impurity metal ions from pregnant leach solution using Zn powder (Jha et al., 2001; Silwamba et al., 2020a). These ZLRs are disposed of in landfills because there is no proper treatment method even though it contains not only Zn but also various cemented heavy metals (e.g., Cd, Pb, etc.) (Abo Atia and Spooren, 2020; Bae and Yoo, 2016; Jha et al., 2001; Martínez-Sánchez et al., 2019). Recently, Silwamba et al. (2020) proposed a technique for treating ZLRs called coupled extraction-cementation (CEC) wherein ZLRs are treated in chloride media (a mixture of NaCl/HCl) together with Al powder. During treatment, Pb and Zn contained in ZLRs are extracted by complexation with chloride ions, and metal-chloride complexes are reductively deposited on Al surface. This technique was effective in removing Pb^{2+} but difficult to remove Zn^{2+}, indicating that an additional process for Zn removal should be followed. Moreover, they only focused on the removal of Pb and Zn, but Cd is also often found in ZLRs (Abo Atia and Spooren, 2020; Bae and Yoo, 2016; Silwamba et al., 2020b). Cadmium is very toxic even at minute concentrations, and long-term exposure to Cd increases the

risks of developing cancers of lung, kidney, liver, stomach, etc. (Bernhoft, 2013; E. Park et al., 2021; Vicentini et al., 2022), so it is necessary to develop an appropriate cementation technique for the removal of Cd in ZLRs.

Therefore, this chapter aimed to investigate the effects of Fe_3O_4 addition on the cementation of Cd^{2+} and Zn^{2+} from sulfate media using Al as an electron donor. In this chapter, Cd^{2+} and Zn^{2+} were selected as target metal ions because among the major heavy metals (Cd, Pb, and Zn) in ZLRs, Pb^{2+} is known to be precipitated as $PbSO_4$ because of its low solubility in sulfate media. Specifically, this chapter conducted cementation experiments as well as surface analysis and electrochemical chapter to confirm the enhanced cementation and its mechanism. Moreover, magnetic separation experiments were also conducted for the cementation products to separate heavy metal-enriched particles and unreacted Al.

5.2 Materials and methods

5.2.1 Cementation experiments

For cementation experiments, solutions containing 1 mM Cd^{2+} or Zn^{2+} were prepared using reagent-grade $CdSO_4 \cdot nH_2O$ (99.5%, Wako Pure Chemical Industries, Ltd., Japan), $ZnSO_4 \cdot 7H_2O$ (99.5%, Wako Pure Chemical Industries, Ltd., Japan), and deionized (DI) water (18 MΩ·cm, Mill-Q® Integral Water Purification System, Merck Millipore, USA). The initial pH of these solutions was adjusted to 5.0 by adding 1 M H_2SO_4 (Wako Pure Chemical Industries, Ltd., Japan) to minimize precipitation of metal ions at high pH in consideration of the increase in pH after the experiment. To normalize the effects of SO_4^{2-} on cementation experiment, total SO_4^{2-} concentration was adjusted to 0.1 M using 1 M Na_2SO_4 (99.0%, Wako Pure Chemical Industries, Ltd., Japan).

The cementation experiments were conducted using a 50-mL Erlenmeyer flask. A 10 mL metal sulfate solution was added to the flask, and ultrapure N_2 gas (99.99%) was introduced for 15 min to remove dissolved oxygen (DO) in the solution. Then, 0.1 g of Al powder (99.99%, Wako Pure Chemical Industries, Ltd., Japan) with and without Fe_3O_4 (0–0.4 g) (> 95.0%, Wako Pure Chemical Industries, Ltd., Japan) was added to the flask, and N_2 was further introduced for 5 min. The median particle sizes (D_{50}) of Al and Fe_3O_4 used were 21.3 μm and 3.4 μm, respectively. After that, the flask was tightly capped with a silicon rubber plug and parafilm and shaken in a thermostat water bath shaker (Cool bath shaker, ML-10F, Taitec Corporation, Japan) maintained at 25 °C with 40 mm shaking amplitude and 120 min^{-1} shaking frequency. After 24 h, the suspension was collected and filtered by a syringe-driven membrane filter (pore size: 0.2 μm, LMS Co., Ltd., Tokyo, Japan). After measuring final pH, the filtrate was diluted with 0.1 M HNO_3 for measuring the change in metal ion

concentration by inductively coupled plasma atomic emission spectroscopy (ICP-AES, ICPE-9820, Shimadzu Corporation, Japan). The removal efficiency (R) of metal ions was calculated according to the following equation:

$$R = \frac{C_i - C_f}{C_i} \times 100 \quad (5\text{-}1)$$

where C_i and C_f are the initial and final concentrations of metal ions (mg/L), respectively. For the case of cementation products, it was thoroughly washed with DI water, dried in a vacuum drying oven at 40 °C for 24 h, and then analyzed by scanning electron microscopy with energy-dispersive X-ray spectroscopy (SEM-EDS, JSM-IT200TM, JEOL Co., Ltd., Japan).

5.2.2 Magnetic separation

The washed cementation product was treated by an ultrasonicator (W-113, Honda Electronics Co., Ltd., Japan) for 10 min in 400 mL DI water to disperse agglomerated particles. After this, the suspension was agitated at 400 rpm, then magnetic separation was conducted for 1 min using a rare earth tube magnet (0.6–0.65 T, 2.5 cm in diameter and 15 cm in length, Eriez Co., Ltd., Japan) attached to outer surface of the beaker as shown in Fig. 5-1. The obtained magnetic and non-magnetic products were processed by an additional magnetic separation to minimize the entrapment of non-magnetic particles in the magnetic fraction as well as to recover magnetic particles remaining in the non-magnetic fraction as shown in the flowchart (Fig. 5-2). After magnetic separation, the black particles were separated as a magnetic fraction and the gray particles were separated as a non-magnetic fraction (Fig. 5-2). The final products were filtered with a membrane filter, rinsed using DI water 5 times, and dried in a vacuum oven for 24 h at 40 °C. The dried products (magnetic and non-magnetic fractions) were dissolved in aqua regia, diluted with DI water, and analyzed by ICP-AES for examining distribution. Moreover, the products were analyzed by SEM-EDS.

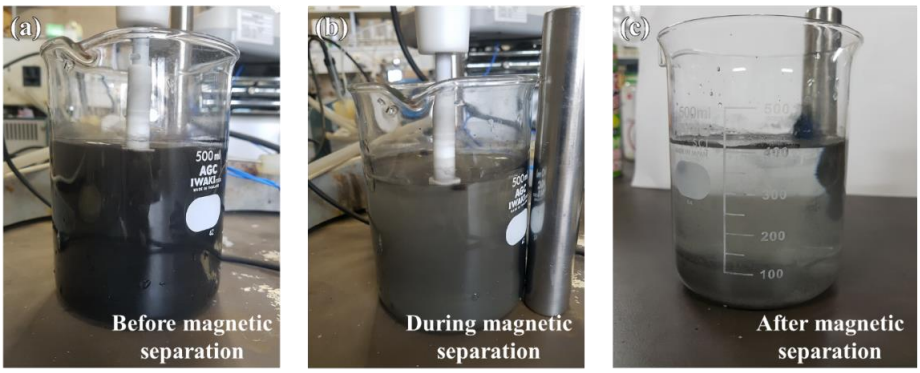


Fig. 5-1 Photographs of the magnetic separation used in this study: (a) before magnetic separation, (b) during magnetic separation with stirring, and (c) after magnetic separation without stirring.

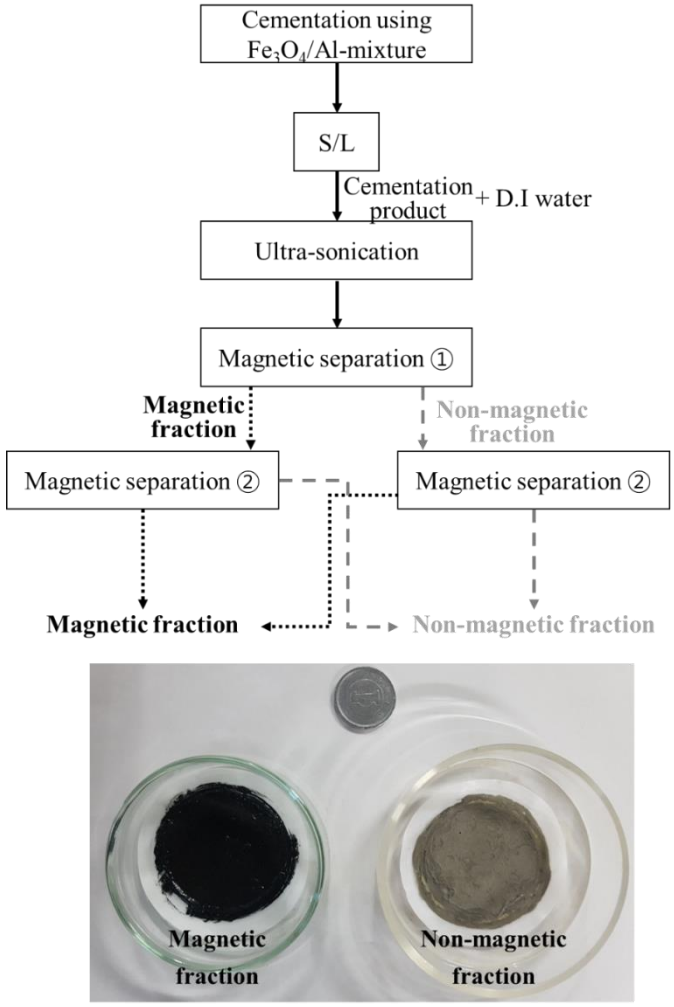


Fig. 5-2 The flowchart of 2-stage magnetic separation and photographs of magnetic and non-magnetic fractions obtained by magnetic separation of Cd cementation products.

5.2.3 Electrochemical measurements

Electrochemical impedance spectroscopy (EIS) was conducted using a potentiostat (SP-300, Biologic, France) with a conventional three-electrode system to elucidate the electrochemical properties of Al electrode with and without the attachment of Fe_3O_4 particles on its surface. For EIS experiments, Al rod (99.999%, 10 mm φ, Nilaco Corp., Japan), Ag/AgCl electrode filled with saturated KCl, and platinum (Pt) electrode were used as working, reference, and counter electrodes, respectively. Al working electrode was polished with a 1200-grit silicon carbide paper followed by 1 μm diamond paste on a polishing cloth plate using a polishing machine (Saphir 250 M1, ATM, Germany). After this, the Al working electrode was ultrasonically cleaned for 3 min to remove impurities, washed with DI water, and exposed to the atmosphere for 7 days to form Al_2O_3 layer on the surface of Al working electrode.

The Fe_3O_4/Al electrode was prepared as follows: (1) 0.1 g of Fe_3O_4 was mixed with 30 ml of acetone and suspended by ultra-sonification, (2) the Fe_3O_4/acetone suspension was put dropwise on the whole surface of Al electrode, and (3) the Fe_3O_4/Al electrode was used as a working electrode after the evaporation of acetone. Three electrodes were immersed into the electrolyte solution (0.1 M Na_2SO_4; pH 5), deoxygenated by N_2 purging, and equilibrated at 25 °C for 30 min. After equilibration at the open circuit potential (OCP), EIS measurement was conducted with a 5 mV sinus amplitude and frequency range of 20 kHz to 0.02 mHz as shown in Fig. 5-3.

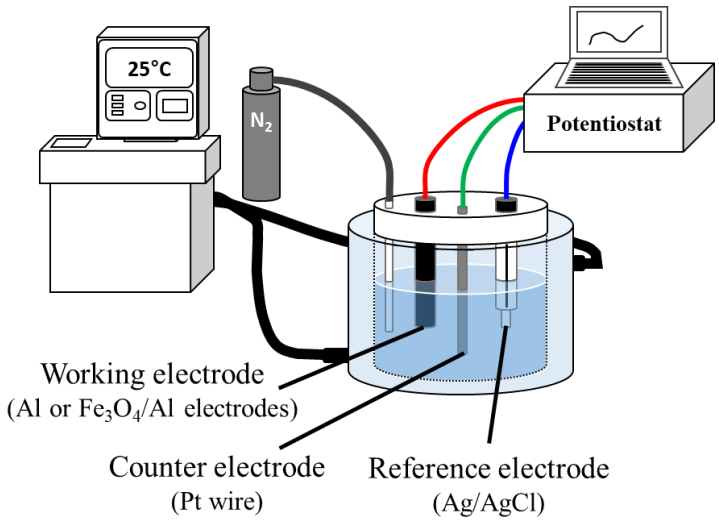


Fig. 5-3 The schematic diagram of electrochemical experiment.

5.3 Results and discussion

5.3.1 Effects of Fe_3O_4 on cementation of Cd^{2+} and Zn^{2+} with Al

5.3.1.1 Cementation experiments

Cementation experiments for removing Cd^{2+} and Zn^{2+} from sulfate solutions were conducted at initial pH of 5.0 using Al powder as an electron donor for 24 h, and the effects of the addition of Fe_3O_4 powder on the metal removal efficiencies were investigated. To clarify the enhanced cementation by the combination of Fe_3O_4 and Al, the experiments using only Fe_3O_4 (without Al) were also done. Figures 5-4(a) and (b) show the results of the average removal efficiencies of Cd^{2+} and Zn^{2+}, respectively. After cementation, the highest final pH was 6.7 for Cd^{2+} (Fig. 5-4(c)) and 6.4 for Zn^{2+} (Fig. 5-4(d)), and at these pH conditions, Cd^{2+} and Zn^{2+} are expected not to be precipitated as $Cd(OH)_2$ and $Zn(OH)_2$ based on equilibrium log activity – pH diagrams (Figs. 5-4(e) and (f)). This indicates that the Cd^{2+} and Zn^{2+} concentrations decreased after experiments are most likely due to the cementation reaction, not to precipitation.

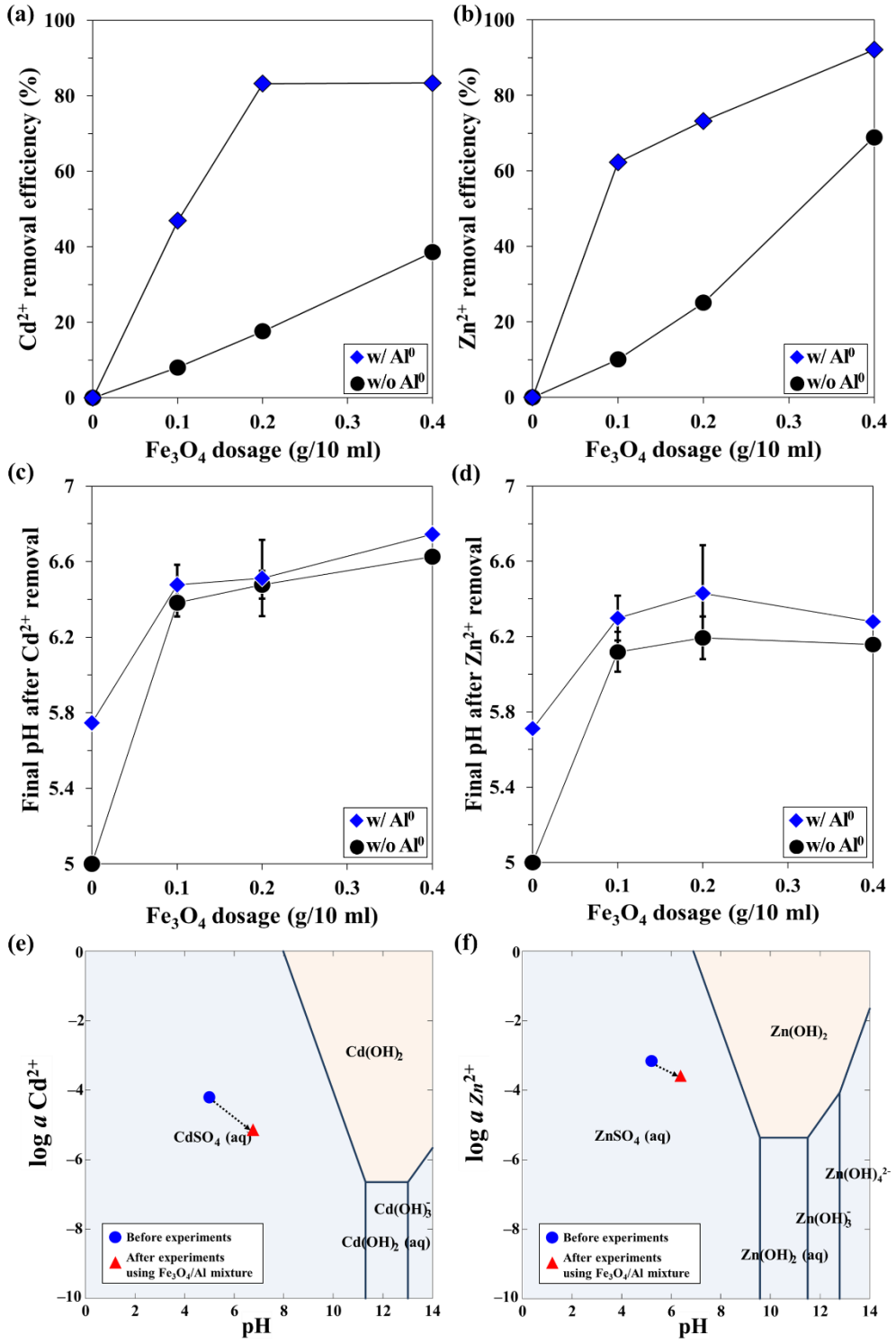


Fig. 5-4 The removal efficiencies of metal ions ((a) Cd^{2+} and (b) Zn^{2+}) and final pH ((c) Cd^{2+} and (d) Zn^{2+}) in sulfate solutions using Al^0 and/or Fe_3O_4 at initial pH 5.0 for 24 h and the activity – pH diagram for 1 mM (e) Cd^{2+} and (f) Zn^{2+} species with 0.1 M SO_4^{2-} at 25 °C (created using the Geochemist's Workbench® Professional Ver. 12.0.3 software with the MINTEQ database).

When only Al was used (without Fe_3O_4), the removal efficiency of Cd^{2+} and Zn^{2+} was closed to zero (Figs. 5-4(a) and (b)). In sulfate solutions at pH > 5, insulating Al_2O_3 layer covers Al surface as discussed in the previous chapters, and inhibits the electron transfer from Al to metal ions (Eqs. 5-2 and 5-3).

$$2Al^0_{(s)} + 3\ Cd^{2+}_{(aq)} \rightarrow 2Al^{3+}_{(aq)} + 3\ Cd^0_{(s)} \quad (5\text{-}2)$$

$$2Al^0_{(s)} + 3\ Zn^{2+}_{(aq)} \rightarrow 2Al^{3+}_{(aq)} + 3\ Zn^0_{(s)} \quad (5\text{-}3)$$

On the other hand, the sole addition of Fe_3O_4 could remove around 8–39% of Cd^{2+} and around 10–69% of Zn^{2+} from solutions. The Fe_2O_3/Fe_3O_4 redox pair is higher than standard electrode potentials of Cd^{2+} and Zn^{2+} (Alorro et al., 2010), which means that these metal ions are impossible to be reductively deposited on the surface of Fe_3O_4. Instead, the removal of metal ions using only Fe_3O_4 was attributed to the adsorption of positively-charged metal ions on negatively-charged Fe_3O_4 surface by electrostatic attraction (i.e., physisorption) (Abdus-Salam and Adekola, 2018; Emadi et al., 2013; Karami, 2013; Shahid et al., 2018).

The removal efficiencies of Cd^{2+} and Zn^{2+} could be significantly enhanced by using Fe_3O_4 and Al simultaneously. Compared to the results of Fe_3O_4 only, the metal removal efficiencies were much higher; for example, at Fe_3O_4 dosage of 0.4 g, the removal efficiencies for Cd^{2+} and Zn^{2+} were 39 and 69% without Al and 83 and 92% with Al, respectively. This suggests that when using Fe_3O_4/Al mixture, not only adsorption but also another chemical process such as cementation occurred, resulting in the enhanced removal of metal ions.

Cementation experiments were conducted several times to obtain reproducibility using Fe_3O_4/Al-mixture and only Fe_3O_4 (without Al) as shown in Fig. 5-5. Without Al, a good reproducibility was achieved regardless of Fe_3O_4 dosages. With Al, a low reproducibility was achieved because cementation efficiency is decided by the probability of contacting Al and Fe_3O_4 particles. As can be seen in Fig. 5-5, the removal efficiencies of Cd^{2+} and Zn^{2+} became less fluctuated with increasing the amount of Fe_3O_4 particles. It is important to note that the removal efficiencies of Cd^{2+} and Zn^{2+} using Fe_3O_4/Al mixture were higher than using Al only or Fe_3O_4 only.

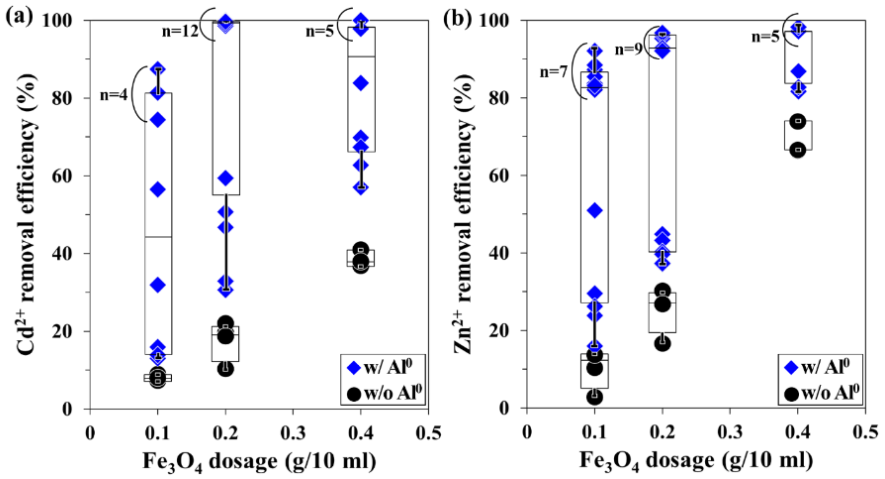


Fig. 5-5 Box plots of removal efficiencies of metal ions ((a) Cd^{2+} and (b) Zn^{2+}) in sulfate solutions using Al^0 and/or Fe_3O_4 at initial pH 5.0 for 24 h.

After cementation experiments, the concentrations of dissolved Al and Fe were also measured apart from Cd^{2+} and Zn^{2+}. When cementation reaction (Eqs. 5-2 and 5-3) occurs, Al should be dissolved stoichiometrically. However, the concentrations of dissolved Al after cementation experiments were less than 1 mg/L, which were lower than the expected values based on the stoichiometry of cementation reactions. This suggests that Al^{3+} dissolved by cementation reactions was precipitated because of increased solution pH to 5.7–6.7 (Figs. 5-4(c) and (d)) where Al oxyhydroxides (e.g., $Al(OH)_3$ and/or AlO(OH)) are thermodynamically stable (Park et al., 2018; Wei et al., 2005). Meanwhile, the concentration of dissolved Fe was significant when Fe_3O_4/Al mixture was used; that is, about 13.7–16.8 mg/L Fe^{2+} was extracted from Fe_3O_4 after 24 h. Since Fe_3O_4 cannot act as an electron donor like Al, the release of Fe^{2+} is most likely attributed to its reductive dissolution by Al (Eq. 5-4):

$$3\ Fe_3O_4 + 2\ Al^0 + 18\ H^+ \rightarrow 3\ FeO + 6\ Fe^{2+} + 2\ Al^{3+} + 9\ H_2O \qquad (5\text{-}4)$$

To meet the effluent discharge limits, therefore, the solution obtained after cementation process needs to be treated for removing Fe^{2+}. This can be achieved by aeration of solution that oxidizes Fe^{2+} to Fe^{3+}, followed by its precipitation as $Fe(OH)_3$ (Li et al., 2019; I. Park et al., 2021; Rose, 2010; Seng et al., 2019); however, this is out of the scope of this study.

5.3.1.2 Surface analysis

Cementation products obtained after 24 h of cementation experiments using 0.1 g Al and 0.2 g Fe_3O_4 were analyzed by SEM-EDS. As shown in the backscattered electron (BSE) image of the Cd-cementation product (Fig. 5-6), small bright particles (e.g., Point 2) were agglomerated with small gray particles (Point 3), and they were attached on the surface of dark and large particles (Point 1).

The EDS point analysis revealed that Point 1 showed strong signals of Al and O, suggesting that a dark particle was Al powder. Meanwhile, Points 2 and 3 showed the intensity of Al signal decreased from 38 kcounts (Point 1) to ~6 kcounts and new signals (e.g., Cd and Fe) were detected, which indicate that these two points were Cd cemented on Fe_3O_4. Specifically, bright particles (Point 2) are considered as Cd metal deposited from solutions based on strong signals of Cd, while gray particles (Point 3) are most likely Fe_3O_4 due to strong signals of Fe.

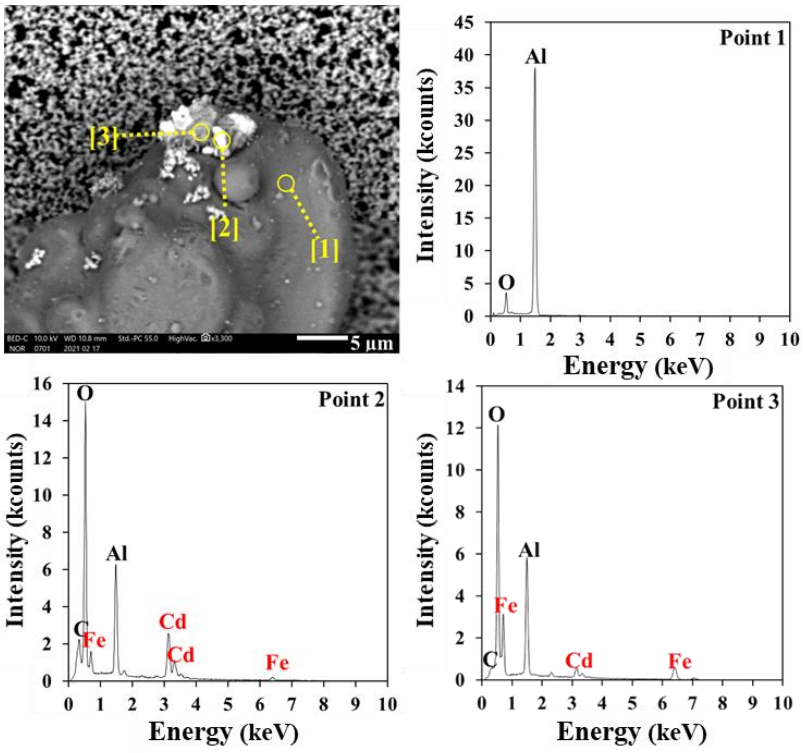


Fig. 5-6 SEM-EDS analysis of Cd- cementation product: BSE image and EDS spectra of the corresponding points.

Similarly, SEM-EDS analysis of Zn-cementation product (Fig. 5-7) also showed agglomerates of cemented Zn (Point 2) and Fe_3O_4 (Point 3) were present on the surface of Al (Point 1). These results suggest that Cd and Zn were reductively deposited on the surface of Fe_3O_4 attached on Al powder.

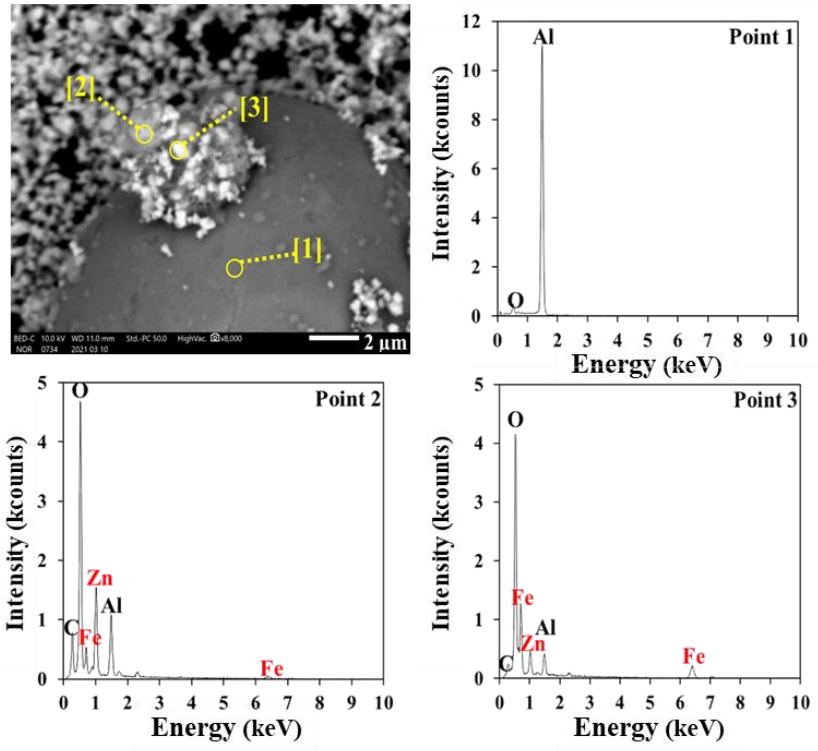


Fig. 5-7 SEM-EDS analysis of Zn- cementation product: BSE image and EDS spectra of the corresponding points.

5.3.1.3 Electrochemical measurements

The results of cementation experiments and surface analysis suggest that Fe_3O_4 attached on Al surface plays an important role in the enhanced cementation of Cd^{2+} and Zn^{2+}. To elucidate how the attachment of Fe_3O_4 on the surface of Al improves the cementation efficiency, electrochemical impedance spectroscopy (EIS) measurements were conducted for Al electrode with and without Fe_3O_4 attachment.

As shown in Fig. 5-8(a), a Nyquist plot of Al electrode (without Fe_3O_4 attachment) was fitted with an equivalent circuit (EC) model composed of a solution resistance (R_s) connected with a parallel circuit of a charge transfer resistance (R_{ct}) and a capacitance (C). The diameter of the flat semi-circle in the Nyquist plot corresponds to the value of charge transfer resistance, R_{ct}, and the observed large value (around 120 kΩ) suggests that Al_2O_3 layer present on Al electrode surface acts as an insulating layer inhibiting electron transfer between Al to chemical species in aqueous solutions.

When Fe_3O_4 particles were attached on the surface of Al electrode (Fig. 5-8(b)), however, the impedance data in the Nyquist plot were drastically changed; that is, an inclined straight line appeared at the end of the plot. Thus, this EIS data was fitted with the EC model consisting of the R–(RC) circuit connected with a Warburg impedance, corresponding to diffusion phenomenon or inclined straight line in the Nyquist plot. An important difference between the impedance data with and without Fe_3O_4 is the diameter of the semi-circle corresponding to RC parallel circuit; that is, the diameter observed with Fe_3O_4 was apparently smaller than that without Fe_3O_4, suggesting that charge transfer resistance (R_{ct}) was reduced from around 120 to 2 kΩ when Fe_3O_4 attached on Al electrode surface.

For the case of the pre-oxidized Al electrode without Fe_3O_4, charge transfer resistance, R_{ct}, is determined by and proportional to the thickness of Al_2O_3 layer, d. Even in this case, time constant ($\boldsymbol{\tau}$) of the parallel circuit, $\boldsymbol{\tau = RC}$, is not changed because C is proportional to $1/d$, minimizing the effect of d. This indicates that the time constant does not change even when the thickness of Al oxide layer becomes thicker. The effect of Fe_3O_4 on time constant was evaluated using the following equation (Bonnel et al., 1999; Dollé et al., 2001):

$$\tau = \frac{1}{2\pi f_{max}} \tag{5-5}$$

where f_{max} is the frequency at the top of semicircle in Nyquist plot. The value of f_{max} was 1.656 Hz with Fe_3O_4, which was approximately 17 times larger than that without Fe_3O_4 (0.097 Hz). This indicates that the time constant was reduced with Fe_3O_4, and that the reduction of R_{ct} with Fe_3O_4 was not caused by Al_2O_3 layer thickness reduction as already discussed. This is also supported by the impedance spectra data (Bode plot) shown in Figs. 5-8(c) and (d). Peak frequency, $f(\theta_{max})$ on θ-F plot was significantly changed when Fe_3O_4 was attached on Al electrode, indicating that different reactions could occur by the presence of Fe_3O_4 on Al electrode surface. The RC parallel circuit for Fe_3O_4/Al electrode was not determined with Al_2O_3 layer, and it was probably corresponding to Fe_3O_4 particles on the electrode surface.

Figure 5-8(e) shows a model explaining the effects of Fe_3O_4 addition on the enhanced cementation of Cd^{2+} and Zn^{2+} using Al as an electron donor. The added Fe_3O_4 particles are attached on Al particle of which surface is covered with an insulating Al_2O_3 layer, and the attached Fe_3O_4 particles then act as an electron mediator to enhance electron transfer from Al to metal ions. The authors reported that cementation of metal ions using Al as electron donor was also enhanced when AC or TiO_2 was added (Choi et al., 2021b, 2021a; Jeon et al., 2020). All these materials are classified as electro-conductive materials. The results obtained by a series of these studies by the authors suggest that any kinds of electro-conductive materials can most likely be used as an electron mediator to enhance the cementation using Al as an electron donor.

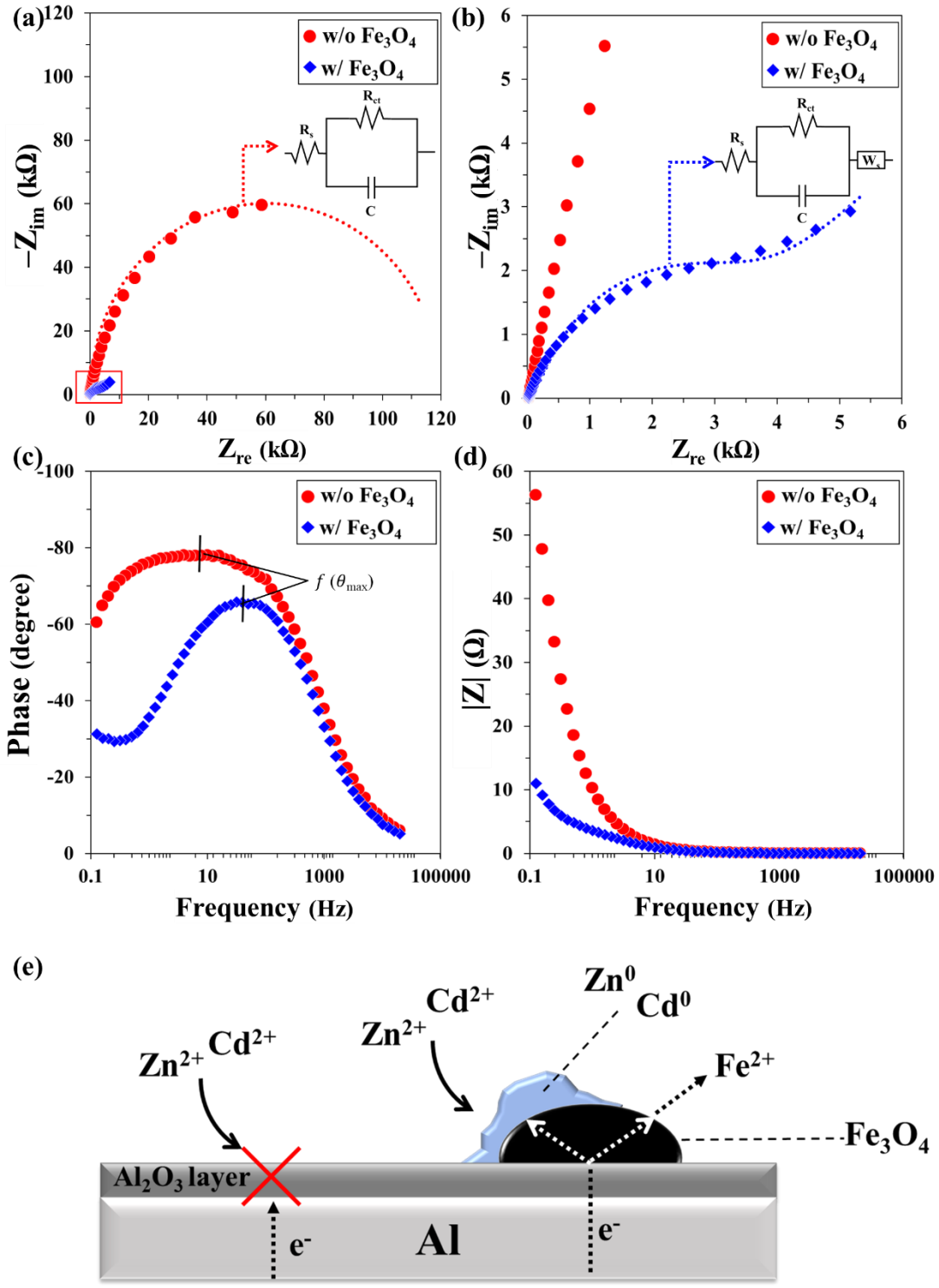


Fig. 5-8 Nyquist plots of (a) Al and (b) Fe_3O_4/Al electrodes (insets are equivalent circuit models for fitting EIS data), the Bode plot of (c) phase angle and (d) magnitude Z as a function of frequency for Al and Fe_3O_4/Al electrodes, and schematic diagram of Cd^{2+} and Zn^{2+} cementation using Fe_3O_4/Al-mixture.

5.3.2 Magnetic separation of cementation products

Magnetic separation of Cd- and Zn- cementation products was conducted to separate metal-deposited Fe_3O_4 particles from clean Al particles. Yield of magnetic fraction was 67.1% for Cd cementation product and 68.7% for Zn cementation product. The photographs of magnetic fraction and non-magnetic fraction were shown in Fig. 5-2. Figures 5-9 and 5-10 show the results of SEM-EDS analysis for magnetic and non-magnetic fractions obtained after magnetic separation of Cd- and Zn-cementation products, respectively. As can be seen in BSE images of magnetic fractions (Figs. 5-9(a) and 5-10(a)), there are many small particles (< 1 μm) and relatively large particles agglomerated. The results of EDS point analysis indicated that small particles (Point a-2 in Figs. 5-9(a) and 5-10(a)) are Fe_3O_4 particles based on strong signals of Fe and O, while large particles (Point a-1 in Figs. 5-9(a) and 5-10(a)) were composed of Al, Fe_3O_4 and cemented metals. The results of SEM-EDS analysis for non-magnetic fractions (Figs. 5-9(b) and 5-10(b)) showed that Al particles were major constituents but a small amount of Cd/Zn-cemented Fe_3O_4 remained, indicating that a part of cemented metals (Cd and Zn), strongly adhered to the surface of Al that was not detached even after 10 min ultra-sonification, was distributed to a non-magnetic fraction.

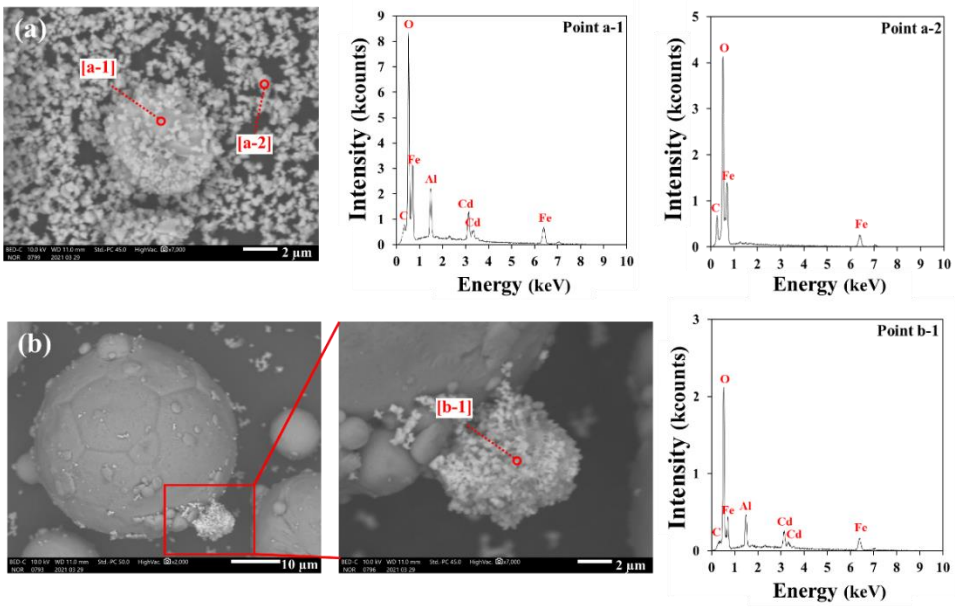


Fig. 5-9 Back-scattered electron (BSE) image of the Cd components in (a) magnetic fraction and (b) non-magnetic fraction, and EDS point analysis of each point (a-1, a-2, and b-1).

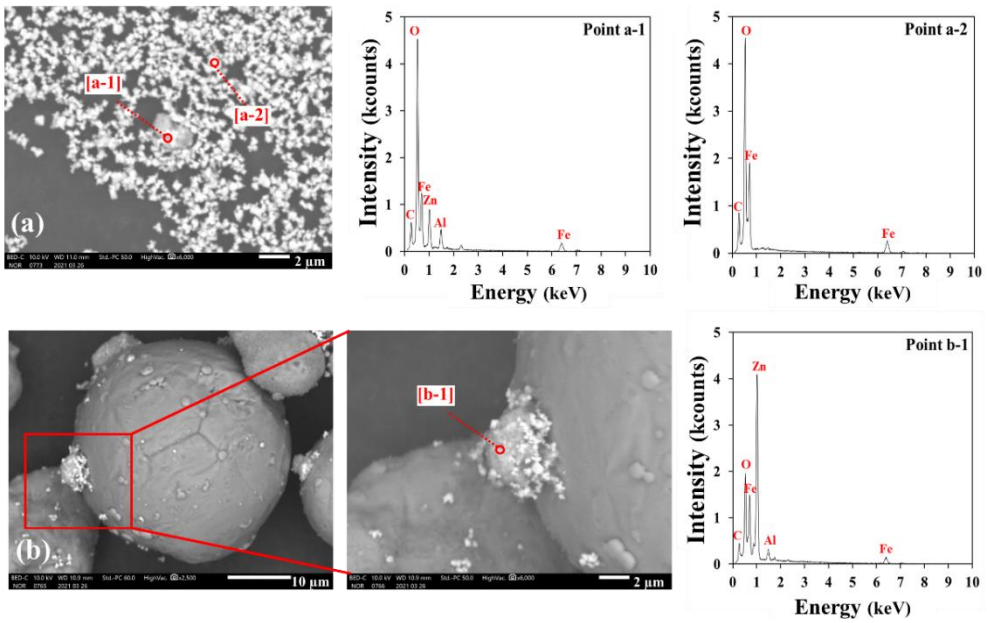


Fig. 5-10 Back-scattered electron (BSE) image of the Zn components in (a) magnetic fraction and (b) non-magnetic fraction, and EDS point analysis of each point (a-1, a-2, and b-1).

Figures 5-11(a) and (b) show the distribution ratio of Al, Fe, and heavy metals (Cd and Zn) to magnetic and non-magnetic fractions. For both Cd- and Zn-cementation products, more than 99% of Fe was distributed to a magnetic fraction, while more than 95% of Al was distributed to a non-magnetic fraction, indicating that their separation was well achieved by applying magnetic separation. Heavy metals were distributed to both magnetic and non-magnetic fractions; however, bulk of Cd (76.5%) and Zn (69.8%) were distributed to a magnetic fraction. As confirmed by SEM-EDS analysis of non-magnetic products (Figs. 5-9(b) and 5-10(b)), the distribution of cemented metals in non-magnetic fractions was mainly due to some cemented products strongly adhered to Al surface. This suggests that recovery of cemented metals attached on the surface of Al could be expected to increase if they are sufficiently liberated by employing strong ultra-sonification, surface grinding techniques, etc.

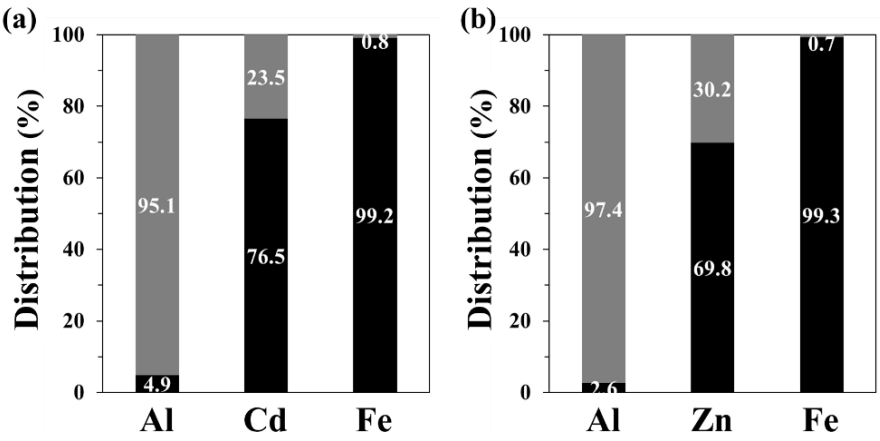


Fig. 5-11 Distribution of magnetic and non-magnetic fractions obtained by magnetic separation of (a) Cd- and (b) Zn- cementation products.

Figure 5-12 shows the proposed flowsheet for ZLRs treatment by cementation using Al and Fe_3O_4. At the first step, heavy metals like Cd and Zn are extracted from ZLRs in sulfate media and simultaneously cemented on Fe_3O_4 with the assistance of Al. Afterward, the suspension is introduced to magnetic separator wherein heavy metal-loaded and fresh Fe_3O_4 particles were separated from ZLRs and Al. Magnetic products consist of large size of Cd/Zn-enriched Fe_3O_4 particles and small size of fresh Fe_3O_4 particles, and they can be separated by employing hydrocyclone. Similarly, non-magnetic products are also composed of fine ZLRs and coarse Al, and these two materials can be separated by size-based separation like a mechanical classifier. Then, the recovered clean Al and Fe_3O_4 are re-utilized as cementation agents, while ZLRs and Cd/Zn-enriched Fe_3O_4 particles are disposed of in landfills.

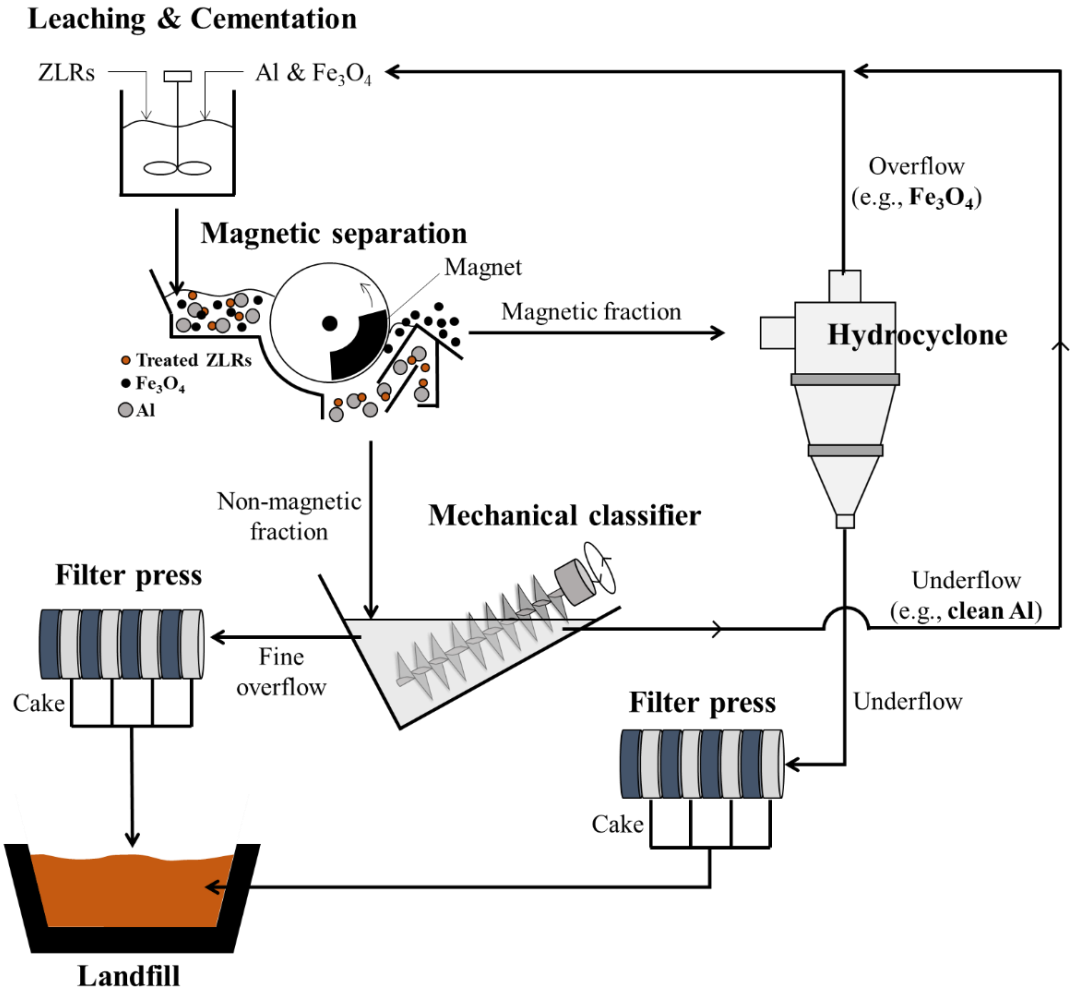


Fig. 5-12 The estimated flowchart for cementation using Fe_3O_4 and Al in this study.

5.4 Summary

In this chapter, cementation of Cd^{2+} and Zn^{2+}, two of the major contaminants released from ZLRs, using Al as an electron donor and Fe_3O_4 as an electron mediator was investigated. The use of Fe_3O_4/Al-mixture significantly enhanced the removal efficiencies of Cd^{2+} and Zn^{2+} from ~0% (0.1 g Al) and 18–25% (0.2 g Fe_3O_4) to 73–83% (0.1 g Al + 0.2 g Fe_3O_4). Electrochemical impedance spectroscopy proved that the charge transfer resistance of the oxidized Al decreased when Fe_3O_4 particles were attached on its surface, indicating that Fe_3O_4 acts as an electron mediator, and thus cementation efficiencies of Cd^{2+} and Zn^{2+} were enhanced. After cementation, the application of magnetic separation to the cementation products could separate Al and Fe_3O_4, where bulk of cemented metals (i.e., 77% for Cd and 70% for Zn) were recovered together with the latter. Magnetic products were composed of small Fe_3O_4 particles (< 1 μm) with no cemented metals and agglomerates containing heavy metals and Fe_3O_4 (~10 μm). Their separation based on the difference in particle size like hydrocyclone should be considered to reduce the amount of heavy metal-rich wastes disposed of in the landfill sites as well as to reutilize clean Fe_3O_4 together with Al (non-magnetic products) as cementing agents.

References

Abdus-Salam, N., Adekola, S.K., 2018. Adsorption studies of zinc(II) on magnetite, baobab (Adansonia digitata) and magnetite–baobab composite. Appl. Water Sci. 8, 1–11. https://doi.org/10.1007/s13201-018-0867-7

Abo Atia, T., Spooren, J., 2020. Microwave assisted chloride leaching of zinc plant residues. J. Hazard. Mater. 398, 122814. https://doi.org/10.1016/j.jhazmat.2020.122814

Alorro, R.D., Hiroyoshi, N., Kijitani, H., Ito, M., Tsunekawa, M., 2010. On the use of magnetite for gold recovery from chloride solution. Miner. Process. Extr. Metall. Rev. 31, 201–213. https://doi.org/10.1080/08827508.2010.483359

Bae, E., Yoo, K., 2016. Leaching behavior of valuable metals from by-product generated during purification of zinc electrolyte. Geosystem Eng. 19, 312–316. https://doi.org/10.1080/12269328.2016.1247754

Bernhoft, R.A., 2013. Cadmium toxicity and treatment. Sci. World J. 2013. https://doi.org/10.1155/2013/394652

Bonnel, K., Le Pen, C., Pébère, N., 1999. E.I.S. characterization of protective coatings on aluminum alloys. Electrochim. Acta 44, 4259–4267. https://doi.org/10.1016/S0013-4686(99)00141-3

Choi, S., Jeon, S., Park, I., Ito, M., Hiroyoshi, N., 2021a. Enhanced cementation of Co2+ and Ni2+ from sulfate and chloride solutions using aluminum as electron donor and conductive particles as an electron pathway. Metals (Basel). 11, 1–12. https://doi.org/10.3390/met11020248

Choi, S., Jeon, S., Park, I., Tabelin, C.B., Ito, M., Hiroyoshi, N., 2021b. Enhanced cementation of Cd2+, Co2+, Ni2+, and Zn2+ on Al from sulfate solutions by activated carbon addition. Hydrometallurgy 201, 105580. https://doi.org/10.1016/j.hydromet.2021.105580

Dollé, M., Orsini, F., Gozdz, A.S., Tarascon, J.-M., 2001. Development of Reliable Three-Electrode Impedance Measurements in Plastic Li-Ion Batteries. J. Electrochem. Soc. 148, A851. https://doi.org/10.1149/1.1381071

Emadi, M., Shams, E., Amini, M.K., 2013. Removal of zinc from aqueous solutions by magnetite silica core-shell nanoparticles. J. Chem. 2013. https://doi.org/10.1155/2013/787682

Jeon, S., Tabelin, C.B., Takahashi, H., Park, I., Ito, M., Hiroyoshi, N., 2020. Enhanced cementation of gold via galvanic interactions using activated carbon and zero-valent aluminum: A novel approach to recover gold ions from ammonium thiosulfate medium. Hydrometallurgy 191, 105165. https://doi.org/10.1016/j.hydromet.2019.105165

Jha, M.K., Kumar, V., Singh, R.J., 2001. Review of hydrometallurgical recovery of zinc from industrial wastes. Resour. Conserv. Recycl. 33, 1–22. https://doi.org/10.1016/S0921-3449(00)00095-1

Karami, H., 2013. Heavy metal removal from water by magnetite nanorods. Chem. Eng. J. 219, 209–216. https://doi.org/10.1016/j.cej.2013.01.022

Li, X., Hiroyoshi, N., Tabelin, C.B., Naruwa, K., Harada, C., Ito, M., 2019. Suppressive effects of ferric-catecholate complexes on pyrite oxidation. Chemosphere 214, 70–78. https://doi.org/10.1016/j.chemosphere.2018.09.086

Martínez-Sánchez, M.J., Solan-Marín, A.M., Hidalgo, A.M., Pérez-Sirvent, C., 2019. Characterization and mobilization of toxic metals from electrolytic zinc waste. Chemosphere 233, 414–421. https://doi.org/10.1016/j.chemosphere.2019.05.257

Park, E., Kim, S., Song, S.H., Lee, C.W., Kwon, J.T., Lim, M.K., Park, E.Y., Won, Y.J., Jung, K.W., Kim, B., 2021. Environmental exposure to cadmium and risk of thyroid cancer from national industrial complex areas: A population-based cohort study. Chemosphere 268, 128819. https://doi.org/10.1016/j.chemosphere.2020.128819

Park, I., Higuchi, K., Tabelin, C.B., Jeon, S., Ito, M., Hiroyoshi, N., 2021. Suppression of arsenopyrite oxidation by microencapsulation using ferric-catecholate complexes and phosphate. Chemosphere

269, 129413. https://doi.org/10.1016/j.chemosphere.2020.129413

Park, I., Tabelin, C.B., Seno, K., Jeon, S., Ito, M., Hiroyoshi, N., 2018. Simultaneous suppression of acid mine drainage formation and arsenic release by Carrier-microencapsulation using aluminum-catecholate complexes. Chemosphere 205, 414–425. https://doi.org/10.1016/j.chemosphere.2018.04.088

Rose, A.W., 2010. Advances in passive treatment of coal mine drainage 1998-2009. Jt. Min. Reclam. Conf. 2010 - 27th Meet. ASMR, 12th Pennsylvania Abandon. Mine Reclam. Conf. 4th Appalach. Reg. Refor. Initiat. Mined L. Refor. Conf. 2, 847–887. https://doi.org/10.21000/jasmr10010847

Seng, S., Tabelin, C.B., Kojima, M., Hiroyoshi, N., Ito, M., 2019. Galvanic microencapsulation (GME) using zero-valent aluminum and zero-valent iron to suppress pyrite oxidation. Mater. Trans. 60, 277–286. https://doi.org/10.2320/matertrans.M-M2018851

Shahid, M.K., Phearom, S., Choi, Y.G., 2018. Synthesis of magnetite from raw mill scale and its application for arsenate adsorption from contaminated water. Chemosphere 203, 90–95. https://doi.org/10.1016/j.chemosphere.2018.03.150

Silwamba, M., Ito, M., Hiroyoshi, N., Tabelin, C.B., 2020a. Recovery of Lead and Zinc from Zinc Plant Leach Residues by Concurrent Dissolution-Cementation. Metals (Basel). 10, 531. https://doi.org/10.3390/met10040531

Silwamba, M., Ito, M., Hiroyoshi, N., Tabelin, C.B., Fukushima, T., Park, I., Jeon, S., Igarashi, T., Sato, T., Nyambe, I., Chirwa, M., Banda, K., Nakata, H., Nakayama, S., Ishizuka, M., 2020b. Detoxification of lead-bearing zinc plant leach residues from Kabwe, Zambia by coupled extraction-cementation method. J. Environ. Chem. Eng. 8, 104197. https://doi.org/10.1016/j.jece.2020.104197

Tabelin, C.B., Igarashi, T., Villacorte-Tabelin, M., Park, I., Opiso, E.M., Ito, M., Hiroyoshi, N., 2018. Arsenic, selenium, boron, lead, cadmium, copper, and zinc in naturally contaminated rocks: A review of their sources, modes of enrichment, mechanisms of release, and mitigation strategies. Sci. Total Environ. 645, 1522–1553. https://doi.org/10.1016/j.scitotenv.2018.07.103

Vicentini, M., Fernandes, L. da S.P., Marques, A.E.M.L., Osório, F.H.T., Baika, L.M., Risso, W.E., Martinez, C.B. dos R., Grassi, M.T., Fávaro, L.F., Mela, M., Cestari, M.M., Silva de Assis, H.C., 2022. Effects of cadmium on the female reproductive axis of a Neotropical fish. Chemosphere 286, 131639. https://doi.org/10.1016/j.chemosphere.2021.131639

Wei, X., Viadero, R.C., Buzby, K.M., 2005. Recovery of iron and aluminum from acid mine drainage by selective precipitation. Environ. Eng. Sci. 22, 745–755. https://doi.org/10.1089/ees.2005.22.745

CHAPTER 6 – GENERAL CONCLUSION

In this dissertation, a new cementation technique using Al as electron donor and electro-conductivity particle as electron mediator was studied to develop the methods for removal and recovery of heavy metal ions from sulfate and chloride solutions. Important results obtained in each chapter are summarized as follows:

Chapter 1 describes the background, objectives of this study, and literature review of the cementation on Al and affecting factors to increase cementation efficiency.

Chapter 2 investigates the effects of AC addition on the cementation of Cd^{2+}, Co^{2+}, Ni^{2+}, and Zn^{2+} from sulfate solutions using Al. The results of cementation experiments showed that cementation efficiencies were enhanced with AC even when insulating Al_2O_3 layer was present. The results of surface analysis and electrochemical study suggest that AC attached on the surface of Al act as electron mediator to enhance electron transfer from Al to metal ions.

Chapter 3 investigates the effects of AC addition on the cementation of Pb^{2+}, Cd^{2+}, Co^{2+}, Ni^{2+}, and Zn^{2+} from chloride solutions at pH 4. In the chloride solutions, Al_2O_3 layer was dissolved due to the formation of soluble Al^{3+} chloride complexes. Because of this, even without AC, almost all Pb^{2+} and Cd^{2+} were cemented. In the case of Co^{2+}, Ni^{2+}, and Zn^{2+}, however, cementation was limited, because of competition with hydrogen evolution and slow reduction rate of the metal. With AC, cementation of Pb^{2+} and Cd^{2+} was suppressed while cementation of Co^{2+}, Ni^{2+}, and Zn^{2+} was enhanced.

Chapter 4 studies alternative electron mediators to AC. Cementation experiments using Al to remove Co^{2+} and Ni^{2+} from sulfate and chloride solutions were conducted with TiO_2 and SiO_2 instead of AC. Cementation efficiency depended on the conductivity of electron mediators: no cementation occurred when using non-conductive SiO_2 while enhanced cementation occurred with conductive TiO_2, and surface analysis showed that elemental Co and Ni were deposited on TiO_2 attached on Al surface. From these results, it is concluded that AC could be replaced by other conductive particles like TiO_2.

Chapter 5 investigates the addition of Fe_3O_4 for cementation of Cd^{2+} and Zn^{2+} from sulfate solutions using Al. Fe_3O_4 enhanced cementation efficiency of Cd^{2+} and Zn^{2+} with Al even in the presence of Al_2O_3 layer, and electrochemical experiments showed that charge transfer resistance significantly decreased when Fe_3O_4 was attached on Al surface. After cementation, a significant portion of cemented Cd and Zn were concentrated together with Fe_3O_4 in magnetic fractions, and used Al was separated as a non-magnetic fraction. Based on these results, it is expected that the application of magnetic separation after cementation process using Fe_3O_4/Al-mixture could be applied as a post-process of cementation using Al.

Finally, Chapter 6 gives the general conclusions of this study.

ACKNOLEDGEMENT

My three-year journey for this dissertation was not easy, but thanks to the help and support of many people, I was able to complete my dissertation, so I would like to express my gratitude to them.

First of all, I would like to express my sincere appreciation to my supervisor, Professor Naoki Hiroyoshi, for giving a lot of constructive advice and strong support for my research at Hokkaido University. He made my research has become more in depth and made me grow a lot as a researcher. Thank you bottom of my heart for all kindness you have shown me.

The assistance provided by Associate Professor Mayumi Ito was greatly appreciated. She gave me critical advice and insightful comments to complete my research successfully. Her advice and comments were always helpful and encouraging.

My deepest appreciation goes to my senior, Assistant professor Ilhwan Park, and my senior and friend Assistant professor Sanghee Jeon. Thanks to you, I was able to withstand my life in Japan and get a lot of advice on research. I will always support your life in Sapporo. Thank you for three years. I wish to extend my special thanks to my two co-examiners, Professor Toshifumi Igarashi (Division of Sustainable Resources Engineering, Faculty of Engineering, Hokkaido University) and Associate Professor Masatoshi Sakairi (Division of Materials Science and Engineering, Faculty of Hokkaido University), for their careful comments and reviewing of my research.

I want to say a big thank you to my former supervisor Professor Kyoungkeun Yoo (Department of Energy & Resources Engineering, Korea Maritime and Ocean University). Thanks to all the constructive advice and warm encouragement that has given me since my undergraduate days. Without his guidance and support, I would never grow up as a researcher.

Special thanks go to all members of the Laboratory of Mineral Processing and Resources Recycling for their kindness to me and for helping me a lot in my life at Hokkaido University. Thanks to the all members I was able to complete the three-year journey.

마지막으로 제가 어떤 선택을 해도 저를 믿고 지지를 보내준 사랑하는 부모님과 동생이 있었기에 저의 박사 학위 논문이 완성될 수 있었습니다. 정말 감사합니다.